Constructed Tidal Marshes

An analysis on how model configurations influence accretion

M. C. van Delden

Civil Engineering and Geosciences, Technische Universiteit Delft

TU Delft

Constructed Tidal Marshes

An analysis on how model configurations influence accretion

by

M. C. van Delden

to obtain the degree of Master of Science
at the Delft University of Technology,
to be defended publicly on Tuesday July 2, 2019 at 3 PM.

Student number: 4231910
Project duration: September 19, 2019 – July 2, 2019
Thesis committee:

Dr. T. A. Bogaard,	TU Delft, chair
Ir. W. M. J. Luxemburg,	TU Delft, supervisor
Ir. E. S. J. van Tuinen,	Witteveen + Bos
Dr. D. S. van Maren,	TU Delft
Dr. Ir. E. Mosselman,	TU Delft

An electronic version of this thesis is available at http://repository.tudelft.nl/.

TU Delft Delft University of Technology

Abstract

Along river banks, on the transition zone between the river and see, tidal marshes can develop. The tidal marshes accommodate multiple plant and fish species. As a result of the stressful conditions in tidal marshes, unique intertidal ecology develops. However, due to the densifying of the river banks, tidal marshes are disappearing.

Restoration of tidal marshes can reintroduce the unique intertidal ecology on several locations in the estuary. To obtain restoration of tidal marshes, constructed tidal marshes come into play, which can be built at designated places along the river. However, constructed tidal marshes are not necessarily built to restore the unique tidal nature, but can also have other functions as recreation and contribution in green city area.

Nevertheless, is it still unknown how constructed tidal marshes behave and what the optimal design is. Namely, a mismatch exists between the policymakers and designers on the one side and academic knowledge on the other side. To fill up this gap, accessible knowledge from the experts should be available for designers.

Therefore, this research provides guidelines for designers and gains more insight into the behaviour of constructed tidal marshes. This thesis focusses on extracting general knowledge from the results of a numerical model, applied on a case study.

Simulations of a numerical 1D Sobek model applied on the case study achieves the influence of model configurations on accretion. Therefore, tidal forcing, marsh design and system adjustments are divided into multiple components. The model simulations of the separate components give the influence on bed shear stress and potential sedimentation.

Furthermore, executed fieldwork calibrates the model on measured flow velocities. Besides, the Manning coefficient is estimated, and cross-sections are obtained by gps measurements. The parameters are subsequently used as model input.

From the simulations, it can be concluded that tidal asymmetry determines the duration of stagnant water and thus the settling of fine particles. A considerable increase in sedimentation is reached when flats are participating. However, an increasing flat area encourages ebb-dominance and can even lead to erosion.

Next, when the width of the cross-section is large compared to the depth, more sedimentation is predicted. With flood-dominant bed shear stresses, a broad cross-section leads to accretion.

In the case study, the presence of sand particles is not expected, as sand is deposited close to the inlet, where the bed shear stress is ebb-dominant. In contrast, silt settles throughout the system. Especially at low energetic conditions, such as bends, silt settles. As the occurring bed shear stress is mostly flood-directed, it is likely that sediment entering the system, does not leave the system anymore, and accretion of the bends is presumed.

The placement of gate culverts in flood direction leads to higher accretion rates due to the longer slack duration. However, at the exact locations of structures, higher bed shear stresses can develop, and erosion is expected.

Preface

This master thesis is the final step in obtaining my master degree in Watermanagement at Delft University of Technology. After eight months of being occupied with the subject of tidal marshes, I can state that I've learned a lot.

Especially the most challenging task for me has been setting up research. There are so many opportunities and not so many rules, which resulted for me in getting lost in very interesting, though somewhat unrelated topics. I'm happy that my supervisors gave me the opportunity and freedom to discover the field of research by just doing it.

Special thanks goes to my supervisors. First of all, Ebbing, who suggested this topic and always came up with other ideas to make this thesis work. Also Wim, thank you for your support and your free walk-in policy. Bas, without your expertise, this thesis would have been on a different level. And also great thanks for Erik, who introduced me to several masterclasses and gave some valuable suggestions.

I would also like to thank Annabelle, Anny, Caroline, Fenno, Leoni, Marte, and Pam for getting up at 5 AM and helping me out with the fieldwork. Without your help, this thesis wasn't even possible.

'Hokje 1' on the 4th floor of Civil Engineering made my life much more relaxed and being so supportive. Also Annette en Arjen, my parents, thank you for hearing the same story over and over, albeit very interesting.

M. C. van Delden
Delft, July 2019

Contents

1 Introduction

Tidal marshes are present along the river banks in the transition zone between the sea and the river, where they experience a salinity gradient and tidal variation. In intertidal areas an interaction exists between hydrodynamics, morphodynamics, and flora and fauna. The existence of nature in a stressful area, experiencing flooding and salinity, makes natural tidal marshes unique. However, since river banks are becoming more densely built and more protected, intertidal areas along river banks are vanishing.

For the restoration of intertidal areas in the built environment, constructed tidal marshes are considered. For instance, nature and ecology can be experienced in a large-scale, constructed tidal marsh with a natural function. For this type of marsh, the aim is to reintroduce distinct species into the estuary. Therefore, in constructed tidal marshes with a natural function, only little interventions are needed for well-functioning of the marsh.

However, constructed tidal marshes are not necessarily built to restore the unique tidal nature, but can also have other functions. In a marsh with a natural function on a city-scale, artificial adaptations facilitate the combination of a nature and ecology function with recreation. Next, a park-like constructed tidal marsh has a recreational function, and contributes to the increase in green city areas. In park-like marshes, the tide should be experienced, but sludge is less desirable. Also constructed tidal marshes with a cultural function can be distinguished. The main purpose of cultural constructed tidal marshes is recreation, and nature has a subordinate function.

Rotterdam is a Dutch city situated in the Rhine-Meuse estuary, with a high potential for tidal marshes. The mouth of this river has open access to sea, enabling salinity gradients to exist and ebb and flood to propagate along the river. Hence, the river banks along the Meuse are appropriate locations for the introduction of constructed tidal marshes.

In this thesis the accretion behaviour of constructed tidal marshes is achieved. Each variation of a constructed tidal marsh requires a different type and amount of sediment. When a tidal marsh exports sediment, the system is ebb-dominant. In contrast, when a tidal marsh imports sediment, the system is flood-dominant. Therefore, in this research, components leading to sedimentation and erosion are split up into external forces applied to the constructed tidal marsh and the lay-out of the marsh to obtain accretion.

The outcomes of the research can function as guidelines in the (re)design of constructed tidal marshes. The examination of multiple factors influencing accretion lead to measurements for the support of sedimentation. On the other hand, when accretion is not desired, the guidelines can be used to prevent sedimentation and support erosion.

Research on marsh development is already done in natural systems. It is found that in natural tidal marshes a large interaction exists between hydrodynamics, vegetation, and morphology. Creeks provide the marsh with water, nutrients, and sediments. If circumstances are mild, the landscape shapes into a heightened area where vegetation can develop, due to the water and nutrient supply from the creeks. The landscape development, in turn, influences the hydrodynamics. Over time, it is observed that vegetation succession and

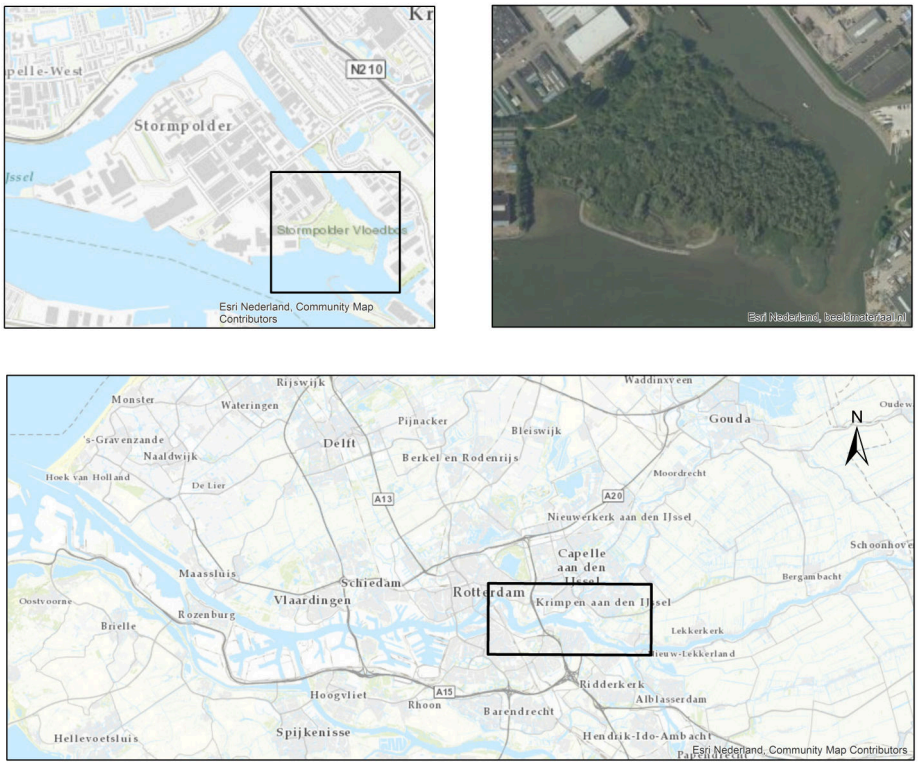

Figure 1.1: Location of Stormpoldervloedbos (SVB)

accretion naturally occur in marshes.

However, constructed tidal marshes differ from natural marshes and their evolution is still unknown. Several models exist to quantify sedimentation and to get insight into the marsh development. The modelling of sediment transport is a challenging task though, and it is often not mastered by designers and policy makers.

Therefore, this research makes expert knowledge accessible and comprehensible for designers. Besides, in this research more insight is given into the contribution of tidal forcing and marsh lay-out to the accretion of constructed tidal marshes.

1.1. Research Objective

The city of Rotterdam wishes to introduce multiple tidal marshes with different functions. Therefore, the city designated places along the Meuse in the order of ten hectares for the reintroduction of the ebb and flood principles. However, a lack of knowledge exists in the behaviour of constructed tidal marshes and comprehensible knowledge is not available. Therefore, policy makers and designers are not able to make well-advised decisions for the construction of new marshes on the designated places.

The aim of this research is to obtain more insight into the contribution of model configurations to accretion. Furthermore the purpose of the research is to develop guidelines to make expert knowledge comprehensible and available for the (re)design of constructed tidal marshes. As the research achieves the effect of external forcing on accretion, the method is applicable for multiple locations along the Rhine-Meuse estuary.

1.1.1. Research Questions

The research goal leads to the following research question:

What is the influence of tidal forcing and system lay-out on the accretion of a constructed tidal marsh?

1.1.2. Sub-questions

To be able to answer the research question, multiple sub-questions are defined:

1. What is the influence of tidal forcing components on bed shear stress and potential sedimentation?
2. What is the influence of marsh design parameters on bed shear stress and potential sedimentation?
3. What is the influence of system adjustments on bed shear stress and potential sedimentation?
4. Where in a constructed tidal marsh does accretion take place?

1.2. Research Approach

In Rotterdam, a constructed tidal marsh is already present, namely the Stormpoldervloedbos (SVB), as can be seen in Figure 1.1. More details of the SVB are given in Chapter 3. The constructed tidal marsh has a natural function on city-scale and used to be in morphodynamic equilibrium. During the research, the SVB is used as case study to test the effect of various model configurations.

Since the aim of the research is to gain more insight into the behaviour of constructed tidal marshes and to generate guidelines for designers, a 1D Sobek model is the model of choice. A 1D model is simplified representation of the system and therefore requires less calculation time and less expert knowledge.

Executing a Sobek 1D model of the constructed marsh obtains mean flow velocities in the constructed tidal marsh. The flow velocities obtained by a Sobek model are verified by some executed fieldwork, as discussed in Chapter 4. After that, the velocities are coupled to bed shear stresses and sediment transport relationships, obtained from previous research, stated in Chapter 2.

Water levels outside the SVB determine the incoming discharges into the SVB, and can be obtained from Rijkswaterstaat (RWS). Chapter 5 elaborates on data analysis in Python on water levels results in design water level time series. The design time series are used as model input to determine the influence of the different tidal forcing on the flow velocities and subsequently on bed shear stress and sedimentation.

Another model configuration, discussed in Chapter 5, is the design of the marsh. The design determines the volume of water entering the system every tidal cycle. Furthermore, the design influences the flow velocities. Therefore, multiple design parameters are examined to achieve the influence on accretion.

An observation from the SVB is that the original lay-out of the creek system has functioned well for many years, but accretion started after modifications of the system. Modelling three situations of the constructed tidal marsh achieves the influence of the system adjustments.

Besides the set-up of the model and the model configurations, Chapter 5 also elaborates on the model results. The comparison of sedimentation with the direction of resulting bed shear stress, determines whether a system is flood- or ebb-dominant and is a qualification of accretion. After that, Chapter 6 compares fieldwork with the model results, discusses the assumptions, and expands on the applicability of the research. Also some case-specific results are discussed here. Chapter 7 is the concluding chapter, where the research questions area answered and recommendations for further research are given.

2

Literature Study

This chapter provides an overview of the existing literature about natural tidal marshes. Here, the distinctions between salt marshes and freshwater marshes are explained as well. Moreover, the behaviour of a reference constructed marsh is compared to natural marshes.

2.1. Natural Tidal Marsh

Marshes are tidal areas located on the border of land and sea, in the presence of herbs and grasses. This area is predominantly salt or brackish and is flooded at least five times a year, with water containing a relatively high concentration of silt. Silt settling occurs when the hydrodynamic energy is low enough, resulting in accretion. The height of the marshes is between mean high water (MHW) and the highest water levels occurring in a year[4].

Due to low hydrodynamic energy, sediment deposits, and tidal flats heighten. The accretion of the surface gives salt-tolerant pioneer vegetation as *Salicornia sp.* and *Spartina sp.* an opportunity to establish in a saline/brackish environment. As a consequence of the heightening and vegetation development, interaction with other animal species establishes. Namely, the vegetation on the marshes provides shelter and food sources for insects, crustaceans and breeding birds, shaping unique areas with high ecological value. Positive feedback mechanisms exist between vegetation, sedimentation and ecology. As vegetation densifies, the flow velocity decreases, causing more sedimentation, and thus heightening of the surface. More vegetation species can develop on higher marshes as the conditions are less stressful, leading again to more animal species[22].

Whether the pioneer vegetation can develop, depends on their tolerance on flooding frequency and salinity. The pioneer zone of the marsh is a distinct area since only small numbers of animal species occur[6]. Vegetation succession drives the marsh towards a high-marsh with a low inundation frequency[18]. After that, the vegetation process is influenced by biotic processes instead of abiotic processes[22].

2.1.1. Formation of Marsh System

Six different stages in salt marshes are distinguished for the morphology, creek patterns and vegetation[22]. An elaboration on the different processes is given below.

Morphology and Creek Patterns

Since the tidal flat is below MHW, development from a tidal flat into a salt marsh is dependent on sedimentation. In this first stage, topography and vegetation determine the pattern of the creeks. When the topography is homogeneous, vegetation enables creek incision[22]. In the case of deep creeks, vegetation on banks has a more stabilizing function.

The marsh evolves to the second stage when vegetation starts to establish. Vegetation leads to lower flow velocities, and result in settling of sediment. During the second stage, the transition between a tidal flat and salt marsh is gradual. Water can enter the area and not many creeks are needed for drainage, resulting in a relatively simple creek system.

The feedback of vegetation on flow velocity is negative on the scale of a vegetation patch. When dense vegetation is present, flow velocity decreases, and sedimentation takes place. However, when two patches are situated next to each other, the flow of water is forced between these two patches. If this flow velocity is larger than a threshold value, incision of channels takes place. When this flow velocity is smaller than the threshold value, merging of the two patches is achieved[19].

The third stage can be observed when the frequency of flooding decreases due to the increase in elevation. In this stage, water and sediment supply no longer cross the edges of the salt marshes anymore, but only creeks carry the water and sediments[22]. The further development of the creeks system takes place by the incision of creeks in the landward direction. Although the creeks are deepening due to erosion, and the salt marshes in between heighten, the location of the creeks remains mainly the same.

Fully developed creeks and continued heightening characterized the fourth stage. During calm periods, sediments settle on the channel bed and sediment concentrations in the water column are low. Parts of the creeks are silting up since less water flows on the higher and more landward parts of the salt marsh.

However, when storm surges or spring tides occur, the flow velocities in these creeks increase. As a result, a considerable amount of sediment is brought in resuspension. The water flows over the channel edges to the marshes, and sediment settles. Flow velocities decrease directly on the channel edges due to vegetation, and larger particles deposit. The residual water flowing towards the land side only contains a fraction of the total sediment and consists of fine clayey particles, subjective to subsidence. As a result, salt marshes typically shape into an area where the seaside is relatively high, and the land side has the shape of a depression[22].

In salt marshes, small ponds exist which are not connected to the creek system. They permanently contain water, except when strong evaporation occurs during summer. The disconnection is caused by the underdevelopment of the creek system and the difference in level between the banks and the depressions. The disconnected ponds are found in the fourth and fifth stage[22].

When the edge of the salt marsh is becoming high and steep, erosion takes place, and a cliff is formed in the fifth stage. Due to erosion, the cliff moves landwards in the sixth stage. A secondary pioneer zone can develop together with a new creek system. The secondary elements will be connected to the creeks of the existing salt marsh since the ebb flow is already concentrated at the exit[22].

Sedimentation rates in a Dutch marsh system, the Wadden Sea, are found to be around 0.5-1 cm a year. Rates are dependent on whether the salt marsh is present on land or on islands. On islands, the sedimentation rate is usually lower. Furthermore, the sedimentation rate is influenced by seasonality. During winter, when storms are present, more sediment is deposited. As time passes by, roots and consolidation strengthen the soil against erosion[4]. It is found that sedimentation is the dominant process over erosion, and salt marshes are growing over time[4]. An exception is an old salt marsh, where consolidation is the dominant process.

Vegetation

Vegetation influences the interaction between morphology and hydrodynamics. As plants dampen waves and flow velocities, silt trapping is enhanced. The roots of the plants hold the nutritious silt and establish further[4], leading to a positive feedback mechanism. Namely, silt trapping and vegetation development heighten the area. As a result, new plants can develop since the circumstances are less stressful: some plants are emerged, and water does not block the light anymore, enabling photosynthesis. This process continues until a situation is reached where the area is only flooded a few times a year, which happens after about 100 years[8].

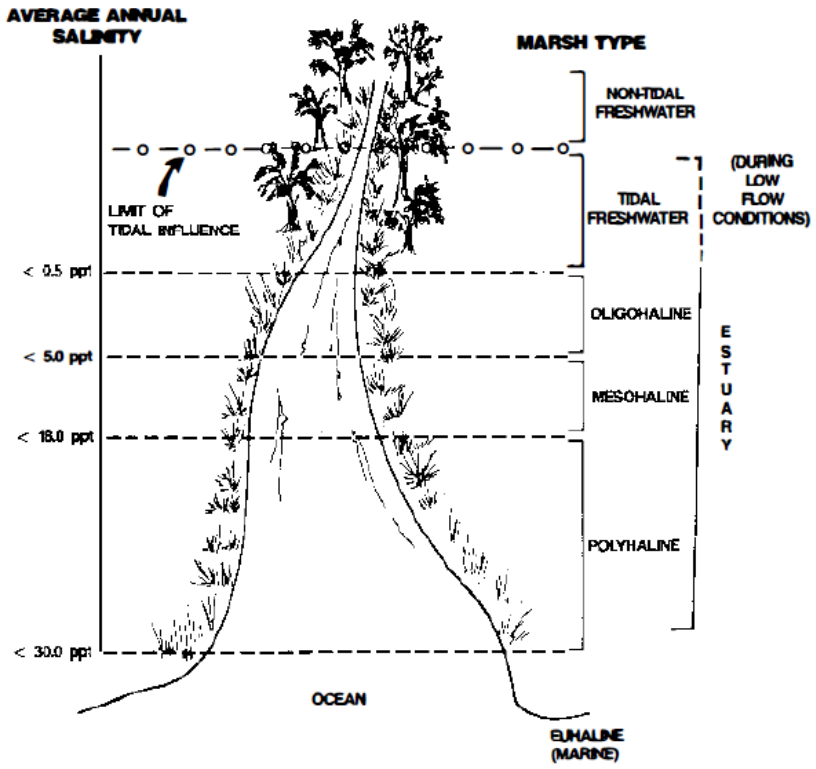

Figure 2.1: The relationship between marsh type and average annual salinity[9].

2.1.2. Variation in Marsh Systems

The development of intertidal areas depends on environmental and hydrologic parameters along the estuary. Close to the ocean, salt marshes are found. When moving in the upstream direction, to the upper boundary, tidal freshwater marshes are present, also depicted in Figure 2.1. This section discusses the variation in salinity, sediments and vegetation along the estuary.

Salinity

Salt marshes are the parts of the estuary where the salinity lies in the range of 18.0-35.0 parts per thousand (ppt). For tidal freshwater marshes, the salinity is below 0.5 ppt. In between these two, the oligohaline and mesohaline exist. However, due to variation in discharge, locations can have seasonal variations on salinity[9]. A summary of the comparison of the physical characteristics between salt marshes and tidal freshwater marshes is given in Figure 2.3.

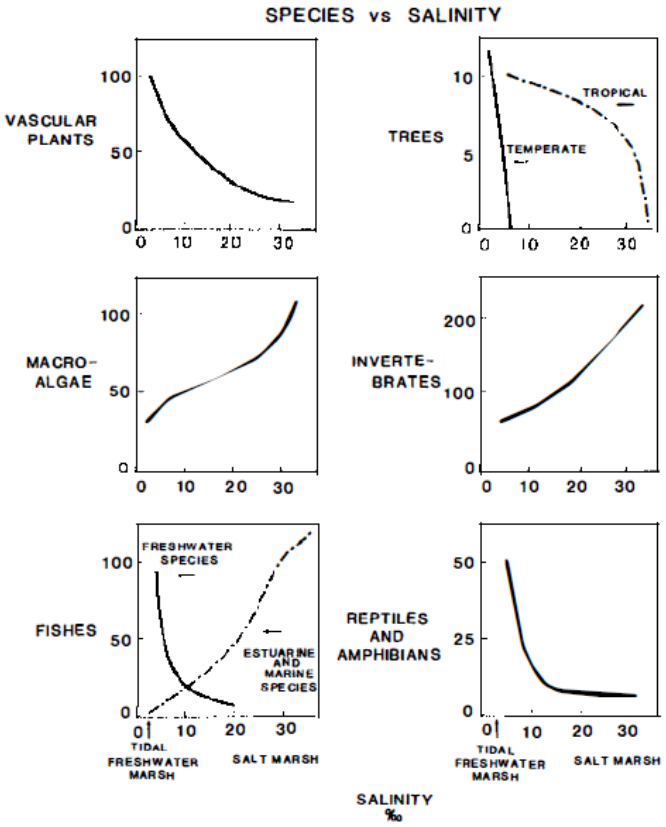

Figure 2.2: Hypothetical trends in total species numbers versus mean annual salinity along the estuarine gradient[9].

	Tidal freshwater marsh	Salt marsh
Location	Head of the estuary (above the oligohaline zone)	Mid and lower estuary
Geographical distribution	Worldwide, usually associated with rivers	Worldwide, not always associated with rivers
Salinity	Annual average below 0.5 ppt	Annual average between 18.0 and 35.0 ppt
Tidal range	Ocean-derived lunar tide, often greater amplitude than nearby salt marshes	Ocean-derived lunar tide
Sediments	Silt-clay, high organic content, low-moderate root and peat content	More sand, lower organic content, higher peat and root content
Sediment erodability	High erodability (particularly in the low marsh)	Generally lower erodability
Streambank morphology	Low gradient, little undercutting	Steeper gradient, more undercutting
Stream channel morphology	Low sinuosity	Moderate to high sinuosity
Dissolved sulfur	Trace (approximately 1 ppm)	Very high (approximately 2500 ppm)
Sediment redox potential	Moderate to strongly reducing (multiple redox pairs)	Strongly reducing (sulfur redox pairs most important)
Reduced iron-sulfur compounds	Rare or absent	Plentiful
Dissolved and particulate organic carbon	High concentrations	Moderate to low concentrations

Figure 2.3: Comparison of physical characteristics between tidal freshwater marshes and salt marshes[9]

Sediment

Sediments vary with respect to their location in the estuary. Sediments in the tidal freshwater estuary are originating from materials upstream and terrestrial sources. These sediments are, for example, clay, silt and fine organic matter. In the freshwater marsh, only small amounts of sand are present. When a tidal freshwater marsh develops naturally, they are usually present close to the section of the estuary where the highest concentrations of sediments of fine, river-borne materials are present[9].

The sediment origin of freshwater marshes is in contrast with the sediment present in the salt marshes. In salt marshes, more fine sands and clays from marine sources are distinguished as a result of tidal pumping. Often, salt marshes have a lower organic carbon content, compared to tidal freshwater marshes. Freshwater marshes have a more significant annual input of riverine and terrestrial carbon, potentially leading to the higher carbon content. The organic carbon in tidal freshwater is a factor two to three higher than further down the estuary at higher salinities.

Vegetation

Vascular plants are plants which use xylem for conducting water and minerals throughout the plant. Many factors influence the distribution of these plants along the estuary. Salinity is the dominant factor, though, inundation time, sulphide concentrations, and substrate composition are important factors as well. As can be seen in Figure 2.4, totally different plant species are present at both ends of the salinity spectrum. In the tidal freshwater marshes, vascular plants, restricted to fresh water with low salinities, are present. These vegetation properties are in contrast with salt marshes where plant species with specialized physiological adaptations are present, tolerating estuarine and marine conditions.

Next, the diversity in regularly flooded parts of the marshes differs substantially. In the salt marshes, only a few different species can be distinguished, while in the freshwater marsh much diversity is present. Due to the saline stress conditions, species on salt marshes are expected not to exceed ten different species in the regularly flooded part. The amount of species increases at the marsh area, which is flooded only monthly. Single species, such as *Spartina* mostly dominate the intertidal low salt marsh. Figure 2.2 shows these relationships between species and salinity as well.

	Tidal freshwater marsh	Salt marsh
Community composition	Freshwater species	Marine and estuarine species
Species diversity	High species diversity, low dominance by single species	Low species diversity, high dominance by single species
Intertidal distribution	Entire intertidal zone	Upper two thirds of intertidal zone
Zonation and habitat overlap	Zonation present, but not always distinct; much habitat overlap	Pronounced zonation; little habitat overlap
Seasonal sequence of dominant species	Pronounced	Absent or minor
Life history strategies	Reproduction both sexual and asexual, seed banks very important	Reproduction principally asexual (through dispersal of pieces of rhizomes), seed dispersal secondary, seed banks not as important
Tree distribution	Present at least to latitude 45°	Disappear north of latitude 30°

Figure 2.4: Comparison of vascular plant community structure between tidal freshwater marshes and salt marshes[9].

In salt marshes, vascular plants usually cover the upper two-third of the intertidal zone of the marsh. The lower one third usually contains only bare mud and micro and macro algae. Bare soil is presumed due to the

stress of exposure to salt water in combination with the duration of flooding and flooding frequency. Exceptions can occur when the tidal amplitude is only small. Here, species as *Spartina* can grow until mean low tide. Low flora and fauna content is in contrast with the tidal freshwater marsh, where vascular plants can grow on the entire intertidal zone when slope, exposure and sediment characteristics are suitable. It is assumed that vegetation development can take place due to the lack of salt stress and the presence of floating-leaved vascular plant species.

In tidal freshwater marshes, seasonality in vegetation peaks is present, since annual and perennial species are combined. Mangroves are trees which can exist on salt marshes when the temperature is above freezing point. When trees are present at higher latitudes and thus colder regions, salinity should be absent, or trees experience increased mortality.

Thus on salt marshes, *Spartina* is the dominant species. When moving to the tidal freshwater marshes, no real dominant species can be distinguished, and a large, diverse group of broad-leafed plants, rushes, shrubs and herbaceous plants are present[10].

2.2. Constructed Tidal Marsh

A constructed marsh is different from a natural tidal marsh since constructions in the outer dike define the volume, timing and sediment concentration of the incoming water. A commonly used structure which enables tide to enter a constructed tidal marsh is the controlled reduced tide (CRT), see Figure 2.5. This construction consists of two culverts or sluices in the embankment, where the tide can propagate through. During high tide, water flows through the higher inlet structure and during low tide, water flows through the lower outlet structure. Due to the construction, tidal water levels are significantly lowered[18]. Furthermore, the inundation time and height depends on the dimensions of the structure[3].

A CRT results in a flattened tidal curve and thus sharply reduced water dynamics[3]. Consequently, sedimentation settling rates are larger compared to a natural marsh. In contrast, for a CRT, the erosion rates are higher since the filling of the area is slow and the emptying is quick[3]. However, in a constructed marsh, the inundation frequency is not a function of height, as is the case for a natural marsh, but is a function of the inlet system.

2.2.1. Lippenbroek

Not many research is yet done in the SVB, resulting in the absence of detailed observations of the elevation of the marsh and the development over time. Therefore, a similar constructed marsh area is considered, namely Lippenbroek. Lippenbroek is a restored embanked land in the Scheldt estuary in Belgium, where a controlled reduced tide (CRT) is allowed. The size of the area is 8 ha, with a reduced tidal range of 1.3 m. For the SVB, the tidal range is around 1.5 m, and the area is 9 ha. Lippenbroek is a freshwater marsh with an average suspended sediment concentration (SSC) of 0.03 to 0.06 gL^{-1}. The CRT consists of a higher culvert, through water enters during high tide and a low sluice system, where water exits during low tide.

During the research on Lippenbroek, the elevation change of the constructed marsh is examined and compared to the elevation change of a natural marsh[18]. It became clear that over a period of four years both marshes respond similarly. The variations in elevation change on a spatial and temporal scale are related to variation in inundation depth, for both a constructed and a natural tidal marsh. However, when the constructed marsh and the natural marsh are compared over a more extended time period, where the mean high water level (MHWL) remains constant, a different conclusion can be drawn. For the natural marsh, an increase in elevation results in a decrease in inundation depth and therefore the elevation rate decreases.

In contrast, the incoming water of constructed marsh is a function of the inlet structure and is constant. Since the elevation of the low areas in the constructed marsh becomes higher, water is redistributed over the area. This results in a decrease in water level for the low elevated areas and an increase in water level for the highly elevated areas. Consequently, the elevation rate will increase for the higher elevated areas and decrease for the lower elevated areas[18].

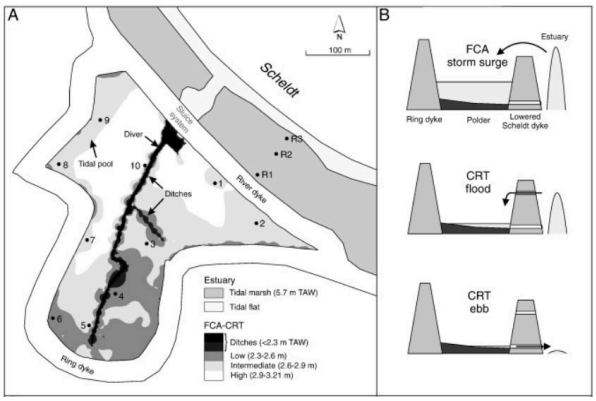

Figure 2.5: Layout of Controlled Reduced Tide[19].

2.3. Theoretical Roughness Coefficient

A challenging task is determining the roughness coefficient since it means estimating the flow resistance in a given channel, which consists of many factors[2]. To get more insight into the determination of Manning's coefficient, the main contributions of the coefficient, leading to energy loss, are discussed below.

Channel-surface Roughness The channel surface roughness is a factor determined by the size, shape, and positioning of the individual grains in the wetted perimeter, and is one of the significant factors affecting Manning's coefficient. Commonly, fine grains have a low n-value, and coarse grains have a high n-value. This difference is the result of the smaller frictional effect for fine material, such as sand, clay, loam, and silt compared to the frictional effect of coarse grains[15]. Next, the n-value for fine material is less dependent on the flow stage, resulting in a constant value for n during both low flows and high flows. The value of n for coarse material, such as gravel or boulders, is dependent on the flow stage. Namely, at high flow stages, the energy is partly used for the rolling of boulders and gravel and results in a higher n-value.

Channel Irregularity Channel irregularity is present when the channel cross-sections does not change smoothly. In natural channels, this is usually the case when sand bars, sand waves, ridges, depressions, and holes and humps are present on the channel bed. Furthermore, obstructions increase the value of n as well.

Cross-section Generally speaking, the n-value of channels decreases when the flow stage and discharge increase, as a result of the less exposed bottom irregularities. However, when the banks are vegetated and rough at high stages, the roughness coefficient is potentially large. When channels are overflowing their banks due to high discharges, a part of the water flows over the floodplain, where the n-value is commonly higher. Next, suspended material and bed load cause an increment of the channel roughness and head loss.

Vegetation Vegetation slows down the flow in channels. The extent of this retarding effect depends on the height, density, distribution, and type of vegetation, and is particularly important in small drainage channels. During summer, vegetations growth results in higher n-values. With a larger depth, the energy loss is less influenced by vegetation as the flow bends over the vegetation. Furthermore, when a higher velocity is present, vegetation is flattened, resulting in lower values of n.

Channel Meandering Due to the meandering of channels, the roughness coefficient increases. However, when the flow velocities are low, the increase in roughness is negligible.

Considering all the above factors, the value of n can be computed by:

$$n = (n_0 + n_1 + n_2 + n_3 + n_4)m_5$$

Channel conditions		Values	
Material involved	Earth	n_0	0.020
	Rock cut		0.025
	Fine gravel		0.024
	Coarse gravel		0.028
Degree of irregularity	Smooth	n_1	0.000
	Minor		0.005
	Moderate		0.010
	Severe		0.020
Variations of channel cross-section	Gradual	n_2	0.000
	Alternating occasionally		0.005
	Alternating frequently		0.010-0.015
Relative effect of obstructions	Negligable	n_3	0.000
	Minor		0.010-0.015
	Appreciable		0.020-0.030
	Severe		0.040-0.060
Vegetation	Low	n_4	0.005-0.010
	Medium		0.010-0.025
	High		0.025-0.050
	Very high		0.050-0.100
Degree of meandering	Minor	m_5	1.000
	Appreciable		1.150
	Severe		1.300

Table 2.1: Values for the major factors contributing to the roughness coefficient[15].

Where n_0 is the channel-surface roughness, n_1 is the degree of irregularity, n_2 is the variation in channel cross-section, n_3 is the relative effect of obstruction, n_4 is the vegetation influence and m_5 is the degree of meandering, Table 2.1 lists the value ranges of the n and m-components.

2.4. Tide

Tide is defined as the periodic water movement with a phase and amplitude determined by the gravitational forces originating from the Earth-Sun system and the Moon-Earth system. The forces of two bodies attracting each other depend on their mass and distance. The attraction force is calculated by:

$$F = G\frac{m_1 m_1}{r^2}, \tag{2.1}$$

where G is the universal gravitational constant.

When two masses are close enough, they are attracted to each other, as happens in the Sun-Earth and Earth-Moon system as well. Due to the attractional force, the masses rotate around their common point of gravity. As the sun is much heavier than the earth, the rotational point of the sun-earth system lies within the sun. The rotational centre of the earth-moon system lies in the earth for the same reason.

The magnitude of the attractional force is proportional to the mass and the inverse distance squared and can be calculated through Equation 2.1.

However, this force is only applied to the earth when it is considered to be a point mass. Only looking at the earth itself, a difference in force at the surface is observed. For the point closest to the attracting mass (Sun or Moon), this force is larger than for the point in the centre of the earth. The difference in force is called differential pull and is calculated by:

$$\Delta a_a = a_{s,nearside} - a_s \tag{2.2}$$

For the sun this gives $\Delta a_s = 0.515 \times 10^{-7}$g. A similarly calculation gives the differential pull for the Moon: $\Delta a_s = 1.13 \times 10^{-7}$g, where g is the gravitational constant of the earth.

Although the mass of the moon is much smaller than the mass of the sun, the differential pull accounts for 69%, due to the smaller distance of the moon to the earth compared to the sun.

The differential pull has a perpendicular and a tangential component. The perpendicular component is negligible when it is compared to the balancing force of the earth, namely its own attraction g. However, the gravity forces of the earth do not balance the tangential component. As a result, water shifts to the side of the earth facing the sun, and to the opposite side. The bulges of water are what we know as the tide, and the water level gradient balances the tangential force.

In the Netherlands, a semi-diurnal tide is observed since the earth rotates along its own axis. Therefore, it passes the two bulges every day. The period of the solar tide is exactly 12h. Since the moon also rotates around the earth, the period of the lunar tide is 12 hours and 25 minutes.

2.4.1. Tidal Asymmetry

A tidal curve for water level and flow velocity in an estuary does not follow a sinusoidal curve, due to the effects of bottom friction and the amplitude variation, as a function of the estuary shape. Bottom friction reduces the tidal amplitude, and a narrower estuary shape leads to an increase in amplitude.

Flood and ebb dominance

Larger friction reduces the tide and establishes a phase difference between horizontal and vertical tide. The influence of friction is higher during ebb than during flood since there is a larger interaction with the bottom during low tides. In a tidal river, where the river flow velocity and tidal flow velocity are of the same order, the ebb flow velocity, and thus the friction, is much larger and slows down the tide even more. When friction can be neglected, the vertical and horizontal tide are in phase. Due to friction, the horizontal tide leads the vertical tide up to a phase difference of $\pi/2$.

Wave celerity, c_w is a function of depth h:

$$c_w = \sqrt{gh} \tag{2.3}$$

When the water during ebb and flood use the same channels and no bank overflow occurs, the wave celerity during flood is higher than during ebb: $c_{flood} = \sqrt{g(\overline{h}+A)}$ and $c_{ebb} = \sqrt{g(\overline{h}-A)}$, where A is the amplitude. A velocity difference in ebb and flood leads to wave-skewness (asymmetry about the horizontal). As the net discharge over one tidal cycle is zero when no non-tidal forces as river discharge and wind are present, the rising period must be shorter than the falling period.

If flow velocities are higher during flood than during ebb, the system is flood-dominant. Shallow channels and a large ratio of $\frac{A}{h}$ enhance flood dominance. The system is ebb-dominant when the ebb velocities are higher than flood velocities and occurs when intertidal flats and deep main channels are present[14]. Flooding of the intertidal flats during high waters results in low water levels, and consequently in a low wave celerity. In contrast, during ebb, the water remains in the main channel, resulting in larger depths, thus higher wave celerity. In general, the mean water level of the flood period is larger than the mean water level of the ebb period. As the net discharge is zero over the tidal cycle, the flood velocities must be lower when the flood duration is the same as the ebb duration. Ebb-dominance is also present in the case of river flows since the river flow leads to an increment of the seaward directed flow velocities.

Besides skewness of the horizontal tide, saw-tooth asymmetry (asymmetry about the vertical) develops as well due to continuity. In a short basin, where the length is much smaller than a quarter of the wavelength, saw-tooth asymmetry is dominant. The water levels in the basin do not vary along the channel axis and h and u are out of phase, leading the lowest flow velocities at the absolute maximum water levels. Slack water is the moment flow reverses and occurs during high water, where $dh/dt = 0$. At this point, the rate of change of the velocity du/dt is a function of the landward basin area, A_b, and the channel cross-section, A_s defined by:

$$u(x,t) = \frac{\partial h}{\partial t}\frac{A_b}{A_s} \tag{2.4}$$

The formula for u is obtained by the general continuity equation:

$$-\frac{\partial Q}{\partial x} = b_s \frac{\partial h}{\partial t}, \tag{2.5}$$

where b_s is the channel width. Integrating this formula over the length of the channel gives:

$$Q(t,x) = \int_x^{L_b} b_s \frac{\partial h}{\partial t} dx, \tag{2.6}$$

Where L_b is the basin length. The water levels in the basin do not vary along the channel axis, thus $\partial h/\partial x = 0$, and gives:

$$Q(t,x) = A_s u = \frac{\partial h}{\partial t}\int_x^{L_b} b_s dx = \frac{\partial h}{\partial t} A_b \tag{2.7}$$

Rewriting this equation leads to Equation 2.4.

When a basin has shallow channels and small intertidal storage, A_s is more extensive during HW than during LW, leading to a small $\partial u/\partial t$. A small $\partial u/\partial t$ results in a longer HWS duration. In contrast, when the basin has a large intertidal storage area and deep channels, A_b is more abundant during HW than during LW, and leads to a large $\partial u/\partial t$. A large $\partial u/\partial t$ results in a shorter HWS compared to the LWS duration.

2.4.2. Overtides

The summation of multiple higher harmonics can describe the asymmetry of the tide. These higher harmonics are tidal periods generated from the non-linear effects in tidal basins. The higher harmonics have periods which are fractions of the basic astronomical constituents, and originate from the attraction forces of earth, moon, and sun. The higher harmonics are also called overtides. Whether asymmetry of the velocity and elevation develops around the horizontal or vertical axis, depends on the phase relationship between the tidal constituents.

Different wave celerities for high tide and low tide induce non-linearity of tidal propagation as discussed above. M4 and S4 are higher harmonics produced from M2 and S2, respectively. The frequency of M4 and S4

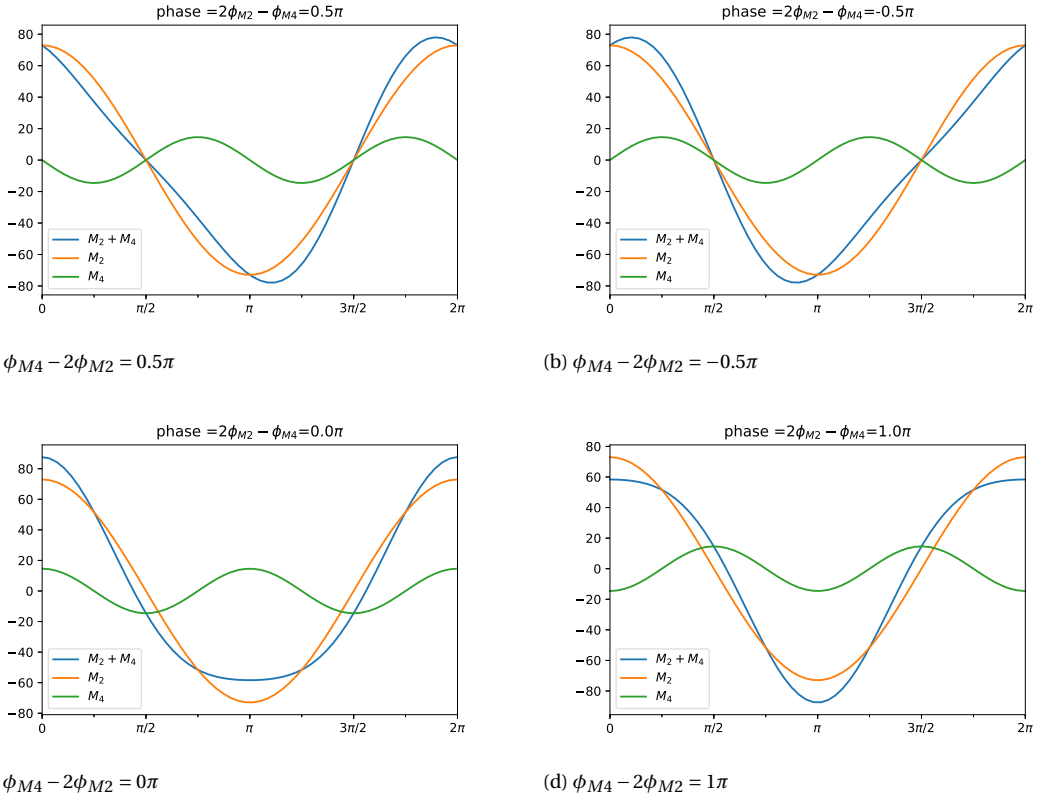

(a) $\phi_{M4} - 2\phi_{M2} = 0.5\pi$

(b) $\phi_{M4} - 2\phi_{M2} = -0.5\pi$

(c) $\phi_{M4} - 2\phi_{M2} = 0\pi$

(d) $\phi_{M4} - 2\phi_{M2} = 1\pi$

Figure 2.6: Water level and flow velocities for multiple phase lags.

is double the frequency of M2 and S2. Furthermore, due to friction, M6 and S6 are produced from M2 and S2, with the frequency of 3 times the frequency of M2 and S2.

The summation of the separate constituents gives:

$$h(t) = A_{M2}cos(\omega_{M2}t - \phi_{M2}) + A_{M4}cos(\omega_{M4}t - \phi_{M4}), \tag{2.8}$$

where h is the water level, A is the amplitude, $\omega = 2\pi \times f$ is the angular frequency, and ϕ is the phase. As $\omega M4 = 2\omega_{M2}$ and $t' = t - \phi_{M2}/\omega_{M2}$ the equation leads to:

$$h(t) = A_{M2}cos(\omega_{M2}t') + A_{M4}cos(2\omega_{M2}t' - (\phi_{M4} - 2\phi_{M2})), \tag{2.9}$$

where $\phi_{M4} - 2\phi_{M2}$ is the phase lag between M2 and M4. When the phase lag is 0, the wave is positively skewed. When the phase lag is $\pm\pi$, the wave is negatively skewed. Asymmetry around the vertical axis is present for a phase lag of $\pm\frac{1}{2}\pi$, where the falling period is unequal to the rising period. The shape of the velocity and water level can be seen in Figure 2.6

2.5. Sediment Transport

Sediment can be transported when the occurring bed shear stress exceeds the critical bed shear stress. When the sediment transport in the water column is larger than the transport capacity, sediment settles. Due to the difference in timing and location of shear velocity, sediment transport is a stochastic process.

A Rouse profile estimates the distribution of the sediment over the water column. For really fine sediment, the distribution over the water column can be assumed to be uniform, and the sediment is in suspension. However, when heavier particles are present, the sediment concentration is higher close to the bed. The

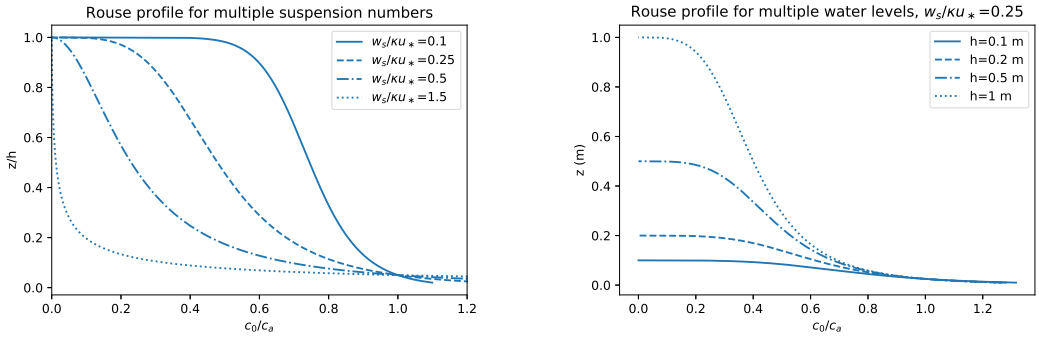

(a) Rouse profile for multiple suspension numbers $Z = w_s/\kappa u*$.

(b) Rouse profile for multiple water levels.

Figure 2.7: Rouse profile for varying suspension number and water level. In accordance with Equation 2.10.

Rouse profile is defined as follow:

$$\frac{c}{c_a} = \left(\frac{h-z}{z}\frac{a}{h-a}\right)^{w_s/\kappa u*}, \tag{2.10}$$

Where h is the water depth , a is the reference level, z the height above the bed, c_a is the reference concentration, w_s the particle fall velocity, $u*$ the bed shear velocity and κ the Von Karman constant[17].

The importance of suspended transport is determined by the factor $Z = w_s/\kappa u*$. If $Z = 0.1$ the sediment distribution is almost uniform over the water column. For $Z = 1$, suspended sediment is present up to the water surface, for $Z = 2$ suspended sediment is present up to half of the water depth, and for $Z = 5$ suspended sediment is present in the near-bed layer[17]. In Figure 2.7, the relation between c_0/c_a and the suspension number, and the relation between c_0/c_a and the water depth is shown.

Bedload transport in unsteady flow responds directly to the hydraulic conditions and therefore can be modelled with a formula. A measure for this response is the bed shear stress compared to the critical bed shear stress. Direct response is not the case for suspended load transport though. Convection and diffusion processes in the vertical determine the suspended load as it takes time to for particles to move in the z-direction[17].

The sediment concentration continuously adapts until it reaches the equilibrium sediment concentration. When the transport is higher than the transport capacity, sedimentation takes place. Erosion takes place when the transport is lower than the transport capacity. The transport capacity relates to u^2, and when $u > u_{crit}$ the transport capacity becomes larger than zero.

The sediment moving along with the flow is determined by:

$$\frac{\partial c}{\partial t} = \frac{c_e - c}{T_a}, \tag{2.11}$$

where c is the depth average sediment concentration, T_a is the adaptation time, and c_e is the equilibrium concentration. c_e Is dependent on the instantaneous velocity and is calculated by[14]:

$$c_{eq} \approx \beta |u|^{n-1}, \tag{2.12}$$

where n=3 and β a constant.

If the flow velocity increases and is larger than u_{crit}, the equilibrium concentration increases, see Figure 2.8. As long as the flow accelerates, the transport capacity is larger than the sediment concentration, and particle transportation is in upward direction[17]. It takes time for the sediment concentration to adapt to the value of the transport capacity. The time between the maximum flow velocity and the moment when the sediment concentration and the transport capacity are equal is called the time lag period[17].
When the flow velocity decreases, the equilibrium concentration decreases too. If the concentration is higher

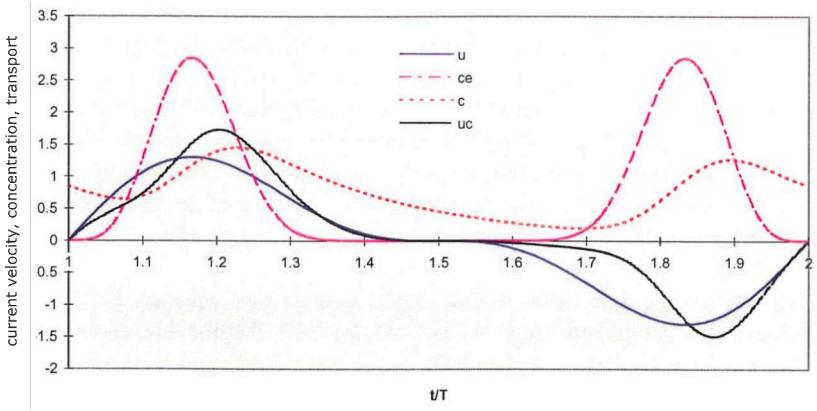

Figure 2.8: The time lag effects for suspended sediment transport. The HWS is longer than the LWS, leading to more sedimentation. u is the flow velocity, c_e is the equilibrium concentration, c is the transport and uc the product of u and c[21].

than the equilibrium concentration, sedimentation takes place. Figure 2.8 shows that the sediment concentration is larger than the transport capacity before they take on the same value. The time between the moment where the transport capacity is zero, and the start of the erosion (when the transport is smaller than the transport capacity) is the time lag during low water.

3

Area Description

In this chapter the case study 'Stormpoldervloedbos' is described. The location of the SVB and the sediment availability are discussed. Furthermore, this chapter elabores the changes in marsh lay-out over time, and on the proposed design.

3.1. Description of Stormpoldervloedbos

The Stormpoldervloedbos (SVB) is a constructed freshwater tidal marsh originating from 1993. The SVB covers an area of around 9 hectares, and is vegetated. The vegetation accommodates multiple butterfly and bird species. Furthermore, a surveyor makes sure the marsh is well functioning by executing maintenance.

3.1.1. Location

The marsh is situated between the Hollandsche IJssel and Lek, as can be seen in Figure 3.1. The Hollandsche IJssel and Lek are connected by the Sliksloot, with a branch discharging into the SVB. The incoming discharge of the SVB goes through structures connecting the branch with the SVB, see Figure 3.1 and Appendix B.

The SVB is also connected directly to the Sliksloot by weirs in the outer dike, and water levels determine the incoming discharge. The Sliksloot lies close to a measuring station of Rijkswaterstaat. This station records water level time series with a frequency of 10 minutes. It is assumed that the water level in the Sliksloot follows the water level of measuring station Krimpen aan den IJssel. The measuring Station Krimpen aan den IJssel is indicated by a red dot in Figure 3.1.

3.1.2. Sediment

The sediment concentration in the Sliksloot determines the amount of sediment entering the SVB. The water level difference between the Hollandsche IJssel and the Lek controls sediment transport in the Sliksloot, as it determines the bed shear stress and thus sediment transport. Figure 3.2 shows the output of two different Delft3D models executed by the Port of Rotterdam. Different forcing is present in the simulations.
Figure 3.2a shows a simulation called Rotterdam swim with a mean river discharge of 2300 m^3/s and a wind velocity of 7 m/s directing from the south west. The second simulation is called Breeddiep and has a discharge of 4000 m^3/s and a wind velocity of 15 m/s, the results are shown in Figure 3.2b. These Figures show a considerably lower velocity in the Sliksloot, compared to the velocity in the Lek. It can be concluded that the head difference between the Hollandsche IJssel and the Lek determines the flow in the Sliksloot. Although river discharge and wind set-up is high, the velocity in the Sliksloot does not increase. The low flow velocities in the Sliksloot lead to settling of the heavier particles, while the particles with a small settling velocity are still in suspension. Fine particles present in the SVB is also confirmed by visual inspection, as shown in Figure 3.3. Figure 3.3b shows the deposited sediment from the river. It can be seen that mainly sandy sediment is present. In contrast, Figures 3.3c and 3.3d show that inside the SVB finer particles are present. The fine particles are in suspension in the entire water column.

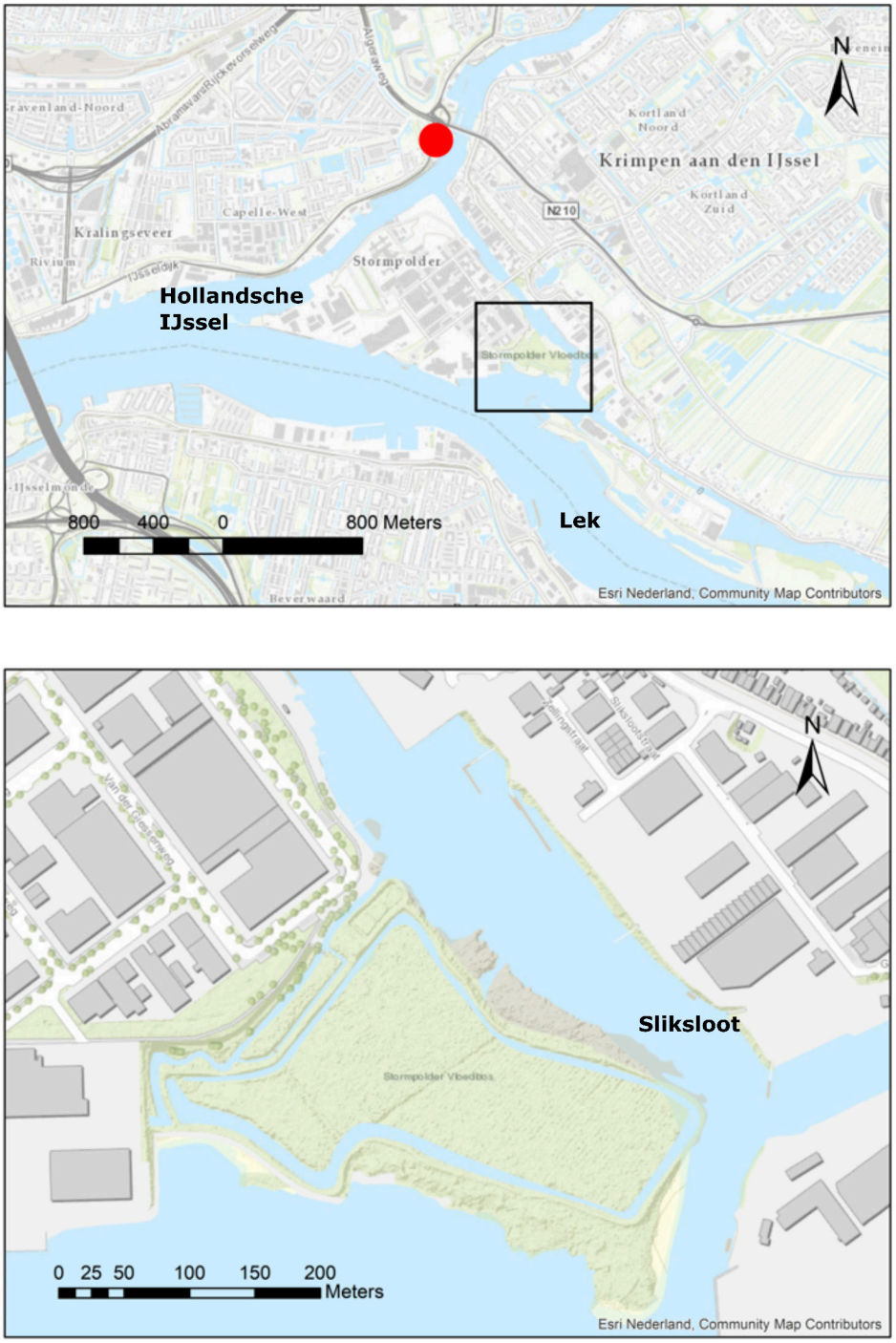

Figure 3.1: In the upper Figure the Hollandsche IJssel on the north and the Lek on the south are depicted. The Sliksloot connects the two rivers. A branch of the Sliksloot flows to the inlet of the SVB. The red dot identifies the RWS measurement location.

Another influencing factor controlling sediment concentrations are the ships mooring in the small port connected to the Sliksloot. Ships stir up sediments due to high shear stresses and can increase the sediment concentration in the water.

3.2. Area Configuration

After some modifications in the Stormpoldervloedbos, accretion and vegetation succession is observed by the designer of the area. The aim for the SVB is a situation where the tide can be experienced in a natural tidal marsh, in the presence of tidal channels, and only little maintenance is required. This section elaborates on three different configurations of the area: the original situation (situation 1), the current situation with the adaptations incorporated (situation 2), and the proposed situation (situation 3).

3.2.1. Original Situation

Situation 1 represents the design of the SVB from 1993. The cross-sections in situation 1 originate from the designer of the SVB and are depicted in Figures 3.4 and 3.5. For water levels around 1.19 m, water overflows banks of the cross-section into the inner area of the SVB. The Figures of the cross-sections clearly show deeper, and somewhat broader cross-sections closer to the SVB inlet. From the inlet towards Weir 1, the elevations of the cross-sections are increasing. The largest and deepest cross-section is the supply channel ab. Furthermore, cross-section bc is much deeper than cross-section bi and water is expected to flow mainly towards the East side during a flood. The locations of the cross-sections are shown in Figure 3.6

In the initial design, only three weirs and four inlet culverts are present, see Table 3.1 and Figure 3.6. The four culverts function as inlet structure and have a round shape with a diameter of 1 m. Table 3.1 lists the structures and their dimensions. In Sobek, the four culverts and the weir first discharge into a basin, from where the flow continues to the East and West side of the SVB.

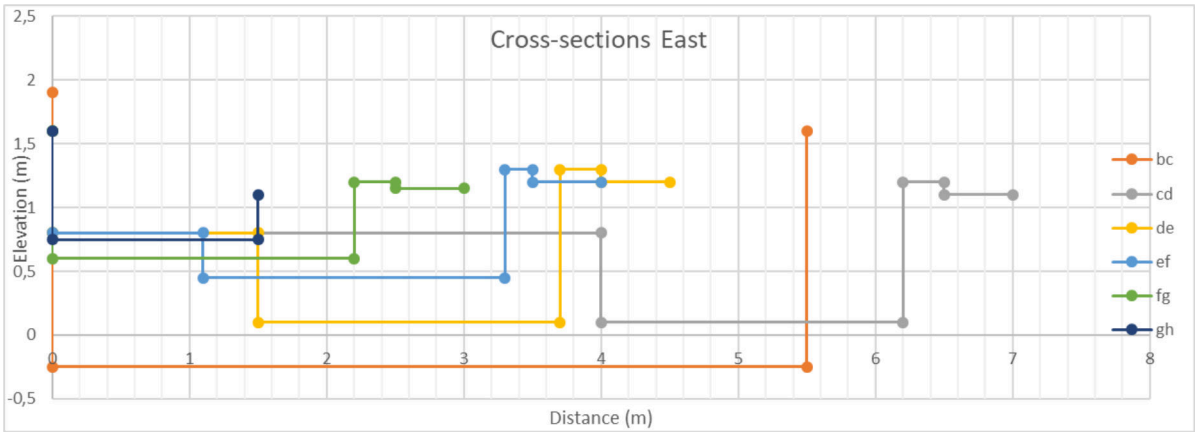

Figure 3.4: The cross-sections present in the right part of the SVB. Locations of the sections can be found in Figure 3.6

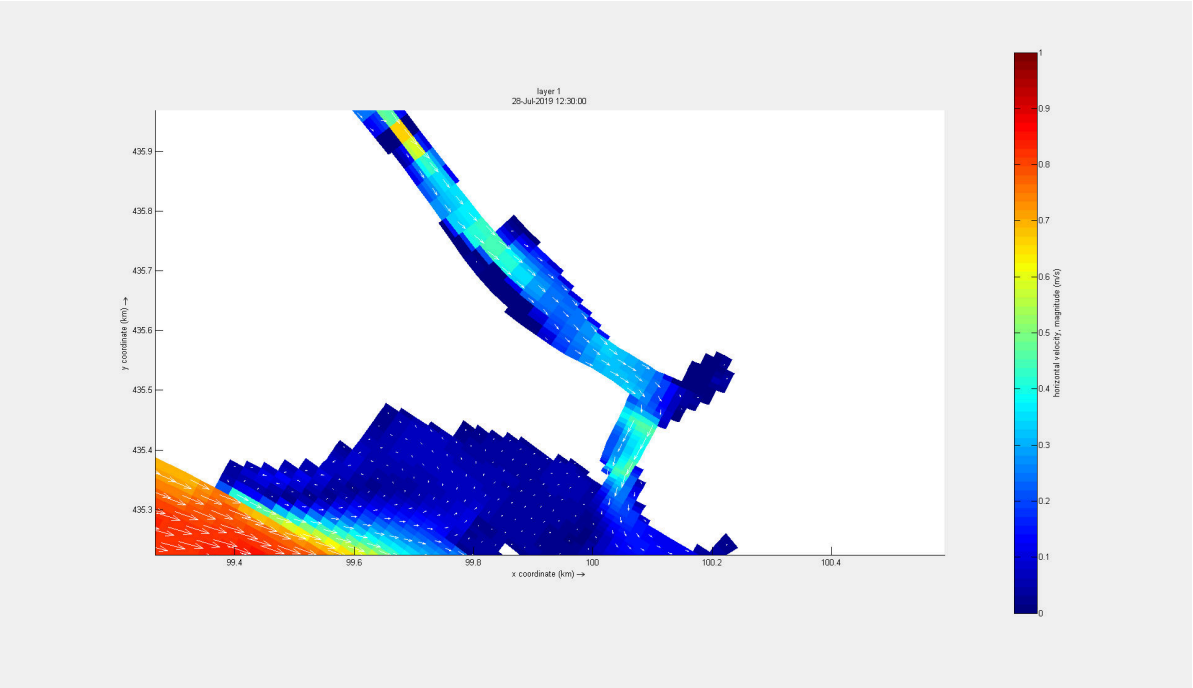

(a) Maximum velocities for the simulation of Rotterdam swim. The river discharge is 2300 m^3/s and the wind velocity is7 m/s.

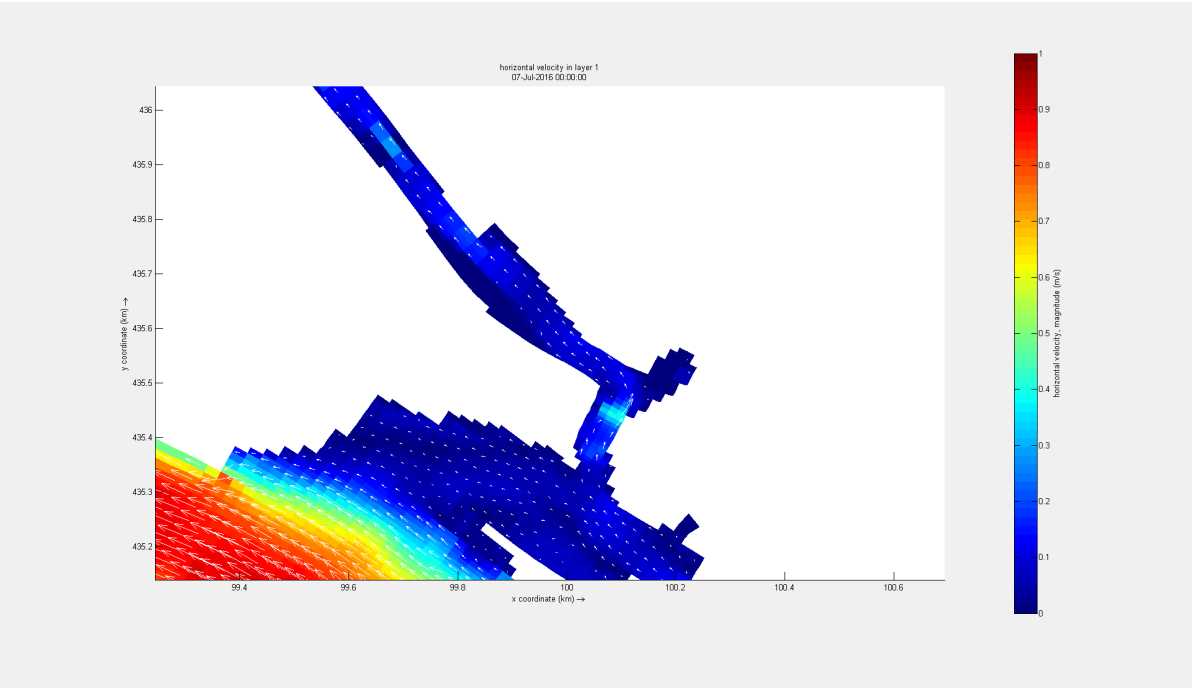

(b) Maximum velocities for the simulation of Breediep. The river discharge is 4000 m^3/s and the wind velocity is 15 m/s.

Figure 3.2: Maximum flow velocities in the Sliksloot for two simulations of the Port of Rotterdam. It is shown in the Figures, the velocity in the Sliksloot is not directly dependent on river discharge and wind set-up.

(a) View from the SVB on the Lek.

(b) Deposited sediment outside the SVB.

(c) Water in the creeks of the SVB containing fine sediment.

(d) Deposited sediment inside the SVB.

Figure 3.3: Visual inspection of sediment inside and outside the SVB.

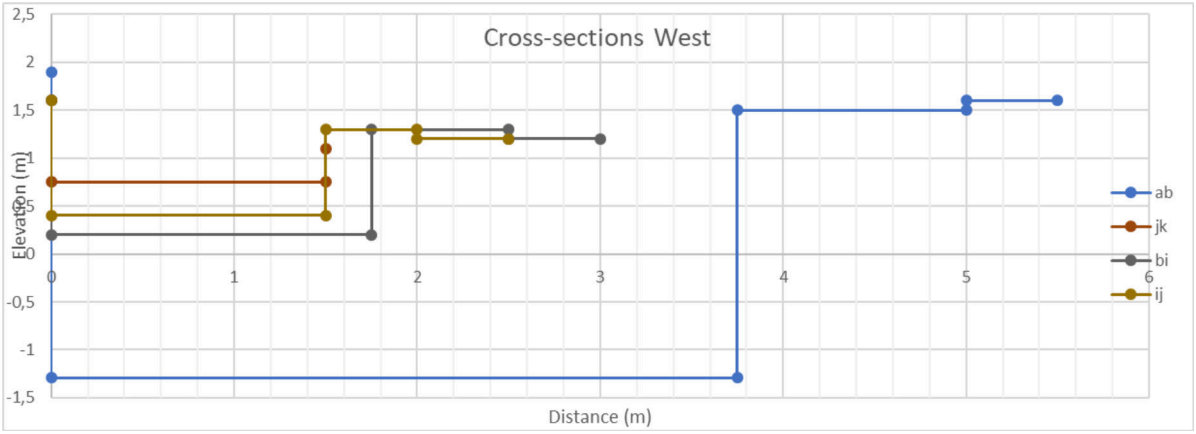

Figure 3.5: The cross-sections present in the left part of the SVB. Locations of the sections can be found in Figure 3.6

Structure	Id	Width/Diameter (m)	Level (m + NAP)
Culvert	C1.1, C1.2, C1.3, C1.4	1	-1.29
Weir	O1	4	0.97
Weir	O2	4	1.14
Weir	O3	4	1.17

Table 3.1: Dimensions of the structures in Situation 1. The weir level is the level when water is coming in with respect to the Dutch ordnance level. The weir Id corresponds to the Id as shown in Figure 3.6.

3.2.2. Current Situation

The modifications of 2017 consisted of the placement of four gate culverts and three weirs, see Figure 3.6. The modifications also included the lowering of the two existing weirs. Table 3.2 shows the dimensions of the weirs. Furthermore, in situation 2, the supply channel is connected to Weir 3. The diameter of the gate culverts is 63 cm, and the bottom level is +70 cm NAP. Next, the north-east corner of the SVB was realigned for shipping purposes, as depicted in the Figure. Artificial land, attached to the south side, compensates for the loss of area.

Situation 2 uses the cross-sections from the field measurements with some additional values from AHN3 data. The resulting cross-sections are shown in Figure 3.7. Appendix B shows the layout of the SVB.

Structure	Id	Width/Diameter (m)	Level (m + NAP)
Culvert	C1.1, C1.2, C1.3, C1.4	1	-1.29
Weir	O1	4	1.38
Weir	O2	4	1.24
Weir	O3	5	1.14
Weir	O4	5	1.34
Weir	O5	4	1.45
Gate culverts	K1.1, K1.2, K13, K1.4	0.64	0.75

Table 3.2: Dimensions of of the structures in Situation 2. The weir level is the level when water is coming in with respect to the Dutch ordnance level. The weir Id corresponds to the Id as shown in Figure 3.6

3.2.3. Proposed Situation

Situation 3 represents the redesign of the SVB, proposed by the designer of the SVB, see Figure 3.6. The cross-sections close to the inlet are now sloping, and fewer structures are present. Only two weirs and six gate culverts are present in the SVB in situation 3, see Table 3.3. The unchanged cross-sections use the same cross-sections as for situation 2.

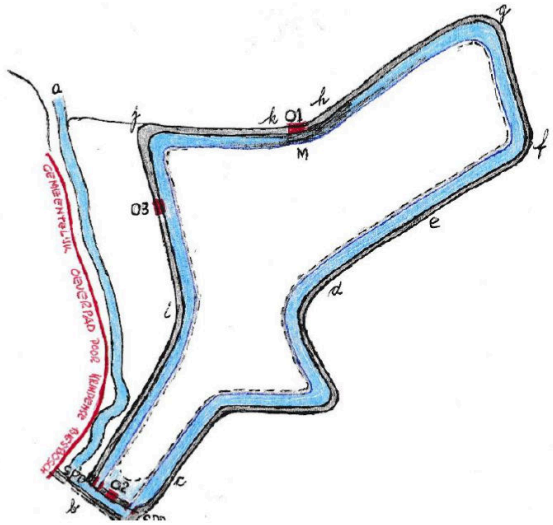

(a) The original design of the SVB with indicated sections. Figure 3.4 and 3.5 show the cross-sections present in the model. Table 3.1 gives the dimensions of the structures.

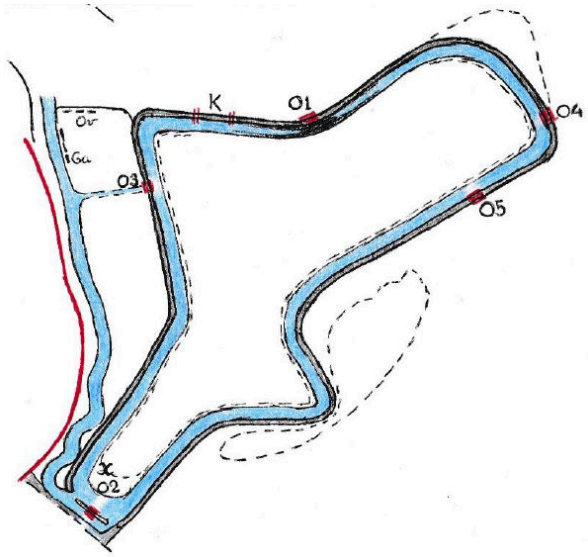

(b) The lay-out of situation 2, where four gate culverts are placed in the north, indicated by K. Three weirs (O3, O4, O5) were placed as well. Next, the upper-right corner is realigned. Table 3.2 gives the dimensions of the structures.

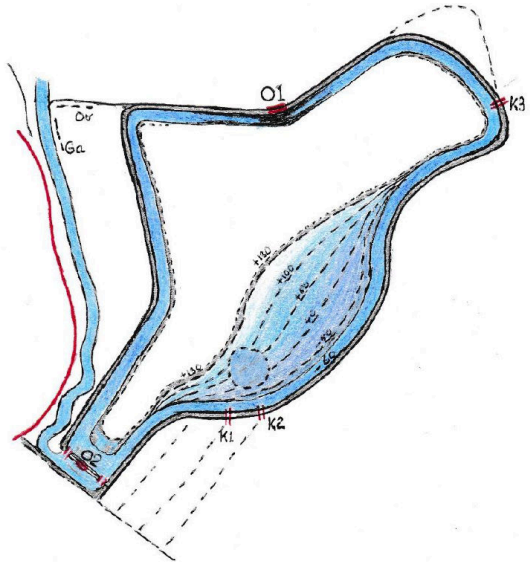

(c) The design of situation 3 with a sloping cross-section and (re)placed gate culverts K1, K2, K3. Table 3.3 gives the dimensions of the structures.

Figure 3.6: Lay-out of the system for the three different situations.

Structure	Id	Width/Diameter (m)	Level (m + NAP)
Culvert	C1.1, C1.2, C1.3, C1.4	1	-1.29
Gate culverts	K1.1, K1.2, K2.1, K2.2	0.63	0.9
Gate culverts	K3.1, K3.2	0.4	1.2
Weir	O1	5	1.45
Weir	O2	7	1.24

Table 3.3: Dimensions of the structures in Situation 3. The weir level is the level when water is coming in with respect to the Dutch ordnance level. The weir Id corresponds to the Id as shown in Figure 3.6

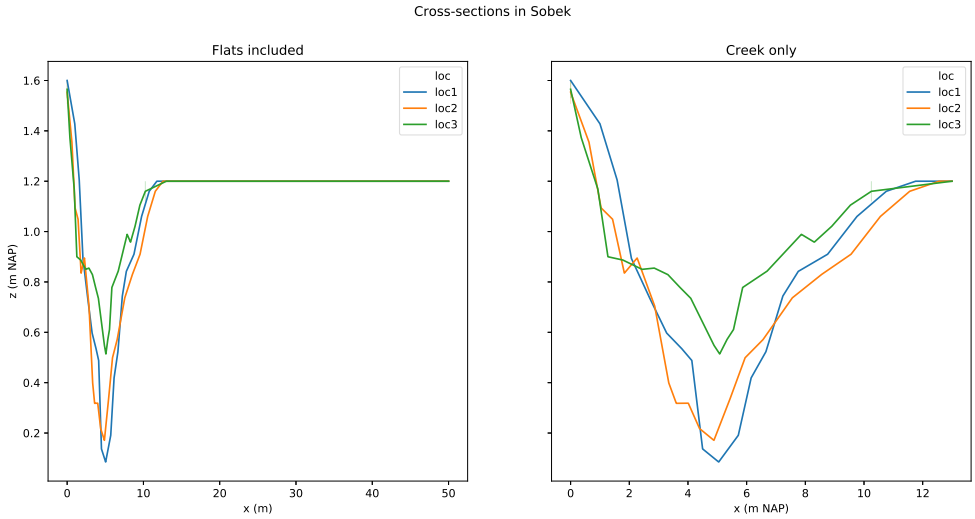

Figure 3.7: The cross-sections achieved by the GPS measurements during fieldwork supplemented with AHN3 data. The locations of the cross-sections can be seen in Appendix B. The cross-sections are used as input for the Sobek model.

4

Field Measurements

On 15 February, fieldwork was done in the SVB. During this day, velocities, depths and elevations of the creeks were measured. The fieldwork aims to verify the model results and to obtain a comprehensive insight into the water system. This chapter covers the preparation, execution, and results of the fieldwork.

4.1. Approach

4.1.1. Streamflow Measurement

The discharge is determined by measuring the mean flow velocity of several heights over multiple sections in the cross-section, see Figure 4.1. These measurements are then repeated for multiple cross-sections varying along the x-axis. Increasing the number of sections and the number of velocity measurements improves the discharge estimation. During fieldwork in the SVB, cross-sections are divided into three sections, containing only one measurement point. The discharge of a cross-section is calculated by:

$$Q = \int^{A_s} u dA_s \approx \sum^{m} u_i \cdot \Delta A_i \tag{4.1}$$

Where u_i is the mean flow velocity in section A_i and m the number of sections. Multiplying u_i by A_i gives partial discharges. The sum of these partial discharges equals the total instantaneous discharge in a cross-section of the channel[1].

4.1.2. Preparation

Before the fieldwork took place, some decisions were made on the measuring methods. Furthermore, instructions were needed for the volunteers executing the measurements.

Velocity Measurement Method

Multiple velocity measurement methods are considered. The first one is the propeller method. The propeller consists of the propeller and a removable blade. The rotations are counted by a counting box attached to the propeller. With a calibration curve, the rotations are linked to flow velocities. The second method is

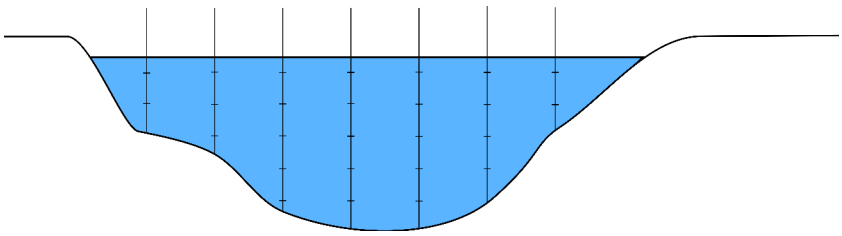

Figure 4.1: The cross-section of the channel is divided in multiple sections, where u_i and A_i are determined. When the mean velocity u_i of a section is multiplied by the area of this section, A_i, partial discharges are calculated. The sum of the partial discharges is the total discharge.

the floats method. For this method, multiple floats are let into the water. De time the floats take to travel a predefined distance is a measure for the flow velocity. Multiple floats exist to reduce the influence of the higher surface velocity. The third method is the salt dilution method. In this method, a volume of salt solution is instantaneously added to the stream. Downstream of the injection, where the mixture is completely mixed over the cross-section in the stream, the electrical conductivity is measured. From the measurements a peak can be distinguished at the moment the salt passes by. The time it takes for the peak to pass by depends on the flow velocity.

Measuring with a propeller is considered to be the most suitable option. Compared to the floats method, the propeller is more practical and precise. Propeller measurements are not dependent on the streamlines of the water, which is the case for floats. The stream potentially drives the floats to the borders of the cross-section, where the flow velocity is lower. As a result, it is hard to determine a mean flow velocity of the channel. This problem does not occur during propeller measurements, as the instrument is held at a fixed point in the stream.

Additionally, a propeller has better precision. Floats potentially follow curved pathways resulting in an inaccurate estimation of the travelled distance, causing an underestimation of the flow velocity.

Moreover, compared to the salt dilution method, the propeller method is better applicable in the SVB. As much vegetation is present in the stream, the vegetation captures the salt solution, resulting in inaccurate outcomes.

Calibration

At the faculty of Civil Engineering, three propellers were available for fieldwork. However, they all originate from different years and have been used many times already, possibly resulting in a deviation of the measurements. The propellers are calibrated, to avoid wrong interpretation of obtained results.

This first propeller was still new and never used. Therefore, propeller 1 is considered to be the most precise and accurate. Propeller 2 and propeller 3 are somewhat older and used many times. It is expected that these propellers are less accurate and less precise compared to propeller 1. Furthermore, the calibration curves of these propellers are lacking and should be determined by lab tests. Multiple blades exist that are used for various velocity ranges. From five blades, two blades are chosen, representing the smallest velocity ranges. As the second blade of propeller 3 is missing, another blade is chosen.

To calibrate the three propellers, they are placed in a laboratory flume. The propellers are arranged over the entire length of the flume, to make sure another propeller does not influence flow velocities. Furthermore, all propellers are placed in the stream midpoint, neglecting wall friction and providing identical conditions. Each propeller is connected to an electrical counting box.

After the system set-up, the tap is opened to discharge water into the flume. All counting boxes are started at approximately the same time, and revolutions are counted for 60 seconds. To ensure high precision of the revolution counting, a period of 60 seconds is chosen. Next, every measurement is performed in duplicate to prevent errors. After the results are written down, the discharge is slightly enlarged, repeating the measurements for the new discharge.

In total, 18 different discharges are applied to the three propellers and 2 types of blades. With the calibration curves of the two blades of propeller 1, the revolutions are coupled to flow velocities. The revolutions and corresponding flow velocities are depicted in Figure 4.2 and 4.3. For blade 1, the smallest blade, the flow velocities for propeller 1 and propeller 2 are comparable. Propeller 3 gives slightly less accurate results, see Figure 4.2. It can be concluded that the calibration curve of propeller 1 can be used for propeller 2 and 3 as well.

The combination propeller 2 and blade 2 deviates quite a lot from the reference combination (propeller 1 and blade 2), see Figure 4.3. This combination is not considered to be very accurate. The combination propeller 3 and blade 3 does not capture the lower flow velocities very well. However, this combination is quite accurate except for one measurement point. Blade 1 and blade 2 are compared in Figure 4.4. This Figure shows blade 1 captures lower flow velocities. The flow velocities in SVB are expected to be lower than 1 m/s.

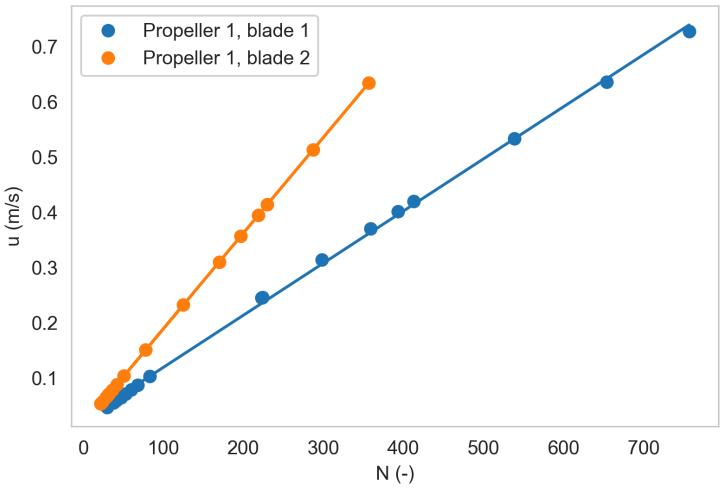

Figure 4.4: Blade 1 is chosen to use in the fieldwork since lower velocities can be measured.

All things considered, blade 1 is used for the field measurements. First, the accuracy of the blades 1 is better than blade 2 or 3. Second, when blade 1 is used, the same blades are used in the field, resulting in coinciding outcomes. Next, blade 1 captures the lower flow velocities likely appearing in the field.

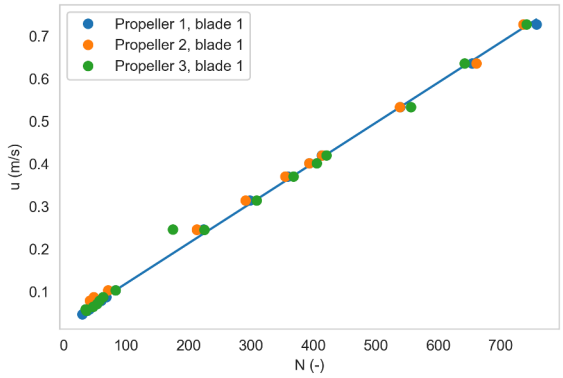

Figure 4.2: Measurements of small blades where the revolutions are coupled to the calibration curve of propeller 1.

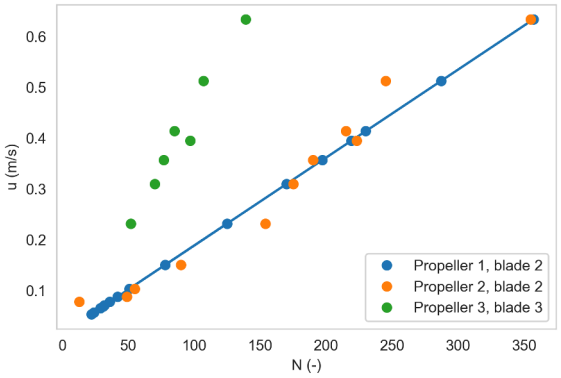

Figure 4.3: Measurements of large blades where the revolutions are coupled to the calibration curve of propeller 1.

4.1.3. Measurements

Measurement Instructions

During fieldwork, some people were needed to execute the measurements. The volunteers consisted of inexperienced people in a technological point of view. Therefore, clear instructions were of great importance. The instructions consisted of explanatory videos of the measurement instrument. Furthermore, some background information and basic principles were explained to the fieldwork participants. To ensure correct execution of the measurements, a guide was offered during fieldwork, attached in Appendix A.

Some fieldwork is done in advance in order to determine the measuring locations. The locations were selected by accessibility, lack of obstacles in the water, position, and recognition. As a result, three locations were chosen to measure, depicted in Appendix B.

(a) Propeller measurement during low water

(b) gps measurement

Figure 4.5: Pictures of the fieldwork on 15 February.

After all the preparations, fieldwork was executed on February the 15th with seven members. According to the prediction of RWS, low water would occur at 6:07h and high water at 12:00h. Therefore, the team was present at the location at 6:00h.

The last explanations were given to the team before they started to measure. Every team member received groin boots to be able to stand in the water. The group was divided into three groups of two persons. Every group received a bag with equipment, containing:

- 15 meter rope
- hammer
- small poles for fixation of the rope
- markers
- tape measure
- long tape measure
- calculator
- pencils
- form
- measurement description, Appendix A

With the equipment, the groups went to their designated location based on the description and photos. After they all found their location, they set-up their measuring station. Small poles were hammered into the ground on both sides of the cross-section, and a rope was attached to the poles.

Figure 4.6: Propeller measurement during high water

Flow Velocity Measurements

Every 10 minutes, a new measurement took place since water levels rise quickly during flood. As a start, the width of the channel was measured with the tape measure and filled in on the form, see Figure 4.6.

After that, propeller measurements were carried out. One propeller measurement consists of a series of three measurements. First, a propeller measurement is executed in the middle of the channel, where the number of revolutions, N1, is obtained. After that two measurements at $\frac{1}{6}$ distance of the channel side obtains N2 and N3. Then the revolutions are converted to flow velocities through the calibration curve of propeller 1.

All the propeller measurements were carried out at 0.6 depth of the water surface, which is approximately the mean velocity, see Figure 4.5a. The measured depth in the middle of the creek is used for the velocity-area method, explained in Section 4.1.1. The revolutions (N1, N2, N3) were filled in on the form together with the flow direction.

Water Levels

During fieldwork, four divers were placed too. The locations of the divers correspond to the measuring locations in SVB. One extra diver was placed in the channel discharging into the SVB. The divers were attached to a concrete tile, ensuring they would stay in the same place during measurements. The tile with the diver was pushed a little into the muddy ground when placed in the field to prevent measurement errors due to settling. The diver used in the fieldwork measures pressure with an accuracy of 1.0 Pa and temperature with an accuracy of 0.1 °C. Measurements automatically took place every 10 minutes.

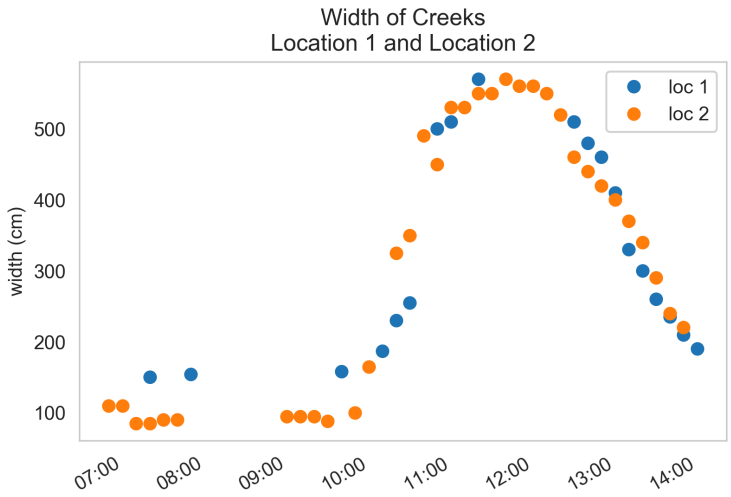

Figure 4.7: Measurements of the creek width over time

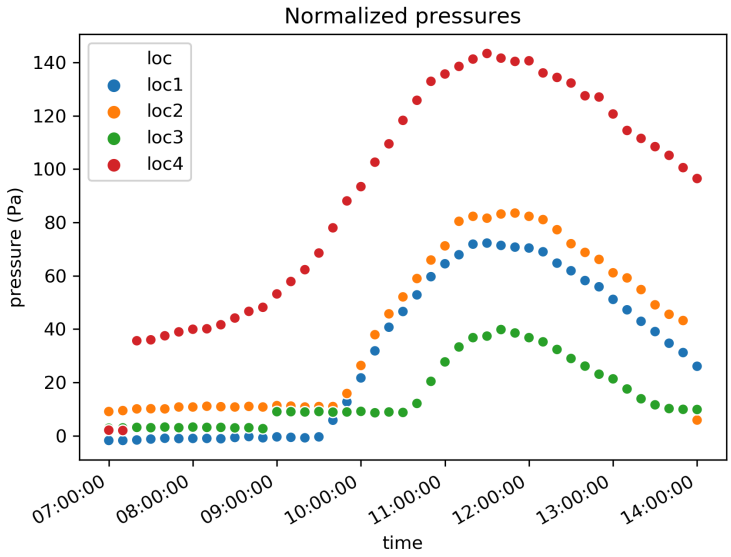

Figure 4.8: Measurements of the diver over time for all the 4 locations. The measurements are corrected for air pressure.

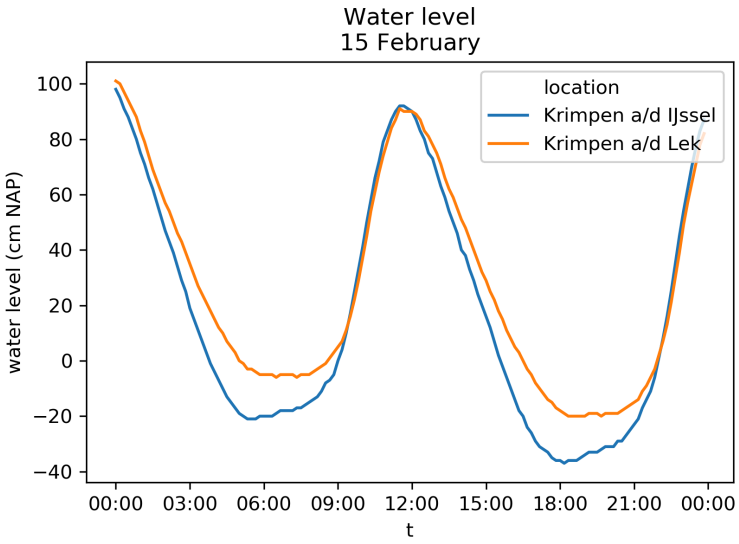

Figure 4.9: The tide measured at two locations close to the SVB on February 15th

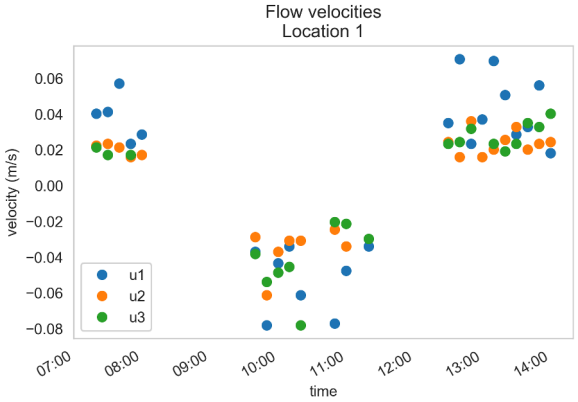

Figure 4.10: The Figure shows the velocity measurements at location 1, where u1 represents the middle measurement, u2 measurement at 1/6 B and u3 measurement at 5/6 B.

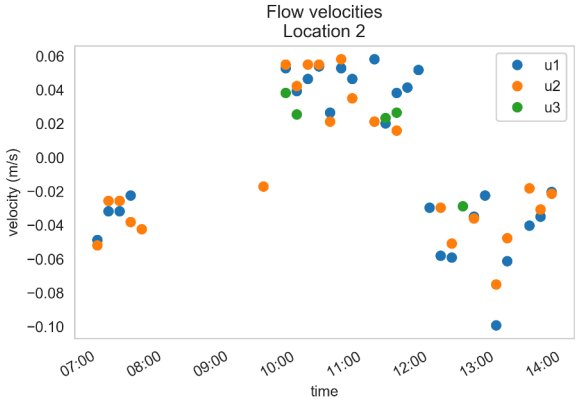

Figure 4.11: The Figure shows the velocity measurements at location 2, where u1 represents the middle measurement, u2 measurement at 1/6 B and u3 measurement at 5/6 B.

Topography

Apart from the flow velocity measurements, GPS measurements were carried out, measuring elevation at every measuring location, see Figure 4.5b. Next, a comparison is made between the measured elevation during fieldwork and data from AHN3 and AHN2 (Algemeen Hoogtebestand Nederland).

AHN is obtained by laser altimetry, resulting in no data points for water. AHN3 is the newest public dataset available and originates from the first term of 2014. AHN2 is older and originates from the first term of 2008. Since the datasets are taken in similar circumstances with respect to vegetation, a comparison is possible. From the AHN data a digital terrain map (dtm) with a resolution of 0.5 m is chosen. In a dtm, trees and buildings are filtered out of the dataset. AHN3-data is freely accessible through `https://www.pdok.nl/nl/ahn3-downloads`.

Data is available on the construction level of the creeks in SVB. For every section indicated in Figure 4.12, a cross-section is available. Measuring location 1 corresponds to section ib, measuring location 2 to section de and measuring location 3 to kj. When the original construction levels are compared to the elevation levels measured with GPS, it becomes clear that the cross-section became smoother throughout the years.

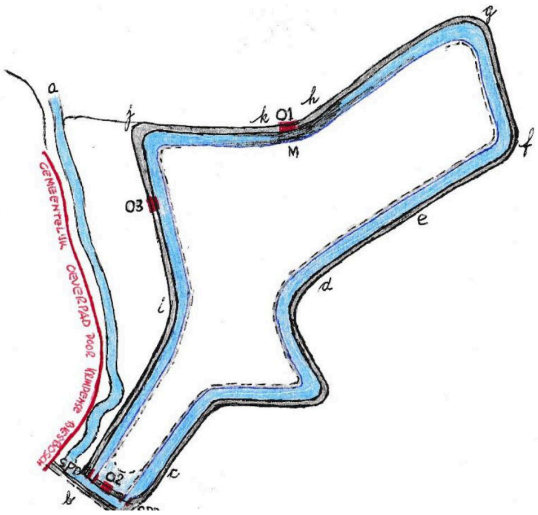

Figure 4.12: The layout of the SVB, with the sections indicated.

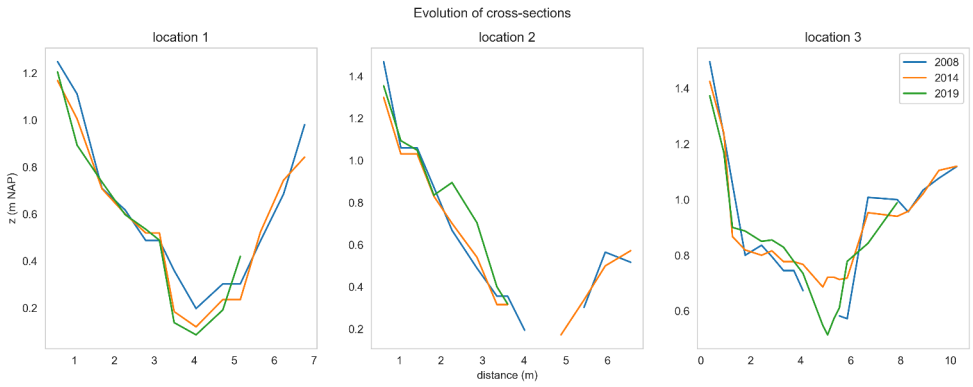

Figure 4.15: The development of the cross-sections over the years. 2008 contains data of AHN2, 2014 of AHN3 and 2019 represents the GPS measurements. The right sides of the plot correspond to the location of the creek closest to the center of SVB.

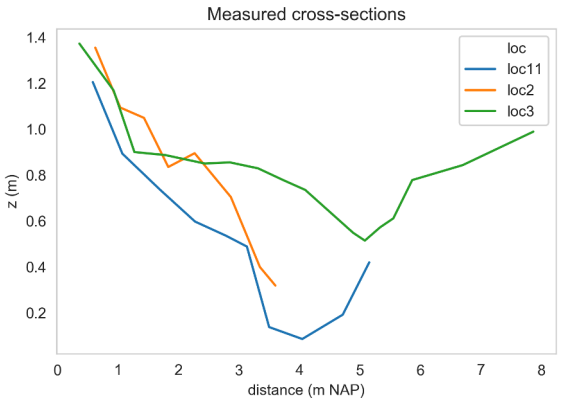

Figure 4.13: At every measuring location, the cross-section is determined by GPS and corrected for measurement errors larger than 0.1 m. loc11 in the figure represents a second execution of the measurement on location 1.

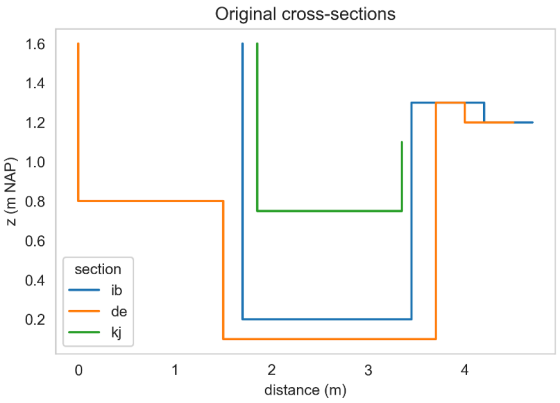

Figure 4.14: For different sections a constructed cross-section is available. Section ib corresponds to location 1, section de to location 2 an section kj to location 3. The location of the sections are shown in Figure 4.12

Furthermore, a comparison at the measuring locations is made between GPS measurements, AHN2 and AHN3. The measuring points from GPS are imported into GIS. From there the corresponding raster tiles are taken from the AHN2 and AHN3 dataset and exported. The result can be seen in Figure 4.15, where the right side of the plots is corresponding to the inner area of SVB. Points with no data are not taken into account.

4.2. Results

4.2.1. Channel Width

As can be seen in Figure 4.7, for both location 1 and location 2, the width increases at 10:00h. The width increment coincides with the rising tide on the 15th of February, Figure 4.9. Around 12:00h, the width for location 2 reaches a maximum, corresponding to the timing of the maximum water level. The maximum width of location 1 is not measured. However, this is possibly identical to location 2. Furthermore, Figure 4.7 shows an initial channel width for location 1, while the channel at location 2 is very narrow.

4.2.2. Flow Velocities

Figures 4.10 and 4.11 show the measured flow velocities. The flow velocities do not exceed 0.1 m/s. The flow velocities in the middle of the stream (u_1) are generally higher than the measured flow velocities on the sides. Furthermore, a difference in the reference frame can be distinguished for location 1 and location 2. During flood, location 1 measures negative velocities, while location 2 measures negative velocities. Location 3 could

not be measured with the propeller during fieldwork since too little water was flowing. Therefore, location 3 was dropped as propeller measuring location.

4.2.3. Water Levels

At location 3, no water was present yet when the diver was placed. Around 9:00h a change of location 3 took place. The diver was replaced to a deeper part of the channel containing more water in the cross-section. This location was more accessible too.

Figure 4.8 shows the diver measurements of the four locations over time. Diver 4 is the diver placed just outside SVB in the supply channel. The Figure shows the direct response of the diver on the water level measured at Krimpen aan den IJssel and Krimpen aan den Lek, without significant delay. The figure clearly shows that water first rises at location 1 at 9:30h. After that, the water reaches location 2 as well, a little before 10:00h. The water rises last at location 3, at 10:30h. The position of the divers explains the delay of the water level for the four locations. Next, the maximum water levels at location 1 and 2 coincide with the timing of maximum width at these locations.

4.2.4. Topography

However, since the area contains many trees, the signal was lost sometimes. Due to the signal loss, large errors occurred. Errors larger than 0.1 m are filtered out. The results are visualized in Figure 4.13.

Especially location 2 shows missing data in the deepest part of the cross-section. No data is a sign for the creek containing water. It is remarkable though that location 1 has data values at elevations lower than 0.2 m NAP, while these data points are lacking for location 2 of the same year. Considering location 1 has data points for elevations lower than 0.2 m NAP, it means that the water level at that time is lower than 0.2 m NAP as well. Since water is present at location 2 at elevations higher than 0.2 m, it is likely that location 2 is located in a depression where water cannot escape.

The evolution over time of the cross-sections differs per location. At location 1 erosion of especially the centre of the creek took place over the past 11 years. The left side of this cross-section did not change significantly. However, for the right side of the cross-section this is less clear. It is shown in the Figure 4.15 that in 2019 the cross-section slightly narrows at the bottom, however, the gradient towards the right side is unclear. For location 2, many data points are missing due to cells containing water or to the signal loss of the GPS. The points available do not show significant erosion, nor sedimentation. Location 3 shows 20 cm of erosion in the centre of the creeks. Just left to the middle part, the creek experiences sedimentation. The right side of the cross-section became more flattened as compared to its initial shape.

5

Numerical Computations

The purpose of the numerical computations is achieving the influence of tidal forcing, design parameters, and hydraulic structures on sedimentation in a constructed tidal marsh. The first part of Chapter 5 elaborates on the hydrodynamic model, the morphodynamic model, and the model configurations. After that, the second part of Chapter 5 discusses the results. To apply the results in a broader perspective, generic results are distracted from the sedimentation in the SVB case.

5.1. Approach

Numerical models of the SVB evaluate the effect of forcing and system lay-out on sedimentation. The first part of the numerical model consists of Sobek simulations, and provides 1D hydrodynamics in nodes and reaches of the system. The Sobek software program enables the integration of rivers, canals, and constructions for a total water management solution. Section 5.1.1 elaborates on the system lay-out of the case study and Section 2.3 discusses the calibration of the numerical model.

In the second part of the numerical model, the output of the 1D model is used in further calculations to obtain the morphodynamics of the constructed tidal marsh. The successive calculations are developed and executed in python to convert hydrodynamics into bed shear stress and sedimentation. The calculation method of parameters relevant for sediment transport are discussed in Section 5.1.3.

To achieve the influence of forcing and lay-out of the system, multiple model configurations are examined in Section 5.1.4. The tidal forcing applied to the numerical model is determined by the amplitude, base flow of the river, and tidal asymmetry. Furthermore, the design and constructions, present in the constructed marsh, determine the lay-out. Section 5.1.4 elaborates on the variation of the two lay-out components.

5.1.1. Case Study

The numerical computations are applied to a case study to be able to compare model results with field measurements and observations. Therefore, the three situations of the SVB is used as the model lay-out. An elaboration of three situations of the SVB can be found in Chapter 3. Furthermore, the model of the current situation is calibrated with field measurements. The field measurements are discussed in Chapter 4.

System Lay-out

Water enters the SVB in the current situation through four culverts, connected to a supply channel. Furthermore, water flows over weirs, present in the outer dike, into the SVB. Inside the SVB creeks distribute the water. The hydrodynamics in the creeks of the SVB are dependent on the water entering the SVB and the elevation and shape of the creeks.

The Hollandsche IJssel encloses SVB on the North-West, and the river Lek encloses the SVB on the South-side, as can be seen in Figure 3.1. The Sliksloot connects the Hollandsche IJssel and the Lek and discharges into the supply channel. The Sliksloot is also connected to the weirs in the outer dike. As the water level in the Sliksloot determines the volume of water entering the SVB, the water level in the Sliksloot serves as a

Point	Reach
Waterlevel (m NAP)	Discharge (m^3/s)
Waterdepth (m)	Velocity (m/s)
Free board (m)	Froude number (-)
	Waterlevel slope (-)

Table 5.1: Output parameters for two Sobek elements

boundary condition for the numerical model.

Appendix B shows the lay-out of the SVB in the Sobek 1D model for the current situation. Here, four culverts, four gate culverts, and five weirs are present, as explained in Chapter 3.

The output of the numerical model is shown along the axis of the main creek system, where x=0 m is the inlet/outlet point, which is at the location of the four culverts. x then increases in counter-clockwise direction and ends at x=1000 m, which is again the inlet/outlet point. The determination of the x-axis results in equal model outputs of x=0 m and x=1000 m, see Figure 5.13.

5.1.2. Hydrodynamic Model

Sobek 1D is used for the hydrodynamic model and calculates parameters in points and reaches, see Table 5.1. The advantage of a Sobek 1D model, compared to a more complex morphodynamic model, is its extensive applicability and user-friendly interface. With only a simple network, a first estimation of the hydrodynamics can be obtained. Next, the results can be easily plotted in either graphs or as an overlay in the area of interest. Therefore, Sobek 1D is a useful tool for rough estimations of hydrodynamics.

Normally, bank overflow is not accounted for in the Sobek calculations, as Sobek only calculates the flows inside the cross-section. Since the cross-section is divided in flats and creeks, the cross-sections in Sobek are elongated to 50 meters width to mimic the flats.

Calibration of Roughness Coefficient

As predicting Manning's roughness is difficult, calibration of the hydrodynamic model leads to an increase in reliability of the numerical model. The velocity measurements of the fieldwork should coincide with the velocity results of the model. Therefore, varying the roughness parameter leads to a calibrated hydrodynamic model.

For the calibration, the model uses the water levels of measurement station Krimpen aan den IJssel from 10 February until 16 February at the boundaries. A spin up time of 7 days ensures the initial conditions of the calculations do not influence the model results anymore. On 15 February, the calibration period for Manning's coefficient starts as this day coincides with the measuring day.

A first estimation of the roughness coefficient for the SVB is n=0.0575 $s/m^{1/3}$, with n_0=0.02 $s/m^{1/3}$, n_1=0 $s/m^{1/3}$, n_2=0.005 $s/m^{1/3}$, n_3=0.020 $s/m^{1/3}$, n_4=0.005 $s/m^{1/3}$, m_5=1.150 $s/m^{1/3}$, as explained in Section 2.3. Calibration of the model with a higher Manning coefficient than 0.0575 $s/m^{1/3}$ shows a better agreement between the flow velocities of the model and the field measurements at the two measuring locations. With Manning's roughness of 0.2 $s/m^{1/3}$, the flow velocities for location 1 become 2 times smaller compared to the outcomes with n=0.0575 $s/m^{1/3}$, see Figure 5.1. For location 2, the flow velocities are even 3 times smaller. The timing for location 1 gets better with a higher Manning coefficient, while the timing of location 2 worsens. For the numerical computations, Manning's coefficient is assumed to be 0.2 $s/m^{1/3}$.

5.1.3. Morphodynamic Model

To transform the output of the hydrodynamic model into morphodynamic results, data modification and consecutive calculations are executed in Python. As the output of Sobek does not directly calculate shear stresses, the bed shear stress is calculated from Sobek output, using Python. Appendix C explains how the Sobek output file is transferred to Python.

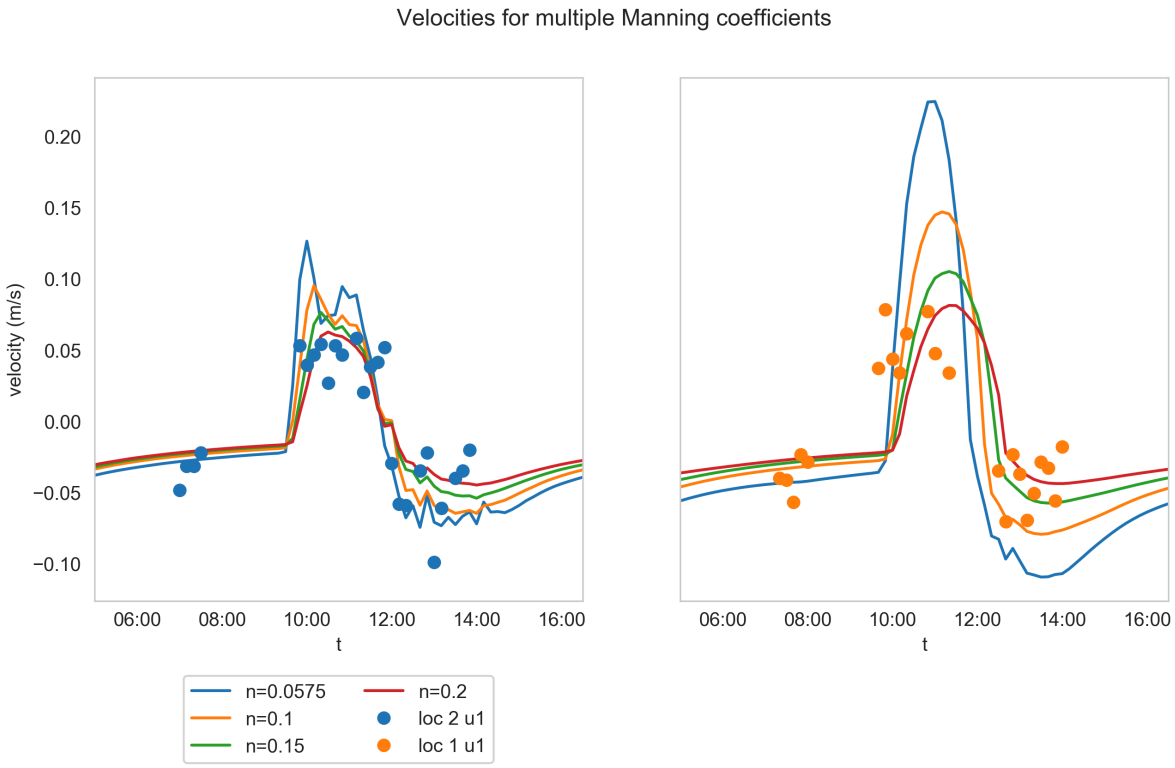

Figure 5.1: The model is calibrated with multiple values of n and shows a better estimation for a higher Manning value.

First, a python script transforms the Sobek output in the nodes and reaches into the desirable order of points and reaches. The order is taken positively from the inlet/outlet point counter-clockwise to the inlet/outlet.

Bed Shear Stress

Bed shear stress is a measure for the force applied to the surface of the bottom of the creek per square meter. When the bed shear stress is larger than the critical bed shear stress, sediment mobilizes, leading to sediment transport. The critical bed shear stress for sand is taken at 0.4 N/m^2, and the critical bed shear stress for silt is between 0.1-0.2 N/m^2.

Sediment transport consists of transport related to currents and transport related to waves, see Section 2.5. As dikes enclose the SVB, dense vegetation is present, and only a small fetch is present, it is assumed the influence of waves on sediment transport is low compared to the current related transport. Therefore, only current related transport, carried out by steady flow, is taken into account. The following formula calculates bed shear stress:

$$\tau_b = \rho U_* |U_*| = \rho \frac{g}{C^2} U^2, \tag{5.1}$$

where τ_b (N/m^2) is the bed shear stress, U_* the friction velocity, ρ the density of water, C the Chézy roughness, and U the mean flow velocity.

After the calibration of the model with the measuring day, the hydraulic roughness value is $n = 0.2 s/m^{1/3}$. The formula:

$$C = \frac{1}{n} R^{\frac{1}{6}} \tag{5.2}$$

transforms Manning's value n into Chézy's roughness coefficient, and is used in Equation 5.1. R represents the hydraulic radius and is calculated by

$$R = \frac{A_w}{P}, \tag{5.3}$$

	Sediment fraction	
	SF1	SF2
w_s (mm/s)	0.87	2.17
$w_s/\kappa u_*$	0.25	1.5

Table 5.2: The sediment fractions used in the analysis for sedimentation. Settling velocities from research on suspended sediment in the Rhine and Meuse[12].

where A_w is the wet cross-section in m^2, and P is the wetted perimeter (m). Both A_w and P vary with water level and are not constant. A_w and P are calculated at every time step at the calculation nodes. This calculation step assumes the cross-section at location 1, as shown in Figure 3.7, is present in the entire area.

With U and C, τ_b can be solved for every time step, using Equation 5.1. Nevertheless, comparison of heights and velocities at the same time force a small data manipulation. z Is the result of a water level in a calculation point, while U is a reach outcome. To be able to compare points with reaches, the location of the reach is relocated to the reach endpoint.

Sedimentation

This research aims to find locations vulnerable to sedimentation. Therefore, potential sedimentation is calculated. The longer the duration of the HWS, the more sediment can settle on the channel bed, as explained in Section 2.5. Absolute flow velocities lower than 0.01 m/s are leading to the settling of fines. The formula:

$$S = \int_{z=0}^{z=\Delta z} c(z) B dz \tag{5.4}$$

gives the potential amount of sedimentation, S. The concentration c is a function of the water depth and is determined by the Rouse profile from Equation 2.10. Δz is the lowest part of the water column from which the suspended sediment settles. $\Delta z = T w_s$, where T is the duration of HWS and w_s is the particle fall velocity. For every location along the creek system, the maximum duration of the HWS is determined. Next, the amount of settling per m^2 is an integration of the sediment concentration, calculated from Equation 2.10, over Δz:

$$\int_{z=0}^{z=\Delta z} \frac{c}{c_a} dz = \int_{z=0}^{z=\Delta z} \left(\frac{h-z}{z} \frac{a}{h-a} \right)^{w_s/\kappa u_*} dz, \tag{5.5}$$

the reference concentration c_a is assumed to be 10 mg/L since the hydrodynamics are low when the water is entering the SVB, see Chapter 3.

Determining the longest HWS at every location enables to calculate the maximum potential sedimentation with Equation 5.4 and 5.5. The width in Equation 5.4 is taken at the mid-time of the HWS, presuming no erosion limit, and the Rouse profile is presumed to be constant and fully developed during the HWS. Sediment entering the system consists of a range of particle sizes and a settling velocities, which are considered constant throughout the system. Typical settling velocities for flocculated particles are in the range of 0.1 mm/s-10 mm/s[18].

The large natural variability in sediment properties is for simplicity characterized by two sediment factions: one fine fraction (SF1) with w_s=0.87 mm/s, and $w_s/\kappa u_*$=0.25, and one fraction (SF2) with a fall velocity of w_s=2.17 m/s, and $w_s/\kappa u_*$=1.5. The sediment fractions, SF1 and SF2, and their settling velocities correspond to the cumulative 50% and 90% present in the Rijn and Meuse delta and are taken from research on suspended sediment in the Rhine and Meuse[12]. Table 5.2 summarizes the fractions and their corresponding variables.

5.1.4. Model Configurations

The model configuration consists of tidal forcing, marsh design and system adjustments, see Figure 5.2. The tidal forcing uses several amplitudes, base flows and tidal asymmetries as input arguments. The determination of these arguments will be discussed below.

Next, the marsh design can vary in depth-width ratio of the creeks, the amount of flat area and the elevation. The arrows in Figure 5.2 indicate that a similarity exists between base flow and elevation. They are

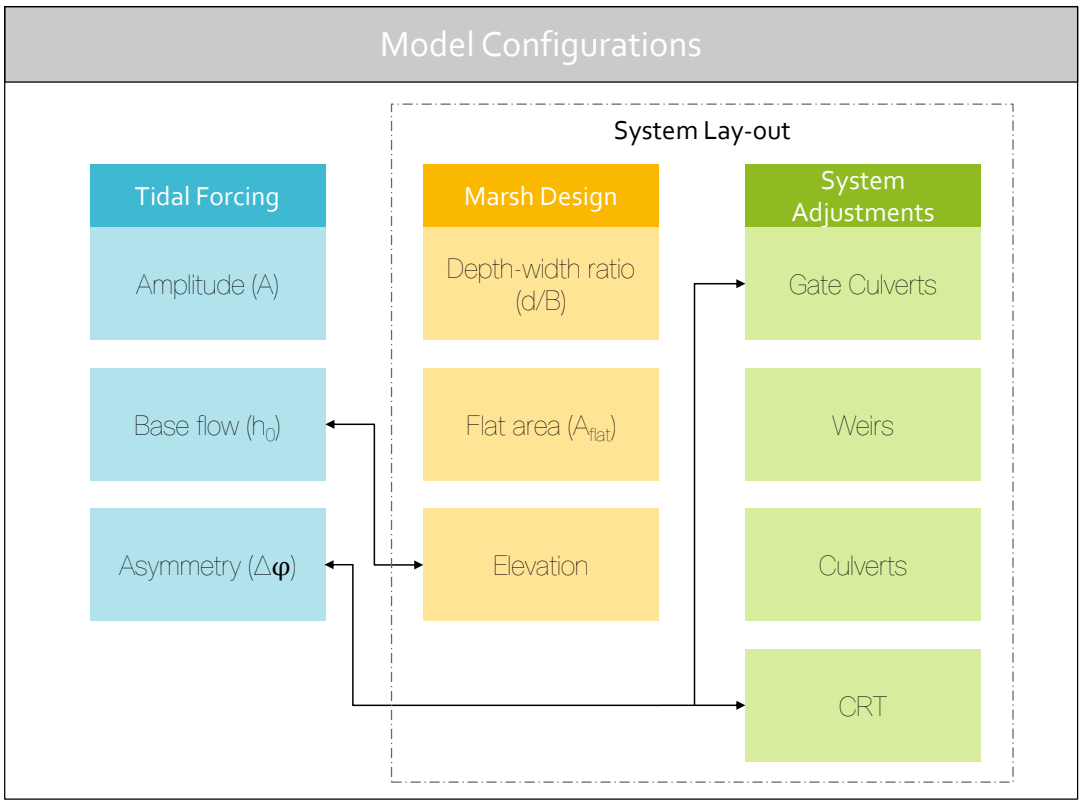

Figure 5.2: Multiple forcing and lay-out components used for model configurations. The arrows indicate a similar effect in forcing or system lay-out

interchangeable, as base flow can be seen as a forcing. However, a high base flow can be counteracted with a high elevation of the tidal marsh.

The system adjustments consist of the structures as (gate) culverts, weirs, and controlled reduced tides built in tidal marshes. Using gate culverts can increase flow velocities, thus mimics tidal asymmetry of $\Delta\phi = 0.5\pi$. In contrast, controlled reduced tides lead to longer period of high water slack and mimics tidal asymmetry of $\Delta\phi = \pi$.

Tidal Forcing

Discharge and tide influence the water level in the Sliksloot, which is the boundary condition in the numerical model. The input at the boundary essential for the output of the Sobek model. Executing the numerical model with multiple input scenarios shows the response of the system. Therefore, several tidal curves, determined by amplitude, base flow, and asymmetry are applied at the boundary to determine the influence on bed shear stress and accretion inside the SVB.

As explained in Chapter 2, the tide varies due to the variation in attractional forces of the moon and sun, leading to spring and neap tide. The astronomical tide is displayed in Figure 5.3.

However, river discharge and wind set-up influence the water level as well. As a result, the maximum observed water levels at Krimpen aan den IJssel do not coincide with the maximum astronomical tide. The graph in Figure 5.4 shows the maximum observed water levels. From this Figure it becomes clear that river discharge and wind set-up have a substantial contribution to the water level, and should be regarded in the determination of characteristic water levels.

	dh_{Rising} (cm)	$dh_{Falling}$ (cm)
min	23	-15
10%	119	-124
mean	146	-146
median	147	-147
90%	171	-166
max	235	-209

Table 5.3: Statistics of rising and falling ranges at Krimpen aan den IJssel

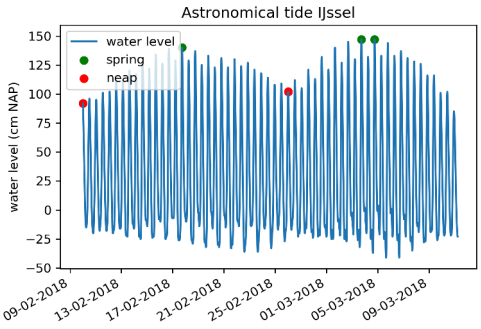

Figure 5.3: Spring tide and neap tide water levels for the astronomical tide. The data originates from RWS.

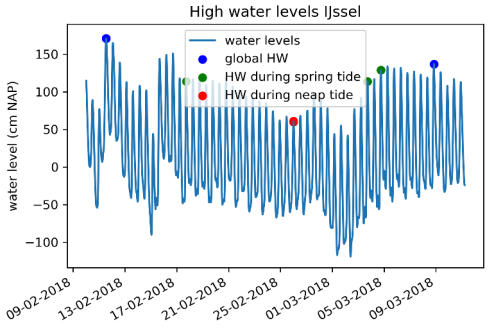

Figure 5.4: The maximum water levels during spring and neap tide do not correspond to the maximum water levels observed at the measuring point in Krimpen aan den IJssel. The data originates from RWS.

Amplitude Statistical analysis on water level data of Krimpen aan de IJssel, with a length of 18.6 years, leads to characteristic water level values, where a period of 18.6 years represents the periodic amplitude variation[5]. The statistical analysis includes the calculation of the rising and falling water levels, leading to characteristic amplitudes of the tide at Krimpen aan den IJssel. Determining the rising and falling head is done by taking the difference between low water and high water, and high water and low water per tidal cycle over 18.6 years. Applying statistical analysis on the ranges gives the mean of the rising and falling tidal range, and the maximum and minimum 10% of the rising and falling tidal range. Table 5.3 shows the result of this analysis. The absolute range of the rising and falling water levels are also displayed in Figure 5.5. The whiskers of the boxplot depict the 10% and 90% values of the dataset.

From Figure 5.5 and Table 5.3 it becomes clear that the spreading of the rising tidal range is somewhat larger than for the falling tidal range. The lowest 10% of the ranges are 119 cm for rising water levels and -124 cm for falling water levels, respectively. The highest 10% of the ranges are 171 cm for rising water levels and -166 cm for falling water levels. The difference in spreading of the ranges may be caused by the stronger wind influence during high waters than during low waters, as river banks and vegetation more protect the water during ebb than during flood, leading to smaller wind set-up. The mean and median do not deviate from each other significantly and are equal for rising and falling water levels.

Dividing the mean ranges of the highest and lowest 10% by two gives the amplitude of the extreme tides. Together with the mean rising/falling heads divided by two, this leads to three characteristic amplitudes: 54, 73 and 90 cm, see Table 5.4. Applying this method introduces a small error. In the determination of the tidal range, a small contribution of the water level is present as well, leading to a slightly larger amplitude.

Base Flow The river discharge shifts the (constructed) tidal curve vertically and is varied in the model input to mimic wind set-up, and multiple base flows of the river. At 1.20 m NAP, the banks of the creeks of the SVB overflow, and water enters the inner area of the SVB, influencing the hydraulics. To determine the water level influence at the boundary, the maximum water level of the tidal curve is taken at 1.20 m NAP, which is bank

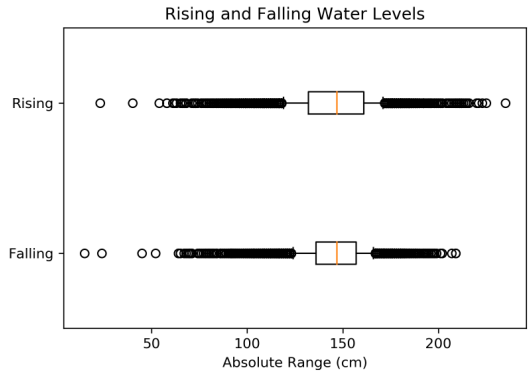

Figure 5.5: The absolute tidal rising and falling tidal ranges at Krimpen aan den IJssel. The orange line represents the median of the data and the wiskers are located at the lowest and highest 10% of the dataset.

Amplitude	Value (cm)
A_{min}	54
A_{max}	90
A_{mean}	73

Table 5.4: The amplitude in the constructed tide takes the minimum 10%, maximum 10%, and mean amplitudes of the data set of Krimpen aan den IJssel

full flow, at 1.30 m NAP, where the flats play a minor role, and at 1.60 m NAP, where the outer dikes of the SVB just does not overflow, and flats play a significant role. To determine the behaviour of the system during mean discharge, a scenario of the mean vertical shift of the tidal curve is included as well. Table 5.5 lists the values of the vertical shift leading to the specific maximum water levels.

Asymmetry A distinction is made between time series resulting in sedimentation of coarse sediment and sedimentation of fine sediment. Therefore, the phase difference of the tide is 0.5π or π, corresponding to the import of coarse sediment and fine sediment respectively, see Section 2.4. When the system imports coarse sediment, the summation of M2 and M4 leads to higher flow velocities during flood compared to the flow velocities during ebb. When the system imports fine sediment, the duration of HWS is more prolonged than of LWS.

Scenarios Varying and combining the three components: amplitude, base flow, and tidal asymmetry leads to 12 scenarios, shown in Table 5.6, and Figure 5.6. The four upper plots use the mean water level of Krimpen aan den IJssel for the vertical shift together with the variation of the amplitudes according to Table 5.4. The two lower plots show multiple vertical offsets as listed in Table 5.5 with the mean amplitude. The plots on the left-hand side differ from the plots on the right-hand side in phase difference. The phase difference is 0.5π and π respectively.

Vertical shift	Value (cm), $\Delta\phi = 0.5\pi$	Value (cm), $\Delta\phi = \pi$	Description
h_0	29	29	Mean water level
h_1	43	62	Bank full flow
h_2	53	72	Minor flat contribution
h_3	83	82	Major flat contribution

Table 5.5: Multiple vertical shifts representing river discharges and flat contribution. The value of the vertical shift is dependent on the phase difference between M2-2M4.

		$\Delta\phi = 0.5\pi$	$\Delta\phi = -0.5\pi$
h_0	A_{min}	Scenario 1	Scenario 2
	A_{max}	Scenario 3	Scenario 4
A_{mean}	h_0	Scenario 5	Scenario 9
	h_1	Scenario 6	Scenario 10
	h_2	Scenario 7	Scenario 11
	h_3	Scenario 8	Scenario 12

Table 5.6: 12 Scenarios for flood and ebb dominance for varying tidal amplitudes and river base flow

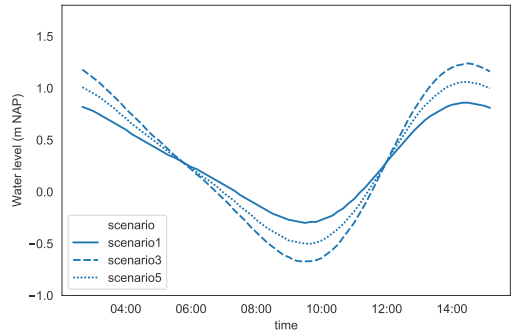

(a) Water levels as function of time for multiple scenarios

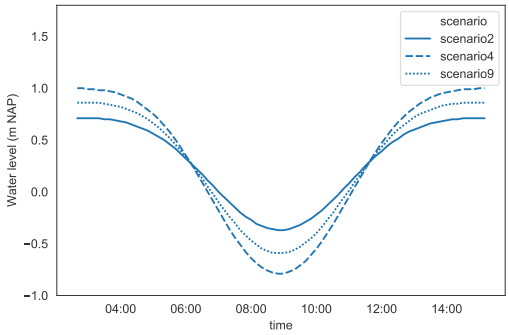

(b) Water levels as function of time for multiple scenarios

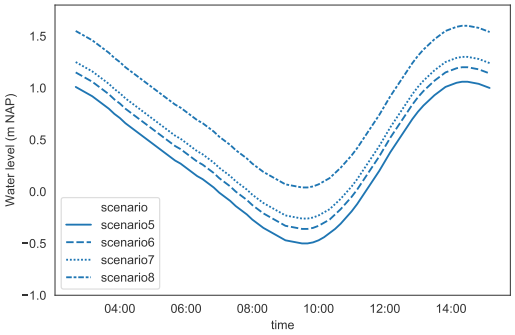

(c) Water levels as function of time for multiple scenarios

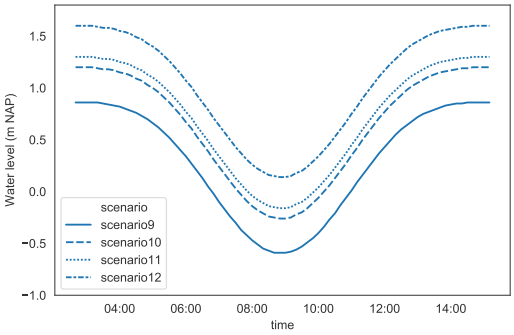

(d) Water levels as function of time for multiple scenarios

Figure 5.6: The upper two plots show the tidal curves for amplitude variation. The lower two plots show the tidal curves for water level variation. The left plots differ from the right plots phase differences.

Marsh Design Parameters

The design of constructed tidal marshes consists of depth-width ratio of the cross-section, flat area and elevation. The shape of the cross-section of the creeks determines the hydraulics and thus the sedimentation. Next, flat area and elevation determine the volume of water entering the constructed tidal marsh.

The three design parameters can be ascertained in the initial design of the marsh. After that, the parameters develop into a dynamic equilibrium, where forcing influences the design parameters, and the design parameters influence hydrodynamic.

System Adjustments

To verify whether the modifications of the SVB are responsible for sedimentation, the situation before the adjustments is compared to the situation after the adjustments. Furthermore, a situation of the proposed new design is examined as well. Therefore, the model simulates three different situations of the SVB, as explained in Chapter 3.

The first situation represents the original designed and constructed situation. The second situation addresses the situation with the following modifications: the replacement of two weirs, placement of four gate culverts, realignment of the north-east corner, and the addition of a small compensation island. The artificial area constructed in the south is not taken into account in the model, as it lies outside the embankment and thus does not influence the SVB. The third situation is the proposed redesign of the area with sloping cross-sections and replaced gate culverts.

The three system lay-outs are implemented in the numerical model, and the effect of on sedimentation is examined. Although in situation 2 and 3, weirs are also present along the Lek, the water levels are assumed to be the same as in the Sliksloot.

5.2. Results

Applying multiple model configurations to the model results in generic conclusions. Variation in tidal forcing leads to the quantification of sedimentation and determination of locations prone to accretion. Furthermore, elaborating on different layouts of the area gives the influence of structures and marsh design on accretion. The reliability of the model is assured by calibrating the model with field measurements. In the results, τ_{diff} is used as a measure of bed shear stress, and is calculated by the difference in maximum ebb and flood velocities, summed over the creek system, see Equation 5.6.

$$\tau_{diff} = \sum |\tau_{max,flood}| - |\tau_{max,ebb}| \tag{5.6}$$

Sobek performs calculations in points and in reaches. For the two types of model elements, different quantities are obtained, listed in Table 5.1. The positive flow direction in Sobek is counterclockwise with respect to the inlet point. In the results, the velocities are taken positive during flood and negative during ebb.

5.2.1. Tidal Forcing

When moving along an estuary, amplitude, base level, and tidal asymmetry change, determining the tidal forcing. In this section the contribution of the three different tidal components are discussed.

Amplitude

Results of a varying amplitude are obtained from the simulations of the numerical model. The model uses Scenario 1, 5, and 3, which have a phase difference of 0.5π and a mean vertical shift. Two tidal periods with amplitudes of 64 cm and 83 cm are added to the simulations. To account mainly for the contribution of the amplitude, and not the shape of the cross-section, a cross-section with a depth-width ratio of 1:8 is chosen and the tidal flats are prolongued to 50 m.

Enlarging the amplitude leads to higher water levels during flood. The Rouse profile is a function of water depth, where more sediment is present for larger depths, see Figure 2.7. As a result, the concentration profile

contains more sediment for larger water depths compared to low water depths. Furthermore, when the water levels during flood increase, the cross-section widens. The increase in concentration profile and larger widths lead to more sedimentation, see Equation 5.4.
Figure 5.7a shows that a rise in amplitude leads to a rise in sedimentation. Especially for an amplitude of 73 cm, the mean amplitude of measurement station Krimpen aan den IJssel, the sedimentation amplifies. An amplitude of 90 cm enables the flats to participate. As a result, the sedimentation rises extensively, and rise of 80% can be obtained.

When the amplitude rises, and the flood duration remains constant, the water level rise is faster, see Figure 5.6a. As a consequence, the flow velocities increase. Equation 5.1 shows τ_b increases quadratically with U. From the results in Figure F.1a it can be concluded that the strengthening of the absolute ebb velocities is more or less equivalent to the strengthening of the absolute flood velocities. Therefore, $\tau_{max,flood}$ and $\tau_{max,ebb}$ rise alike, resulting in a linear rise of τ_{diff}, see Equation 5.6. This result is also obtained by the numerical model, see Figure 5.7a.

The increment of velocities, due to amplitude rise, leads to a shorter duration of HWS. However, an increment of the water level enables the flats to participate. As a result, when flats participate, the flow velocities decrease, leading to a longer duration of stagnant water. Furthermore, participation of the flats leads to a larger incoming water volume. As a consequence, when flats participate, more sedimentation occurs on the flats.
The bed shear stress increases linearly with the amplitude, and remains flood dominant, see Figure 5.7a. Equation 5.1 states the bed shear stress is at maximum during maximum flow velocities, occurring at bankfull flow, see the figure of the case study: Figure 5.16. From 1.20 m on, the participation of the flats leads to a decrease in flow velocities. Although the enabling of flats leads to a decrease in flow velocities, the system remains flood-dominant. The flood-dominance is the consequence of the shape of the cross-section. Namely, the cross-section is shallow and broad. As a result, high bed shear stresses in ebb direction do not develop due to friction.

Base Flow

For the determination of the influence of the base flow, the numerical model uses Scenarios 5-8. Also, two additional simulations are added: one tidal input with a mean water level of 19 cm NAP and one with 68 cm NAP. The cross-sections of the simulation are taken from the GPS measurements of the current situation.

The base flow of a constructed tidal marsh influences the volume of water coming in, and is directly related to the marsh elevation. When the river base flow is high, the difference in the hydraulic head between the marsh and river is high during flood. Hence, the flow velocities in the marsh are larger, leading to a shorter duration of stagnant water and increasing bed shear stresses.

For water levels ranging from 19 cm to 43 cm, the decrease in bed shear stress is an effect of the Chézy value. This value depends on the hydraulic radius, and is increasing with water level. As a result, the bed shear stress decreases, see Equation 5.1.

Although the mean water level increases, Figure 5.7c shows a decrease in τ_{diff}. When the base flow is lower than 53 cm + NAP, the flats are not participating, and the flow is restricted inside the creeks. The averaged flow velocities in the cross-section are high and lead to higher bed shear stresses as explained above.

A change from bankfull flow (mean water level is 43 cm) to a minor participation of the tidal flats (mean water level is 53 cm) leads to an excessive increase in sedimentation. An explanation can be found in the flat participation. When the flats participate to a small extent, the flow velocities decrease substantially. As a result, the duration of the HWS increases. Since the water depth in Sobek is specified as the largest water depth in the cross-section, much sedimentation is calculated. However in reality, since the participation is only minor, not much sediment will settle during small flat participation.

If the flats participate to a larger extent, a larger volume of water can enter, leading to more sedimentation. In contrast, due to the larger volume of water, flow velocities increase, resulting in a shorter duration of

stagnant water. Hence, a balancing effect exists between the rise in water volume and the decrease in HWS.

Asymmetry

For achieving the influence of asymmetry on accretion, the scenarios explained in Section 5.1.4 are used.

Asymmetry of the tide leads to the import of sediment, as explained in Chapter 2. When the phase difference is 0.5π, higher flow velocities are present. For a phase difference of π the duration of slack water is longer. As a consequence, higher sedimentation rates of SF1 are expected for asymmetry of 0.5π compared to π. And higher sedimentation rates of SF2, the denser particle, for asymmetry of π compared to 0.5π.

Figure 5.7b shows a larger contribution to the sedimentation of SF1, compared to SF2, as a result of the difference in suspension number. The suspension number for SF1 is 0.25 and is 1.5 for SF2. Figure 2.7 shows higher concentrations at the same height for smaller suspension numbers, resulting in the higher sedimentation rates of SF1. However, since sediment for larger suspension numbers is more concentrated close to the bed, SF2 only needs a short HWS compared to SF1 to settle a significant portion of the total sediment.

From Figure 5.7b it becomes clear that larger discharges over one tidal cycle lead to an increase in sedimentation. A larger volume of water enters the area for tides with a phase difference of π as the high waters are more prolonged compared to tides with a phase difference of 0.5π. Furthermore, sedimentation increases as a result of the participation of flats, as they elongate the period of stagnant water.

Figure 5.7d shows τ_{diff}, as defined in Equation 5.6, for every scenario. It becomes clear that every scenario is flood dominant, expect for the scenarios with an asymmetry of π, a mean amplitude, and base flow of h_2 or h_3. The scenarios are corresponding to the scenarios with a long slack period and flat contribution.

The reason for the ebb-dominance is that flooding of the flats during rising tide results in low water levels on the flats, and low flow velocities. In contrast, during ebb, the water remains in the main channel, resulting in larger depths and higher velocities. Next, ebb-dominance is present for scenarios with a phase difference of 0.5π and not for the scenarios with a phase difference of π. This is as expected since the bed shear stress is determined by the mean velocity, see Equation 5.1. The velocity is flood-dominant for the asymmetry of 0.5π, as explained before. Furthermore, the tidal curves are shifted vertically in the numerical computations to obtain flat contribution. As a result, the tides with a phase difference of π are shifted to a greater extent. Therefore, a larger volume of water enters the area for tides with a phase difference of π, resulting in amplification of the ebb-dominance.

However, the ebb-dominance is not observed for the effect of tidal asymmetry with a phase difference of 0.5π. Although flats are participating, τ_{diff} remains more or less constant. This is a result of the balancing effect between the shape of the tidal curve, where an increase in amplitude leads to amplification of flood-dominance. And the counter-effect of the ebb-dominance when flats are participating.

5.2.2. Marsh Design Parameters

To develop guidelines for the (re)design of constructed tidal marshes, the influence of multiple design parameters is examined. This section elaborates theoretically on the influence of tidal flats, the width-depth ratio of the cross-section, the amplitude variation, and the elevation of a constructed tidal marsh. Subsequently, parameter simulations are executed in the numerical model, obtaining total sedimentation and resulting bed shear stresses. Summation of sediment fractions SF1, and SF2 during one tidal cycle for the entire area acquires total sedimentation. The resulting bed shear stress, τ_{diff}, is calculated by the sum of τ_{max} during flood and τ_{max} during ebb, determined at every location, see Equation 5.6. Furthermore, the results of the theoretical model and the results in the numerical model are compared.

Tidal Flat

Executing the numerical model with multiple flat widths leads to a qualitative insight into the influence of the tidal flats. The lengths of the flats are simulated for 25 m, 50 m, 100 m and 150 m. Applying the tidal curve of Scenario 8 ensures the shape of the curve is similar to the shape of the tide occurring in Krimpen aan den IJssel. Next, Scenario 8 has water levels higher than the tidal flat; thus they are participating.

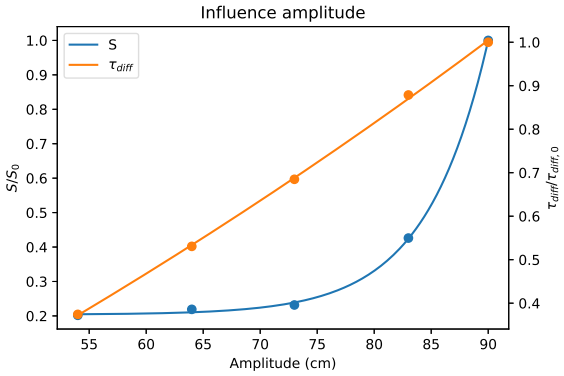

(a) Relationship between ampitude and sedimentation and bed shear stress

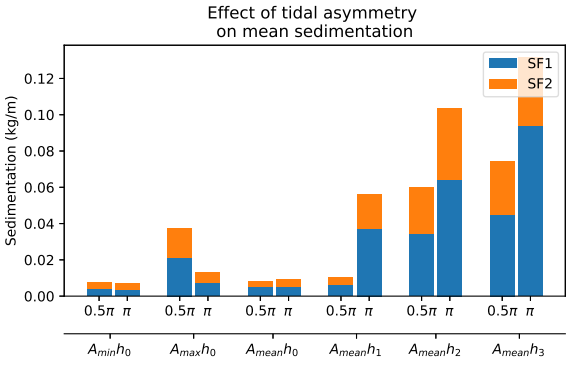

(b) Relationship between asymmetry and sedimentation

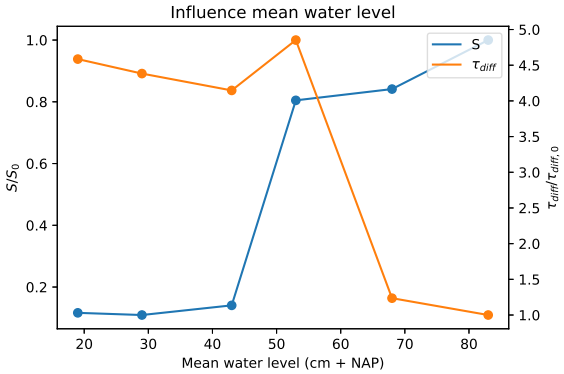

(c) Relationship between base flow and sedimentation

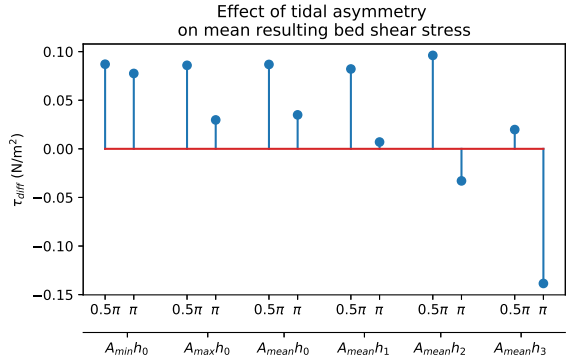

(d) Relationship between asymmetry and bed shear stress

Figure 5.7: Influence of design parameters on sedimentation

When tidal flats in the constructed tidal marsh are contributing during flood, the volume of water entering the system increases. The incoming discharge is defined as:

$$Q = BL\frac{dh}{dt}, \tag{5.7}$$

where BL represents the flooded area. If the wetted area increases, the discharge increases linearly. A rise in water volume entering the area leads higher flood velocities in the creeks, as friction is suppressed for larger depths. Hence, the threshold velocity value for sedimentation is reached later, and ends earlier, leading to a shorter duration of stagnant water. During ebb, the total volume of water leaves the system through the creeks again. Due to lower water levels during ebb, the flats are not participating. As a result, higher outgoing bed shear stresses are obtained and erosion in the creeks is expected.

Although the HWS decreases in the creeks, the threshold velocity for stagnant water is reached earlier at the flats, due to higher friction values. Therefore, sediment settles on the flats. Although the water depth on the flats is relatively low, the suspended sediment present in the water column settles. The model does not account for a distinction between the flats and the creeks, thus a division between eroding creeks and accreting flats is not present.

Figure 5.8a shows that increasing the width of the flats leads to a reduction in total sedimentation. Especially the reduction from $\frac{A_f}{A_{f,0}} = 1$ to $\frac{A_f}{A_{f,0}} = 2$ is large, with a reduction of 17%. After that, the influence of flat contribution decreases.

Although the duration of HWS decreases for larger flat widths, the sedimentation increases as result of increasing cross-section widths. Presumably, the effect of the increase in width of the cross-section is more pronounced for larger flat widths, explaining the small reduction in sedimentation from $\frac{A_f}{A_{f,0}} = 2$ to $\frac{A_f}{A_{f,0}} = 4$.

The difference in maximum bed shear stress during flood and maximum bed shear stress during ebb, τ_{diff}, decreases when the area of the flats increases. τ_{diff} even becomes ebb-dominant for a flat area larger than 40 m as a result of higher ebb-velocities. For a flat area of 25 to 40 m, sedimentation is likely to happen, with the largest sedimentation for $A = 25m$. From 40 m, τ_{diff} becomes negative and the sedimentation decreases, resulting in expected erosion of the creeks.

Depth-width ratio

As a parameter of interest is the cross-section, the numerical model uses Scenario 6 as input. For this scenario, the water remains inside the cross-section, and flats are not contributing. The shape of the cross-section in the numerical computations is rectangular and has a constant area of 8 m^2, approximately corresponding to the surface of the cross-section present in the SVB at location 1. Depth-width ratios of 1.25, 0.65, 0.5, 0.125, 0.08, 0.031 are used in the numerical model.

When the depth-width ratio of the cross-section is high, the depth of the cross-section is larger than the width. The deeper the cross-section, the less influence does the bed roughness have on the flow velocities. However, when the cross-section gets too small, the banks can contribute to friction substantially. Thus, cross-sections with a higher depth-with ratio experience less bottom friction, resulting in higher flow velocities. Though, cross-sections experience friction from the banks when the depth-width ratio increases much. Next, broader cross-sections have lower flow velocities, hence they reach the stagnant water phase earlier, and more sedimentation occurs.

Figure 5.8b shows a critical value of $\frac{d}{B} = 0.5$, meaning that the width is twice the depth. A wide cross-section has shallow water depths, leading to low velocities and longer slack durations, resulting in high sedimentation rates. After this critical value, increasing the depth does not influence sedimentation anymore. However, when the depth continues to increase compared to the width, a situation with considerable bank friction is present.

The value where the shape of the cross-section does not have influence on the bed shear stress anymore is at 0.3. From there on, the resulting bed shear stress reaches a maximum value and is flood-dominant. From values where the width is much larger than the depth, and $\frac{d}{B}$ approaches zero, to $\frac{d}{B} = 0.5$, the sedimentation decreases significantly. A change in the depth-width ratio can acquire a loss of almost 40% in sedimentation.

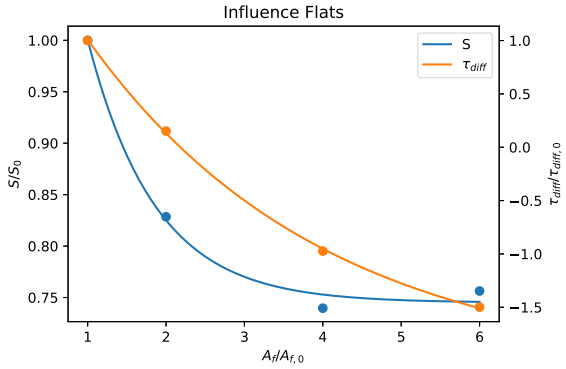

(a) Relationship between flat area and sedimentation, where $A_{f,0} = 25$ m and is the length of the flat.

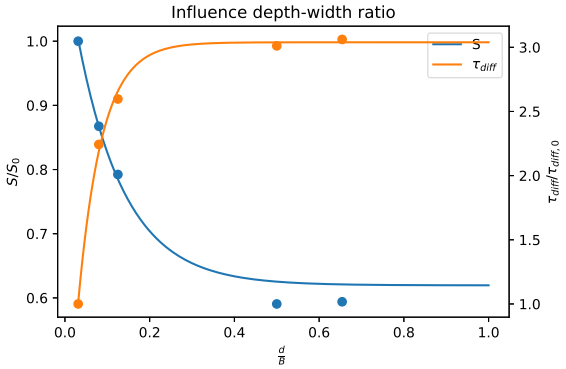

(b) Relationship between depth-width ratio and sedimentation

Figure 5.8: Influence of design parameters on sedimentation

Although the resulting bed shear stress lowers with a factor 3 by decreasing the depth-width ratio, τ_{diff} remains flood-dominant, and the system does not export sediment.

5.2.3. System Adjustments

Comparing the three different situations, as explained in Section 5.1.1, on flow velocity, bed shear stress, and sedimentation gives the influence of structures on different output parameters of the numerical model. The tidal input for the model situations is different from the 12 scenarios as used before. For the different situations only a mean, a maximum, and an extreme tidal force is considered. The mean forcing originates from the mean amplitude in Table 5.4 and a value of h_0 with a $\Delta\phi$ of 0.5π from Table 5.5. The maximum tidal input consists of A_{max} from Table 5.4 and a vertical shift leading to a fully filled tidal marsh (the dikes do not overflow). The most extreme case is when the dikes overflow with a height of 10 cm. The graphs of the tidal forcing are given in Appendix E.

Flow Velocites

Figure 5.9 shows the outcomes of the numerical model for maximum tidal input for the three different situations, where the green line segments mark ebb-dominance. The figure clearly indicates a peak in the maximum flow velocity for situation 1 around 680 m. This peak is the consequence of water flowing over Weir 1 (O1) with a crest height of +0.97 m NAP, see Tabel 3.1. This peak is absent in situation 2 and 3 as the weir has a higher crest level or is lacking. Remarkable is also the lower flow velocity at a distance around 200 m due to the sloping cross-section.

Furthermore, changing from situation 1 to situation 2 or 3, leads to a decrease in flow velocities. A striking difference between the scenarios before and after the modification is the resultant flow velocity. In Scenario 1, the maximum flow velocity is larger in ebb direction for locations ranging from 400-550 m for maximum tidal input, and even 250-550 m for mean tidal input, see Appendix F.1. The ebb-dominant flow velocities are the result of the relative deep cross-section and existing flat area, enhancing ebb-dominance. In contrast, the ebb-dominance is absent in the situations 2 and 3, except from the locations close to the inlet. This is the result of the gate culverts since they lead to a quick filling of the area, leading to high flow velocities. As the gate culverts only function during flood, a quick emptying is not present and therefore flood-dominance is enhanced. For the mean and extreme tidal input, the flow velocities show similar results, as shown in the Figures in Appendix F.2.

Bed Shear Stress

The bed shear stresses are more smooth for situation 1 for each tidal forcing compared to the other situations, see Figure 5.9 and is the result of less inlet points. From around 700 m to 1000 m, the maximum occurring bed shear stress is lower than the critical bed shear stress of both sand and silt, respectively 0.4 N/m^2 and 0.1-0.2 N/m^2. situation 2 and 3 show peaks in the bed shear stress for every forcing when constructions as

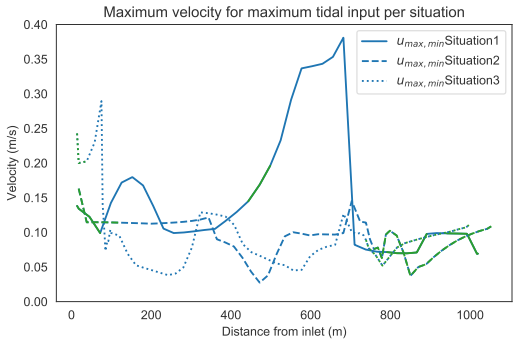

Figure 5.9: Maximum velocity along the x-axis of the creek system for three tidal curves (Appendix E). The green line segments indicate ebb-dominance.

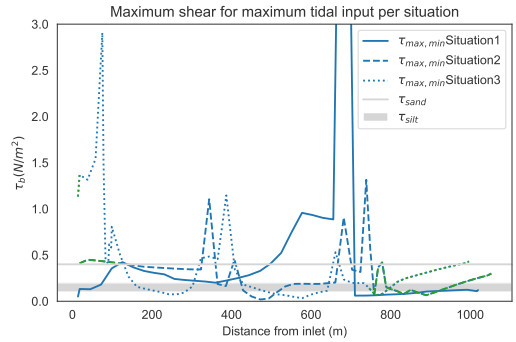

Figure 5.10: Maximum shear along the x-axis of the creek system for three tidal curves and three different scenarios. The green line segments indicate ebb-dominance.

weirs or gate valves are present.

The bed shear stress of situation 3 remains below the critical bed shear stress of silt for the mean tidal forcing, excluding the locations with structures, see Appendix F.2. For situation 2, the bed shear stress for mean tidal input from the inlet to 400 m is around the critical bed shear stress of silt. situation 2 transports silt at some locations, as the critical bed shear stress is exceeded. For situation 1, silt is transported at most locations, and sand is transported at some locations. Sand transport exists at the locations where structures are present. The system is mainly flood-dominant, except for the locations at the outlet point.

When the tidal forcing increases, the bed shear stress increases too as a result of higher flow velocities. For the maximum and extreme tidal forcing, the maximum bed shear stress is above the critical bed shear stress of silt for every location but 200, 450, 600, and 800 m, and sediment is transported. The bed shear stress exceeds the critical bed shear stress of sand close to the inlet. The bed shear stresses close to the inlet are large for situation 3, due to the large storage volume in the sloping cross-section. Namely, the large storage volume leads to a large volume of water entering the system, resulting in high flow velocities and high bed shear stresses. For situation 2, at around 450 m, the location just before the bend, the bed shear stress approaches zero.

However, high flow velocities do not lead per definition to high bed shear stresses. As can be seen in Equation 5.1, the Chézy roughness has the same order of influence on the bed shear stress as the flow velocity. This also explains why the flow velocities in situation 1 are ebb-dominant, but the bed shear stresses are not. For instance, at a location of 200-400 m, ebb-dominant flow velocities are calculated. However, the bed shear stresses are flood-dominant. This is the result of the large in Chézy roughness during the flood stage, compared to the ebb stage. The effect of the broadening of the cross-section from ebb to flood is larger than the ebb-dominance of flow velocity. As a result, the bed shear stress is flood-dominant.

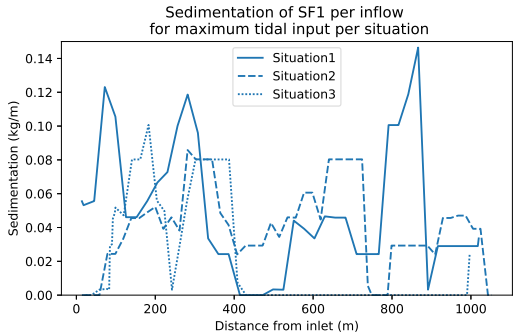

Figure 5.11: Maximum sedimentation of sediment fraction 1 along the x-axis of the creek system for maximum tidal input and three different scenarios.

Sedimentation

In situation 1, potential sedimentation of sediment fraction 1 occurs at 50 m, 250 m, and 850 m for maximum tidal input. For situation 2, the potential sedimentation is more pronounced around 350 and 700 m, which is at the location of a weir and the gate culverts. The large amount of potential sedimentation is presumably the result of water flowing in converging direction from the gate culverts and Weir 1, leading to long periods of stagnant water. For situation 3, sedimentation of sediment fraction 1 and 2 is present in the first 400 m of the tidal marsh, where the cross-section is sloping and a larger volume of water is present. After that, no sedimentation is present.

The potential sedimentation of SF1 for the mean and extreme tidal input are given in Appendix F.2. The potential sedimentation for mean tidal input is much lower for situation 3 compared to the situation 1 and 2 for mean tidal input, as a result of shorter duration of stagnant water. However, the potential sedimentation for mean tidal input decreases for all situations with a factor 7 compared to maximum tidal input as a result of the lower water volume.

Table 5.7 gives the mean sedimentation per meter for the different situations and the three different scenarios in g/m. From this table, it can be concluded that the for the mean tidal forcing, the situations do not differ much. However, when the system is submerged, which happens around 5% of the time, the sedimentation of situation 3 is only half the sedimentation of situation 1 and 2.

situation	mean	max	submerged
1	5.05	49.81	43.76
2	5.51	40.98	40.58
3	4.28	20.00	18.51

Table 5.7: Mean sedimentation during flood over the area for three situations and three tidal curves in g/m.

5.2.4. Locations of Accretion

Model simulations of the SVB show spatial variations in flow velocity, bed shear stress and potential sedimentation. In this section the spatial variations and their explanations are discussed. In Figure 5.13 some x-coordinates are shown corresponding to the locations in the SVB.

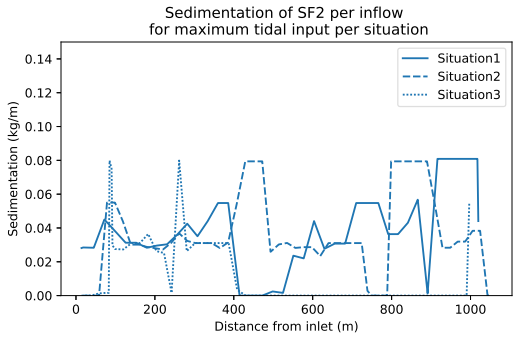

Figure 5.12: Maximum sedimentation of sediment fraction 2 along the x-axis of the creek system for maximum tidal input and three different scenarios.

Figure 5.13: x-coordinates corresponding to locations in the SVB.

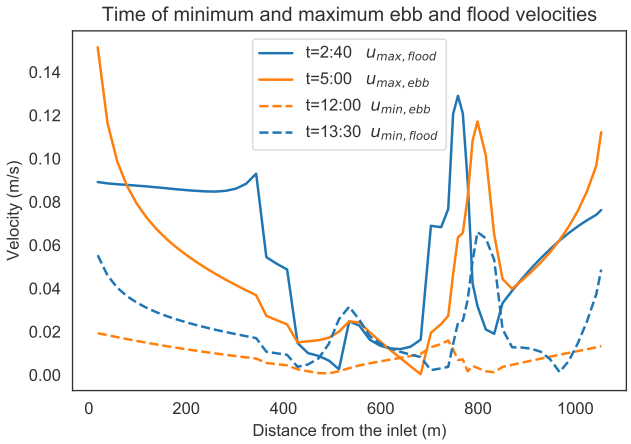

Figure 5.14: Four characteristic times for maximum and minimum ebb and flood velocities calculated for Scenario 5 in the current situation. The blue line represents the flood velocities and the orange lines are the ebb velocities.

Flow Velocities

Figure 5.14 shows a plot of timings of maximum and minimum ebb and flood velocities. The shape of the maximum velocities for ebb and flood is comparable, though the flood velocities are somewhat higher. The minimum flood velocities are higher than the minimum ebb velocities, since the system is flood-dominant. Large peaks are present at the location of the weir, around 800 m. Although the cross-sections do not change abruptly, still the transition to a higher elevated cross-section is visible, explaining the small peaks at x = 550 m.

In general, the graphs in Figure 5.14 show higher flow velocities close to the inlet and almost zero velocities at 400-500 m. The location where the velocity of zero occurs, is around the fierce bend, see Figure 5.13. Furthermore, the influence of the gate culverts and weir is clearly visible in the plot at 700-800 meters distance of the inlet. Although water is not exiting through the gate culverts, high ebb velocities are reached. The ebb velocities are mainly lower than the flood velocities, except for the first 100 m.

Furthermore, the flow velocities at location 1 and 2 for two tidal asymmetries are considered, see Figures 5.15c, 5.15d, 5.15e, and 5.15f respectively. The Figures show how the flow velocity is related to the shape of the cross-section. Shortly after 12:00 the flow velocities start to rise. Appendix D shows from 12:00 the lower part of the cross-section is filled, and flow velocities are able to develop.

The increase in maximum flow velocities in Scenario 1, 3, 5 at location 1 and 2 is the result of increase in water volume entering the the cross-section. Besides, higher velocities are present for location 1, compared to location 2, as the cross-section has a lower elevation, and more water enters during flood.

Scenario 2 shows higher flow velocities than expected for both location 1 as location 2. An explanation can be found in the shape of the cross-section, see Appendix D. For location 1, from an elevation of +0.75 m NAP the cross-section broadens. When the water level is below +0.75 m NAP, which is the case for Scenario 2, the friction of the banks have less influence and the flow velocity reaches a maximum. An equal argumentation applies for location 2.
The reason why the flow velocities at location 2 peak earlier than at location 1 is because large flow velocities are present at +0.5 m NAP in stead of +0.75 m NAP, see also the cross-section of location 2 in Figure 3.7. Besides, location 2 is situated closer to the inlet point, thus the tide arrives earlier at this point.

The right hand plots of Figure 5.16 show a longer HWS compared to the plots of the left hand side, as is expected from the prolonged high water of the tidal curve. When the water levels of the rivers Hollandsche IJssel and Lek increase for Scenarios 9-12, the flat contribution increases too. When the flats are participating, the maximum flow velocity and volume of water increases. The flow velocities at location 2 are lower than at location 1 since the cross-section is broader compared to location 1, see Figure 3.7.

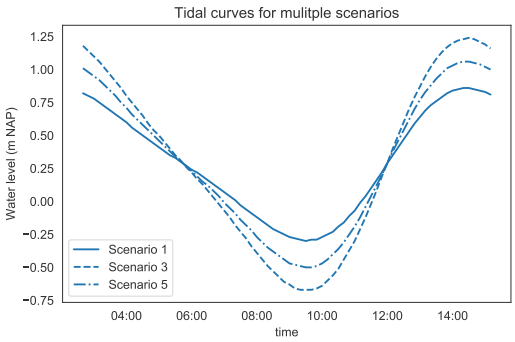

(a) Water levels as function of time for multiple scenarios

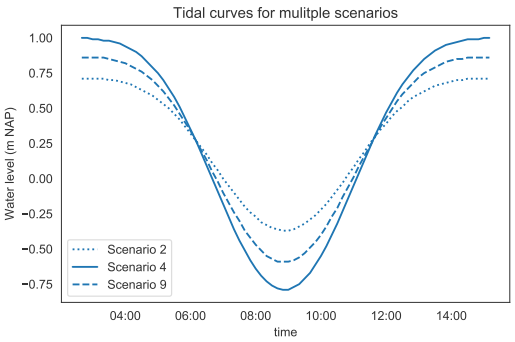

(b) Water levels as function of time for multiple scenarios

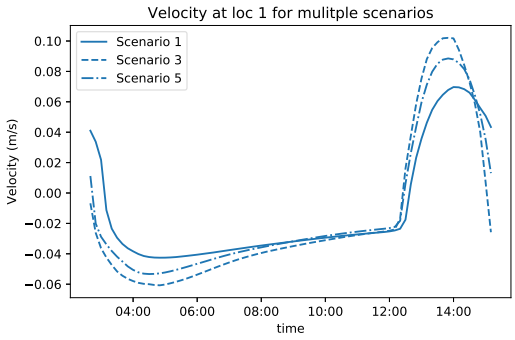

(c) Flow velocities at location 1 for multiple scenarios

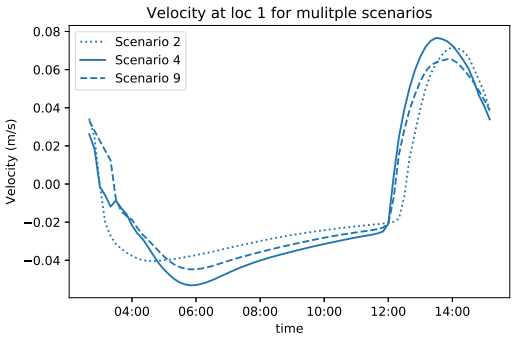

(d) Flow velocities at location 1 for multiple scenarios

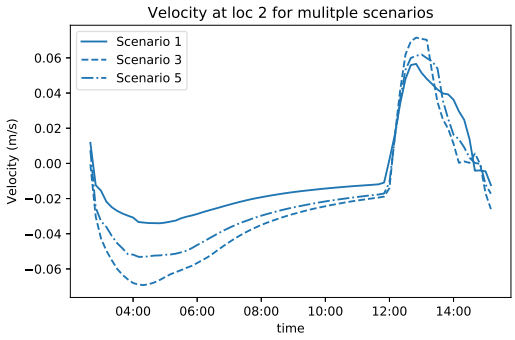

(e) Flow velocities at location 2 for multiple scenarios

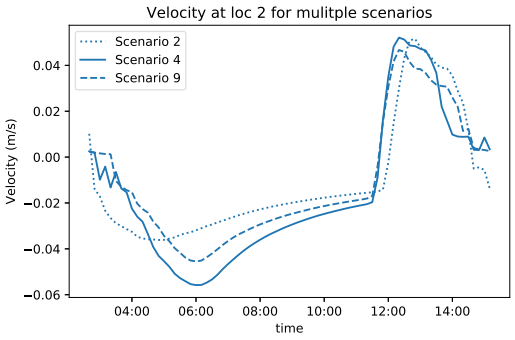

(f) Flow velocities at location 2 for multiple scenarios

Figure 5.15: The upper two plots show the tidal curves for two phase differences. The lower four plots show the velocities at location 1 and location 2 in the SVB.

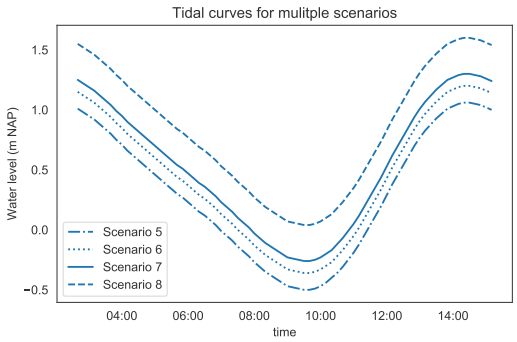

(a) Water levels for multiple scenarios

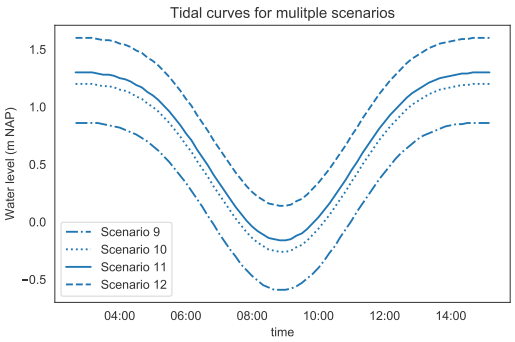

(b) Water levels for multiple scenarios

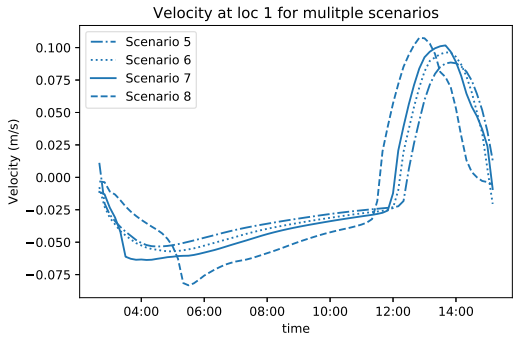

(c) Flow velocities at location 1 for multiple scenarios

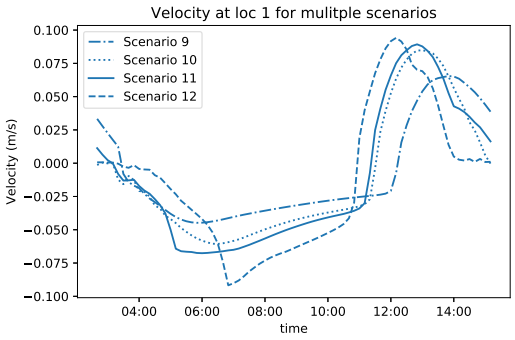

(d) Flow velocities at location 1 for multiple scenarios

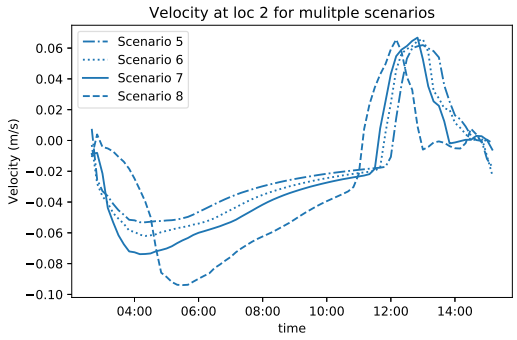

(e) Flow velocities at location 2 for multiple scenarios

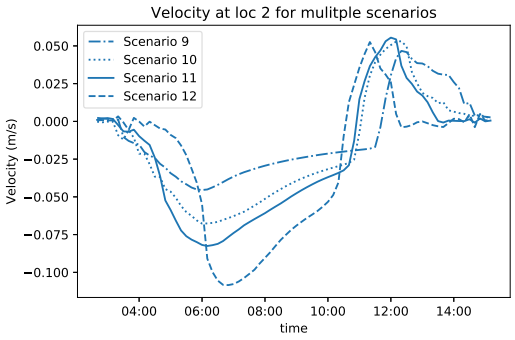

(f) Flow velocities at location 2 for multiple scenarios

Figure 5.16: The upper two plots show the tidal curves for two phase differences. The lower four plots show the velocities at location 1 and location 2.

The volume of water entering the SVB increases when higher water levels are present in the Hollandsche IJssel and Lek, and leads to higher flow velocities. However, when the flats contribute, the frictional effect on the flats is larger, resulting in a reduced flow velocity. Due to this balancing effect, the maximum flow velocities of location 2 are more or less equal. However, for Scenario 8 and Scenario 12, the water entering the system rises to such extend the system becomes ebb-dominant. This can be seen from the difference in velocity peak between ebb and flood of Scenario 8 and Scenario 12. During ebb, the velocity is much larger, since all the water which entered the area during flood, is exported through the creeks.

The flow velocity from Scenario 7 to 8 and from Scenario 11 to 12 only shows a small increase, although the discharge increases substantially. This small effect might be the effect of multiple water inlet points flowing in opposite direction. As a consequence, flow velocities are lower, and a large volume of water is present. Therefore, the sedimentation increases significantly under conditions where the marsh is filled to the outer dikes.

Bed Shear Stress

With the method described in Section 5.1.3, the bed shear stress for every scenario is calculated, see Figure F.2. Scenario 5 is the Scenario with a mean amplitude and a mean vertical shift in the Hollandsche IJssel and Lek. When the amplitude increases/decreases, the bed shear stress increases/decreases as well, see Figure F.2a.

The change of the bed shear stress for multiple times can be seen in 5.17. This Figure shows significant increments of bed shear stresses at the gate culverts at $x = 789$ m. This is the result of high discharges entering though the gate culverts, see Figure 5.18. At the inlet, the flow velocities and discharges are larger than further land inward, resulting in higher bed shear stresses. The peaks at 350 m and 400 m are the result of two weirs which increase the bed shear stress.

The bed shear stresses inside the system are at most locations lower than the critical bed shear stress of sand. Therefore, when sand is imported in the system, the probability of sand being transported is low. It is much more likely that the critical bed shear stress is exceeded for fine sediment.

The incoming volume of water determines the bed shear stress in the creek system since it effects the flow velocity and Chézy roughness, see Equation 5.1. Comparing the bed shear stress in the first 300 m of Scenarios 5 and 6 in Figure F.2c only leads to a small increment in bed shear stress. Scenario 5 represents the mean amplitude with the mean vertical shift and the maximum water level of this scenario is lower than the height of the banks. Scenario 6 represents bankfull flow. For both Scenarios the flats are not participating, and only a small increase in bed shear stress is observed.

However, comparing Scenario 6 with Scenario 7 results in a larger amplification of the bed shear stress as a result of the flats participating. The participation of the flats lead to a larger amount of incoming discharge, resulting in a higher flow velocity inside the creeks.

Equation 5.1 shows that a higher flow velocity leads to an enlargement in the bed shear stress. Remarkable is the remote increase in bed shear stress when Scenario 7 and 8 are compared. The increase in discharge between Scenario 7 and 8 is equal to the increase between Scenario 6 and 7. However, a larger depth is present in Scenario 8, resulting in a lower friction velocity, see Equation 5.2.

Increasing the amplitude in Scenario 1,3, and 5 results in higher bed shear stresses. This is the result of the higher flow velocities, present when the tidal range increases for the same rising period, see Figure F.1. The system is predominantly flood-dominant. When the absolute maximum bed shear stresses during ebb are larger than the absolute maximum bed shear stresses during flood, the line segment is green in Figure F.1, and the system exports sediment. Flood-dominance leads to the import of sediment into the system, as explained in Chapter 2. Furthermore, as the maximum bed shear stress decreases, less sediment can be transported, and sediment deposits.

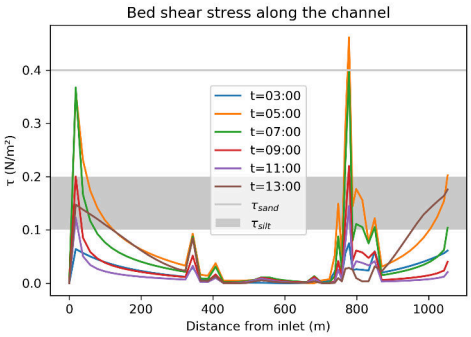

Figure 5.17: The development of the bed shear stress along the channel axis. The figure shows a large increment in bed shear stress at the gate culverts. For the other parts of the creeks this increment is remote.

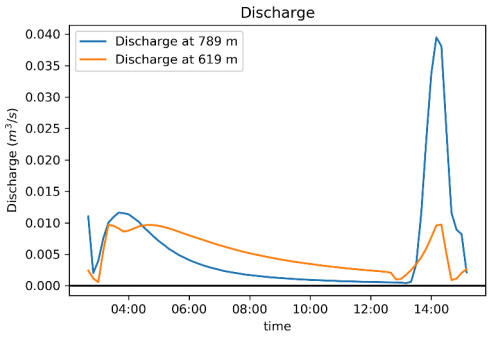

Figure 5.18: The figure shows a higher discharge at the location next to the gate culverts, compared to the discharge at halfway of the creek.

Sedimentation

Using the method described in Section 2.5 gives the sedimentation for the twelve scenarios. The sedimentation of the first sediment fraction is depicted in Figure F.3. Although the HWS is larger for the Scenario 2,4,9 compared to Scenario 1, 3, 5, almost no sedimentation is present, which might be the consequence of the somewhat lower water level forcing. Due to the lower water level forcing, the water levels inside the area are lower too, resulting in a Rouse profile with a smaller total sediment concentration. Next, it is possible that the water level is lower than Δz, the part of the water column from which the sediment settles, resulting in a situation where all the sediment is settled before the HWS is finished. Thus more settling would occur, when a higher water level is present.

When the water levels increase, sedimentation increases abundantly. Especially the difference between Scenario 7 and 8 and between Scenario 11 and 12 is distinct due to the large increase in water levels. The scenarios with a larger vertical shift show a typical sedimentation profile. At the locations close to the inlet, sedimentation is low. When the distance from the inlet increases, the sedimentation is more pronounced. This coincides with the expected energetic conditions in an area like this. Close to the inlet, energy is available for fine sediment transport, but further away, energy dissipates and smaller sediment fractions can settle. Furthermore, at the locations of the gate culverts ($x \approx 790$ m) almost no sedimentation is present. Between the gate culverts and the weir (O1) at $x \approx 600$ m, sedimentation is maximum. The maximum sedimentation is presumably the result of water flowing in converging direction and leading to long periods of stagnant water.

The sediment pattern of SF2 is in contrast with the sediment pattern of SF1. For SF2, the largest sedimentation is present at the inlet and decreases from there on. The suspension number for SF2 is 1.5 and has a relation as shown in Figure 2.7. Therefore, a small high water slack results already in a high amount of sedimentation. Since the water depths and widths of the cross-section are larger closer to the inlet, more sediment is available. Consequently, more sediment settles close to the inlet compared to the sedimentation halfway of the creek system. The integral of the Rouse profile for the same depth is smaller for SF2, compared to SF1, resulting in a lower sedimentation per meter.

6 Discussion

This chapter critically examines the findings compared to previous research and discusses the assumptions of the numerical model. Furthermore, the conclusions are compared with the observations done during fieldwork. Moreover, an elaboration on the applicability of the research is given.

6.1. Discussion of Numerical Model

6.1.1. Model Set-up

The numerical model uses a reference concentration to scale the concentration profile in the water column. The value of the reference concentration is taken relatively low in the numerical computations since the flow velocities entering the SVB are relatively low. Namely, first the flow velocities decease substantially from the Hollandsche IJssel and Lek to the Sliksloot. After that, the velocity decreases further when the branch perpendicular to the Sliksloot discharges into the SVB. The transport capacity has decreased such when entering the SVB, less sediment is available in the water column, and a low reference concentration is taken. However, a wrong estimation of this value leads to errors in the potential sedimentation.

With statistical analysis, tidal curves are constructed for combinations of minimum, mean, and maximum amplitudes, varying water levels, and two types of tidal asymmetry. The constructed tides are then used in the simulation. However, the frequency of occurrence is not taken into account in the evolution of the constructed tidal marsh. It should be considered though that the water level in the Hollandsche IJssel only exceeds 160 cm NAP in 5% of the cases. Therefore, Scenario 8 and 12 do not occur very often. Water levels higher than 120 cm NAP occur in 46% of the cases. Thus, cases disturbing the system occur, while the evolution towards an equilibrium is the common situation.

In the numerical computations, a manning roughness of n=0.2 $s/m^{1/3}$ is obtained from the fieldwork. However, the water level remained below 120 cm NAP, therefore flats did not contribute. This has led to an underestimation of the manning value on the flats. As a result, the velocities when flats are participating are overestimated, leading to higher bed shear stresses and less sedimentation. Consequently, the accretion during flat participation is underestimated.

τ_{diff} is calculated as the sum of the maximum bed shear stress during flood for every location minus the sum of the maximum bed shear stress during ebb for every location. This results in outliers at a location having a significant contribution to the calculation of τ_{diff}. Besides, not only the maximum bed shear stress is of importance for sediment transport, but the duration of the exceedance of the critical bed shear stress as well.

6.1.2. Model Results

For an increment in the flat area, the resulting bed shear stress becomes ebb-dominant, and potential sedimentation is low, based on the numerical model. As a result, the model predicts no sedimentation or even erosion. This is in line with earlier theories of Stive who states that flooding of the intertidal flats during high

waters results in low water levels, and consequently in a low wave celerity. In contrast, during ebb, the water remains in the main channel, resulting in larger depths, thus higher wave celerity[14].

Flow on the tidal flats has only a small depth, leading to enhanced friction and a longer slack duration. Although the system is ebb-dominant, sediment settles on the flat area as result of the high friction. As the bed shear stress on the flats is presumably smaller than the critical bed shear stress, ebb flow is not able to resuspend the particles, resulting in accretion of the flats. In contrast, the creeks have a longer duration of bankfull flow due to the large volume exiting the marsh, leading to high outgoing flow velocities. Therefore, no sedimentation and even erosion is expected in the creeks.

When flow remains inside the creeks, a higher amplitude leads increasing flood-dominant bed shear stresses. In combination with a larger volume of water entering, net sedimentation is expected. Sedimentation for higher amplitudes is in correspondence with theory[14], stating that influence of friction is higher during ebb than during flood since there is a larger interaction with the bottom during low tides. If flow velocities are higher during flood than during ebb, the system is flood-dominant. Furthermore, shallow channels and a large ratio of $\frac{A}{h}$ enhance flood dominance.

6.2. Integration Fieldwork and Numerical Model

The calculations show that the potential sedimentation of the SVB is larger after the system adjustments (situation 2), compared to the original situation (situation 1), and is confirmed by the designer. However, these effects are not observed by the surveyor of the area, who has been monitoring and maintaining the system for over 20 years. Furthermore, the evolution of the cross-section, based on gps measurements and AHN data do not confirm sedimentation.

An explanation might be that the sediment present in the SVB mainly consists of vegetation debris and fine/clayey particles, subjective to subsidence and oxidation. This hypothesis coincides with the research of Wesenbeeck[22] stating that the landside of marshes have the shape of a depression due to compaction of the soil.

Furthermore, sedimentation is likely to occur between 400 and 650 m, the area halfway of the creek system, and at 800-950 m. No accretion is expected closer to the inlet. Possibly the locations of sedimentation are not defined clearly, and miscommunications exists between the designer and the surveyor.

Next, no sedimentation is found, based on gps measurements and AHN data. However, these measurements are limited to the creek, and no measurements of the flats are taken. It is reasonable that the sedimentation only occurs on the flats, and the bed shear stresses in the creeks are high enough to prevent accretion.

In order to reduce accretion in the SVB, the system should become ebb-dominant. This can be obtained by introducing structures that make the bed shear stress during ebb larger than during flood and the duration of HWS is only short. In the current situation, gate culverts functioning in flood-direction area applied, leading to high flood velocities. Gate culverts functioning in ebb-direction can enable high ebb velocities and export of sediment. Also an increasing flat area leads to ebb-dominance

Ebb-dominance of the flow velocity does not per definition lead to ebb-dominance in the bed shear stress. Namely, the Chézy roughness, determined by Manning's coefficient and the hydraulic radius, has a large contribution in the determination of the bed shear stress. Although the system is ebb-dominant with respect to flow velocity, when roughness from ebb to flood increases to a larger extent, the resulting bed shear stress is flood-dominant.

6.3. Research Applicability

The city of Rotterdam aims to build more constructed tidal marshes. In response to this development, the question rises how to embed single pilot projects in integrated delta management or urban development strategies. Masterclasses are organized to share knowledge and to brainstorm about the approach.

By attending two of these sessions with policy makers, designers, and academics, it became clear a mismatch exists between the policymakers and designers on the one side and academic knowledge on the other

side. To fill up this gap, accessible knowledge from the experts should be available for designers.

A functional tidal marsh depends on the aspirations of the management. Constructed tidal marshes can have a natural, cultural or recreational function. A cultural marsh, for instance, should be accessible for a large range of people during the entire year. Furthermore, sludge is not desired and nature has a subordinate function. But how does a marsh develop at a different location in the estuary? The guidelines developed in this research lead to well-informed decisions.

Erosion and sedimentation are dependent on tidal forcing, marsh design, and system adjustments. Tidal forcing are boundary conditions, but can be influenced by the design of the marsh or system adjustments. To prevent or support sedimentation, the participation of the tidal flats is essential. As shown in Figure 5.7c, sedimentation increases when the flats participate. However, when the flat area increases, the system becomes dominant.

Flat participation is determined by the water level at the boundary. But on the other hand, participation of the flats can be fulfilled by setting the elevation of the area. Therefore, the water level in relation to the elevation of the tidal flat should be examined thoroughly for the (re)design of constructed tidal marshes.

Furthermore, the shape of the cross-section is an important parameter in the marsh design. When the centre of the cross-section is small and deep, and then widens with a slight slope, the behaviour is comparable to that of the participation of tidal flats in a lesser extent and lead to sedimentation. Besides, wide cross-sections strengthen sedimentation, while in smaller cross-sections less sedimentation occurs.

Another opportunity for the design of constructed tidal marshes lies in the mimicking of the tidal asymmetry. Although, tidal asymmetry is given for an estuary, the components of the asymmetry important for sedimentation can be imitated. One important asymmetry component is the duration of stagnant water.

Structures exist to regulate water levels inside a constructed tidal marsh. For instance a controlled reduced tide (CRT) can be introduced, as suggested in earlier research[3]. At a predefined level, water flows into the constructed marsh area through a culvert. A gate culvert, at a certain distance below the culvert, is installed as well. The gate culvert enables the water to exit when the water level inside the marsh is higher than outside the marsh. These (gate) culverts result in a longer duration of stagnant water, reinforcing sedimentation.

The incoming water in a CRT is a function of the inlet structure, thus is constant. As a result, the total deposition remains constant too. This is in contrast with sedimentation in a natural marsh, where sedimentation decreases as the area heightens.

Moreover, with the use of a CRT, the amplitudes of the tide can be suppressed, leading to little less sedimentation. The elevation of the (gate) culverts determine at which level water is able to flow in and out. When the level of the inflow culvert is high and the level of the outflow gate culvert is low, the amplitude decreases.

7

Conclusions and Recommendations

This Chapter answers the research questions and recommends how the research can be improved and expanded.

7.1. Conclusions

The objective of this thesis is to determine the influence of tidal forcing and system lay-out on the accretion of a constructed tidal marsh. Therefore, multiple tidal forces are applied to a numerical model, and flow velocities, bed shear stresses and sedimentation are compared for the different scenarios. Furthermore, the influence of structures and the design of the marsh are important for the determination of the accretion of a constructed tidal marsh. The influence of the marsh design parameters and system adjustments are obtained by executing the numerical model with different system lay-outs.

7.1.1. Tidal Forcing

To achieve the influence of tidal forcing on potential sedimentation and bed shear stress in a tidal marsh, the tidal forcing is split up in three components. Namely, the amplitude, base flow, and asymmetry of the tidal curve. This division is made as the three components determine the incoming water volume and the hydrodynamics during one tidal cycle.

In general, when a larger volume of water enters the constructed marsh, larger depths and widths are present in the creek system. The water depth controls the shape of the sediment concentration profile. Furthermore, larger widths lead to a larger sum of sediment in the cross-section. The depth and width, together with the duration of stagnant water, are important in the determination of potential sedimentation.

The duration of stagnant water governs potential sedimentation, and is dependent on the asymmetry of the tide. Besides, the suspension number controls the potential sedimentation. When the suspension number is high, only a short period of slack water is needed for a relatively large amount of sediment settling. For a lower suspension number however, the sediment is more distributed over the water column, and a longer slack duration is needed for the settling of a substantial part of the sediment.

Whether the duration of stagnant water increases with increasing water volumes, depends on the wetted cross-section. When the area of the wetted cross-section increases substantially, and flats are just participating, a longer HWS (high water slack) is expected. Therefore, more sedimentation is predicted for larger water volumes. However, only a small increase in wetted cross-section, leading to bankfull flow, does not lead to sedimentation.

The bed shear stress is governed by the flow velocity and the inverse of Chézy roughness. As a result of amplitude enlargement, the effect of tidal asymmetry amplifies, leading to more pronounced flood-dominance.

Furthermore, when the amplitude increases, flats start to play a role. Contrary to the effect of tidal asymmetry, the participation of flats decreases the bed shear stress during flood, while the flow during ebb is restricted inside the cross-section, resulting in higher bed shear stresses.

The magnitude of the ebb-dominance depends on the shape of the cross-section. Deep cross-sections encounter higher flood-dominance since the effect of bottom friction is low during flood and high during ebb. Broader cross-sections are less flood-dominant as the difference in water level during ebb and flood is

less distinct. When flats are participating, due to a higher mean water level or higher amplitude, water flows over the flats during flood, but remains in the creek during ebb. As a consequence, the resulting bed shear stress is in ebb direction.

To conclude, tidal asymmetry determines the duration of stagnant water. Furthermore, increasing the amplitude and base flow leads to a small increase in sedimentation. However, a considerable increase in sedimentation is reached when flats are participating. Nevertheless, an increasing flat area encourages ebb-dominance and can even lead to erosion. The magnitude of the ebb-dominance depends on the shape of the cross-section.

7.1.2. Marsh Design Parameters

To determine whether flat area and depth-width ratio influence accretion in a constructed tidal marsh, the potential sedimentation and bed shear stresses are obtained for multiple simulations with varying marsh parameters.

The application of flats in a tidal marsh influences the sedimentation. When the area of the flats is only small, sedimentation is likely to happen. However, when the flat area increases, the resulting bed shear stress becomes ebb-dominant. Ebb-dominant bed shear stress, in combination with small sedimentation, leads to the export of sediment.

If the width of the cross-section is large compared to the depth, for a constant cross-sectional area, sediment settles due to higher friction values. The larger the width, the more sediment will settle in the case of bankfull flow. The cross-sections of the creeks approach a critical value when the width is twice the depth. If the width then decreases and the depth increases, no effect in sedimentation is found. However, when the cross-section becomes too small, the influence of the bank friction becomes more pronounced. Due to higher water depths in the cross-section for large depth-width ratios, bed shear stress is able to develop. The flow during flood is less vulnerable to friction due to the higher water depth. As a result, τ_{diff} increases with increasing depth-width ratio.

To conclude, small tidal flats result in sedimentation, but when the flat area increases, erosion is present. Next, when the width of the cross-section is large compared to the depth, more sedimentation is predicted. With flood-dominant bed shear stresses, a broad cross-section leads to accretion.

7.1.3. System Adjustments

To govern the influence of system adjustments on the bed shear stress and potential sedimentation, the three situations of the case study, combined with three tidal forcings are used in the simulations. The three situations correspond to the original design, the current design and the proposed design, respectively. Furthermore, to obtain the locations of accretion in a tidal marsh, the current situation of the SVB is examined thoroughly as a case study.

It can be concluded that the presence and elevation levels of weirs are essential for the magnitude of the flow velocity. In the presence of a weir, a considerable amount of water is able to flow in and out, leading to high velocities.

From the simulations it is observed that the system is ebb-dominant when flood-directed gate culverts are present. The gate culverts allow the constructed tidal marsh to be filled quickly. However, since the gate culverts only function in flood direction, a quick emptying is not present during ebb. As a result, higher maximum flow velocities are obtained during flood compared to the maximum flow velocities during ebb. Next, structures have a notable influence on the bed shear stress too. At locations where structures are present, the bed shear stress increases considerably.

When the amount of potential sedimentation of situation 3 is compared to the amount of potential sedimentation of situation 1 and 2 for submerged conditions, it can be concluded that the potential sedimentation of situation 3 is only half of the potential sedimentation of situation 1 and 2. Potential sedimentation for mean tidal forcing is low for every situation, and no sediment transport is present for situation 3 at all. Since

situation 3 has the smallest amount of potential sedimentation, this situation will probably accrete slowest. However, the system remains flood-dominant and imports sediment.

Furthermore, situation 3 shows only sedimentation in the first 400 meters of the creek system. This corresponds to the location where the cross-section is sloping and larger water volumes are present. For locations larger than 400 m, no potential sedimentation is obtained from the model simulations.

A bed shear higher than 0.4 N/m^2 results in the transport of sand, while the critical bed shear stress for silt is in the range 0.1-0.2 N/m^2. At 450 m distance from the inlet, corresponding to the location of a distinct bend, the maximum flow velocities are almost zero. As a result, the critical bed shear stress of silt at this location is never exceeded, independent on the applied scenario and situation. Therefore, sediment is not transported at the location of the bend.

From the research it became clear that fine sediment (SF1) settles halfway of the creek system, while sediment with a higher fall velocity (SF2) settles closer to the inlet. The deposition of fine sediment increases remarkably land inwards (Figure F.3), while the bed shear stresses decrease land inwards (Figure F.2). The combination of a small bed shear stress and a relatively high deposition rate leads to accretion halfway of the creek system. In contrast, the deposition of sediment fraction 2 is more present close to the inlet (Figure F.4), where the system is ebb-dominant (Figure F.2). These counteracting processes lead to only small resulting accretion/deposition.

To conclude, in the SVB, the presence of sand particles is not expected. Namely, sand is deposited close to the inlet, where the bed shear stress is ebb-dominant. Therefore, when sand is present in the system, it remains close to the inlet. In contrast, silt settles throughout the system. Especially at low energetic conditions, such as bends, silt settles. As the occurring bed shear stress is mostly flood-directed for every situation, it is likely that sediment entering the system, does not leave the system anymore, and accretion of the bends is presumed. The placement of gate culverts in flood direction leads to higher accretion rates due to the longer slack duration. However, at the exact locations of structures, higher bed shear stresses can develop and erosion is expected. Compared to the original and current situation, situation 3 has the smallest amount of potential sedimentation. Therefore, situation 3 probably accretes slowest.

7.2. Recommendations

In this research, the influence of vegetation on the flats is not taken into account and the hydraulic roughness is captured in one manning value. Vegetation is important in tidal marshes, as for marshes in a pioneer stadium, vegetation patches influence the location of the creeks, and inside the patches more particles are able to settle[20]. Despite the SVB is in a more developed stage, where the creeks do not rearrange, but incision is the dominant process[4], vegetation is still an important parameter. Namely, vegetation is responsible for the production of debris, which is a source of sediment leading to accretion. Furthermore, inside the vegetation patch, the flow velocity is lowered, resulting in longer stagnant water, and enabling sediments to settle.

During fieldwork the flow remained inside the creek, resulting in a hydraulic roughness value for the creek system. Since water did not flow on the flats, the hydraulic roughness of this part of the cross-section could not be estimated. Therefore, it is recommended to execute new field measurements during higher occurring water levels. As a result, a partitioning between the hydraulic roughness of creeks and flats can be made, mimicking the influence of the vegetation on the flats.

To estimate whether a cross-section is vulnerable to accretion, the total sedimentation is compared to the difference in maximum and minimum bed shear stress, occurring during one tidal cycle. This difference in bed shear stress determines whether the system is flood- or ebb-dominant. However, not only ebb- or flood-dominance is of importance for sediment transport, the absolute value of the bed shear stress determines whether sediment transport takes place. Besides, the duration of the exceedance of the critical bed shear stress is relevant as well. Therefore, it is advised to use a model where the duration and absolute values of the bed shear stress are taken into account.

Erosion of cohesive sediment is more complex than erosion of non-cohesive sediment. The bed of cohesive sediment normally consists of an easily erodible top layer. However, the critical bed shear stress varies

with time and location as a result of consolidation[23]. Since the sediment in the SVB contains fine and cohesive sediments, the critical bed shear stress increases due to interacting forces between the (flocculated) sediments and the bed[17]. As a result, the bed shear stress during ebb may not be able to re-suspend the particles[18], and accretion is expected. To get more insight in the critical bed shear stress, fieldwork measurements achieving the soil strength are recommended.

Furthermore, the numerical model does not calculate the resulting accretion. The total sedimentation during flood is achieved and the direction of sediment transport. Thus the model is valuable for the predicting whether sedimentation or erosion takes place. However, the amount of accretion is not calculated, as this is dependent on both sedimentation and in and outgoing bed shear stresses. It is suggested to use a model that calculates the resulting accretion.

Moreover, the results of the numerical model give the areas susceptible to sedimentation. When time passes by, sedimentation leads to a change in elevation levels and the locations vulnerable to sedimentation change over time. The numerical model only calculates the potential sedimentation and difference in maximum and minimum bed shear stress during one tidal cycle. The accretion is not updated in the model, thus the accretion of the constructed tidal marsh is only given on a short term. Therefore, if accretion on long term is of interest, it is recommended to execute simulations with updated bed levels.

Furthermore, when accretion on long term is demanded, it is suggested to execute simulations for a longer time period. In this thesis, the effect of one constructed tidal cycle is simulated. However, when the constructed marsh area moves towards an morphological equilibrium, longer times series of occurring water levels should be simulated.

The flow velocities in the numerical model are in 1D, resulting in a mean flow velocity for every location. Though, this is not representative for the flow occurring in the cross-section. Namely, the velocity in the creeks is higher, as a result of a larger depth and discharge compared to the flats. Since friction is high on the flats, sedimentation therefore mainly occurs here and to a lesser extend in the creek system. Also, the ebb velocities are lower on the flats, not able to resuspend particles. Concluding, for further research it is recommended to execute numerical computations in 2D or 3D for the examination of the spatial variation of sedimentation.

Appendices

A

Propeller Measurement

Propeller

Stap 1

- Meet de breedte (=B) van het water
- Schrijf B en de tijd HH:MM op het formulier
- Plaats markeringen op 1/6 B, 1/2 B en 5/6 B

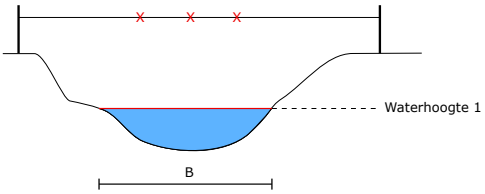

Stap 2

- Meet de diepte (=d) van het water op punt 1
- Schrijf d op het formulier

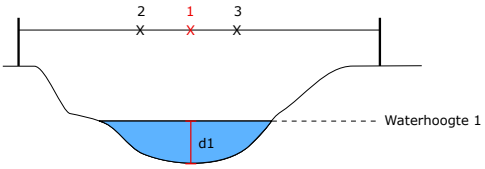

Stap 3

- Hou de propeller op 0.6 d om de meting te starten
- Schrijf het resultaat van de propeller op het formulier

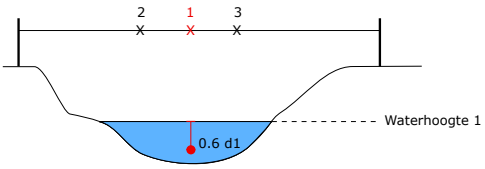

Stap 4

- Herlaal stap 2 en 3 voor punt 2 en punt 3

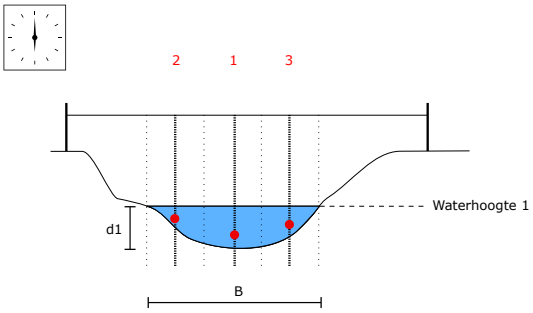

Stap 5

- Begin weer met stap 1 na 10 min met een nieuwe waterhoogte

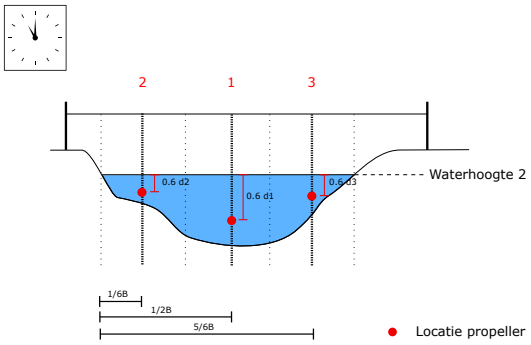

B

Layout SVB

B.1. System Layout

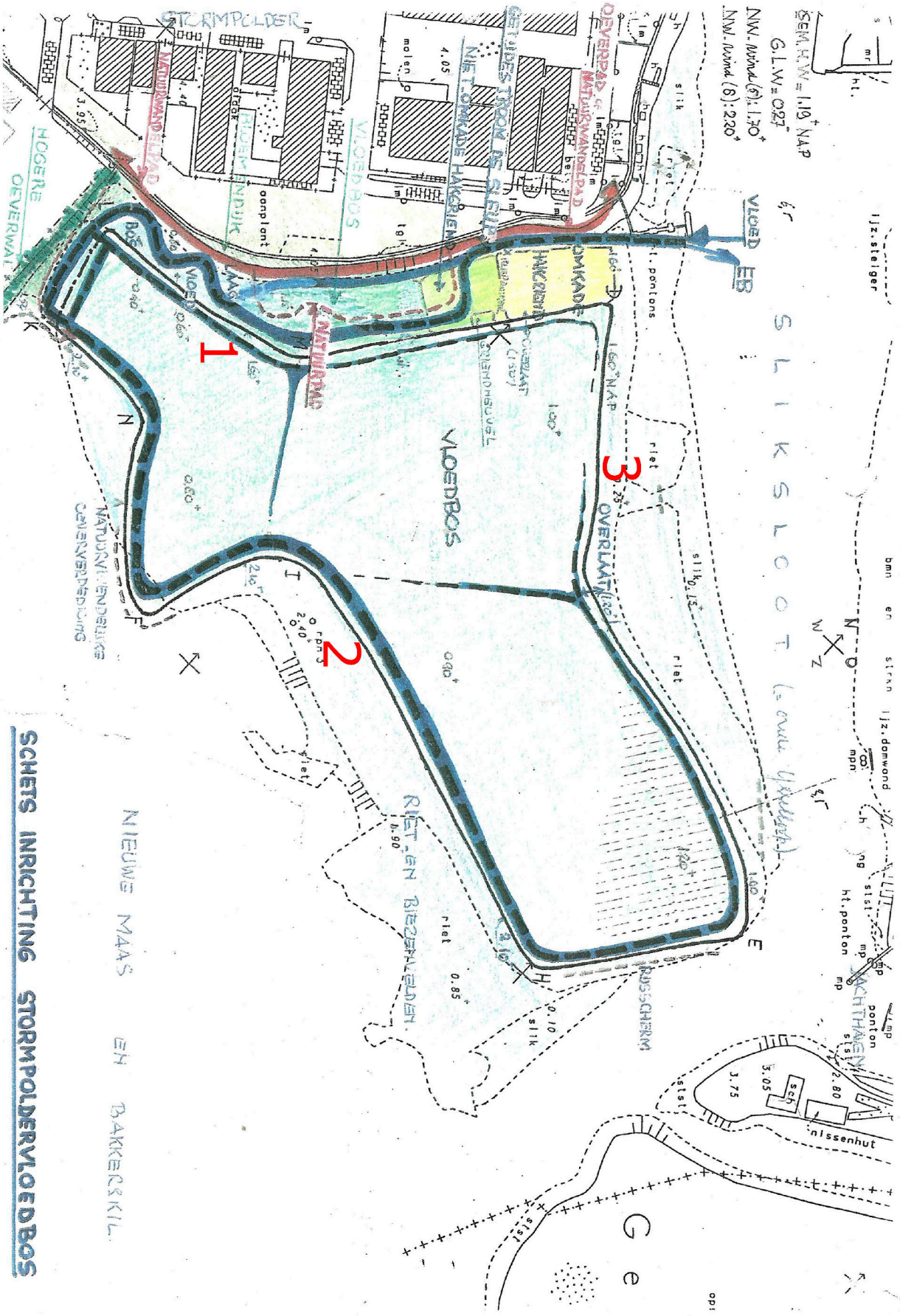

Figure B.1: Design of SVB

B.2. Model Layout

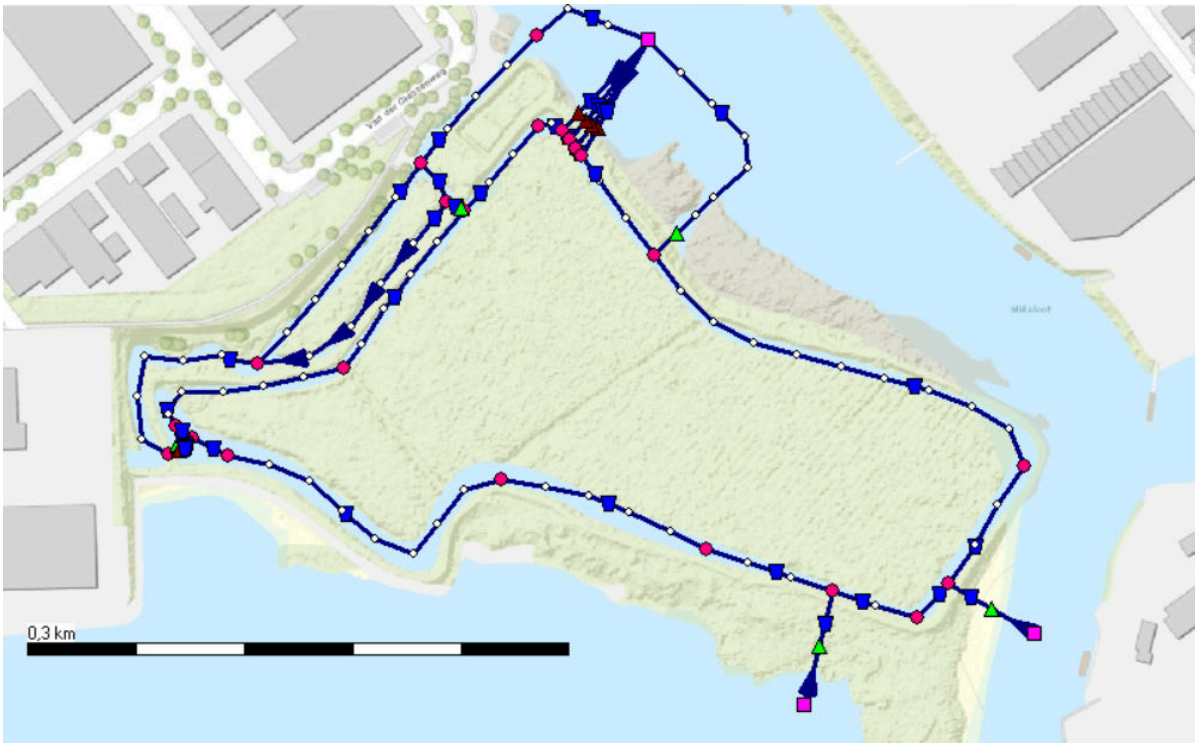

Figure B.2: Lay-out of Sobek model

C

Sobek to Python

As the output of Sobek does not directly calculates shear stresses, they are achieved via Python. In this Appendix it is explained how the Sobek output file is transferred to Python.

C.1. hkvsobekpy

HKV has developed a very useful package for reading Sobek output. It provides access to a his-file, which is a binary file object communicating with Sobek. hkvsobekpy can be installed by `pip install hvsobekpy` after installing the following dependencies with `conda install ...`:

- numpy
- scipy
- pandas
- GDAL
- shapely
- Fiona
- geopandas
- matplotlib
- fire
- tqdm

C.2. Sobek Output

The requested case is run by Sobek. This automatically saves a his-file in the WORK directory. All the his-files are then copied to a Python destination and imported from there. However, as the SVB model is dealing with a loop and tidal water levels, the arrangement of locations in the his-file is not correct.

To be able to work with appearing order of calculation points and reaches, they are imported manually by selecting them and exporting via side view. Thereafter, the arranged locations are imported in Python again.

D

Water Level and Cross-sections

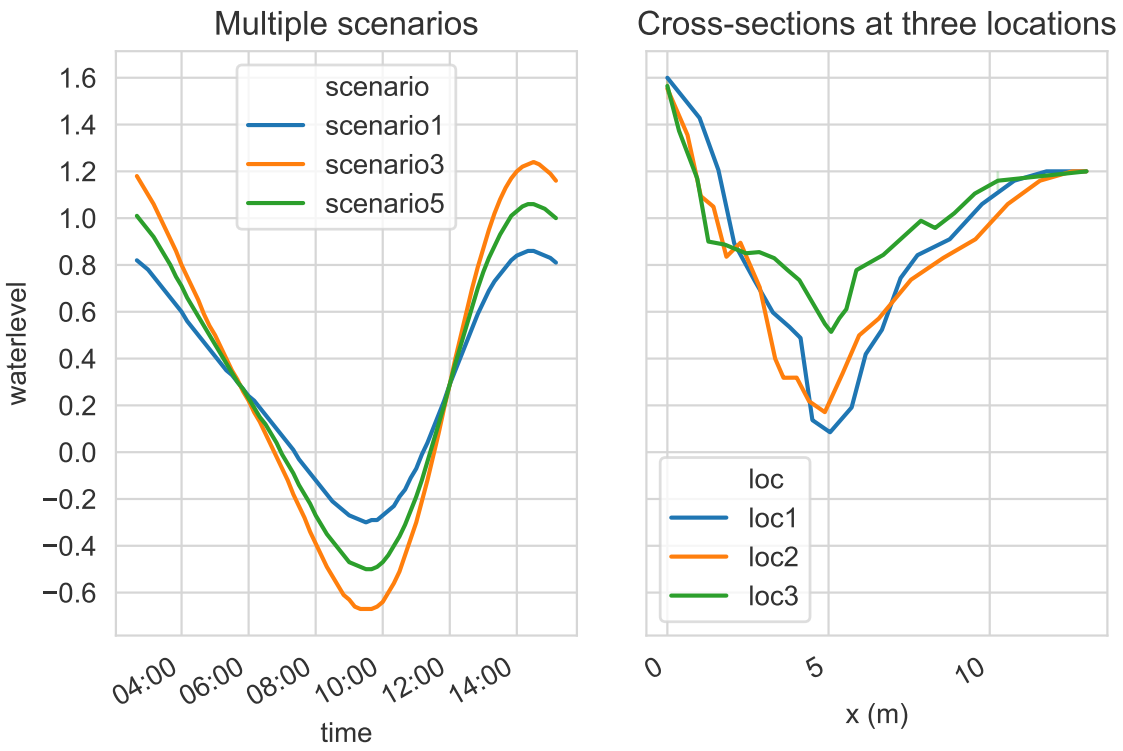
Multiple scenarios
scenario
scenario1
scenario3
scenario5
waterlevel
1.6
1.4
1.2
1.0
0.8
0.6
0.4
0.2
0.0
−0.2
−0.4
−0.6
04:00
06:00
08:00
10:00
12:00
14:00
time
Cross-sections at three locations
loc
loc1
loc2
loc3
0
5
10
x (m)

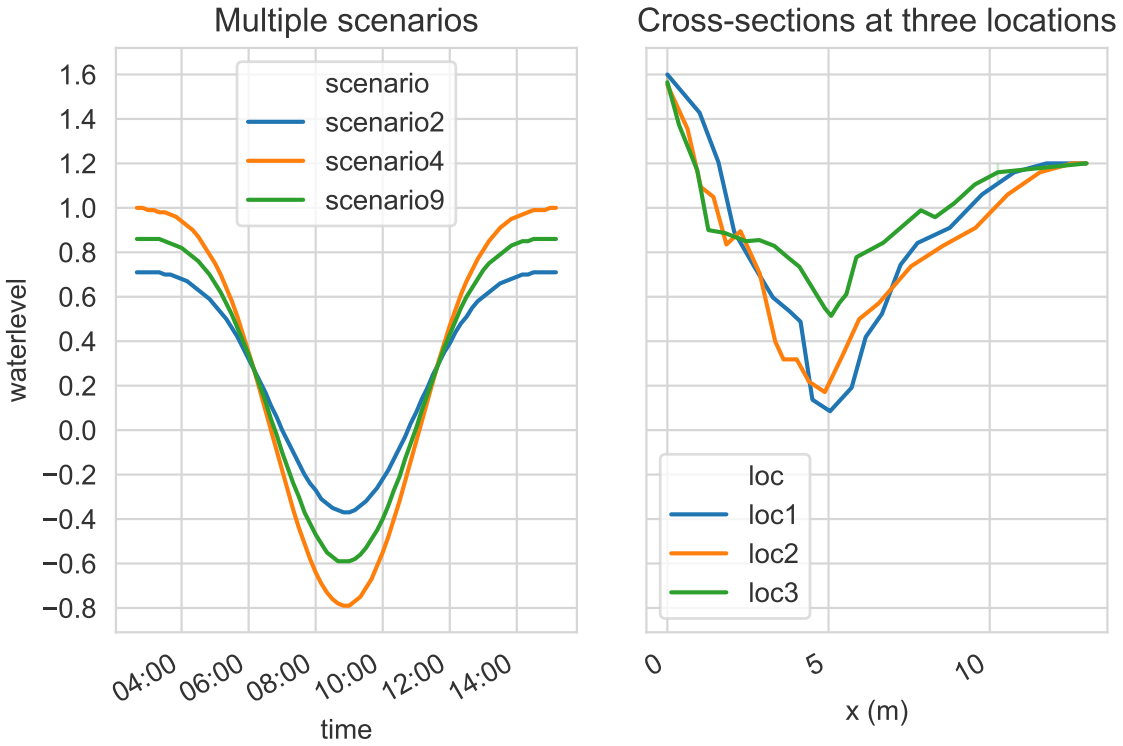
Multiple scenarios
scenario
scenario2
scenario4
scenario9
waterlevel
1.6
1.4
1.2
1.0
0.8
0.6
0.4
0.2
0.0
−0.2
−0.4
−0.6
−0.8
04:00
06:00
08:00
10:00
12:00
14:00
time
Cross-sections at three locations
loc
loc1
loc2
loc3
0
5
10
x (m)

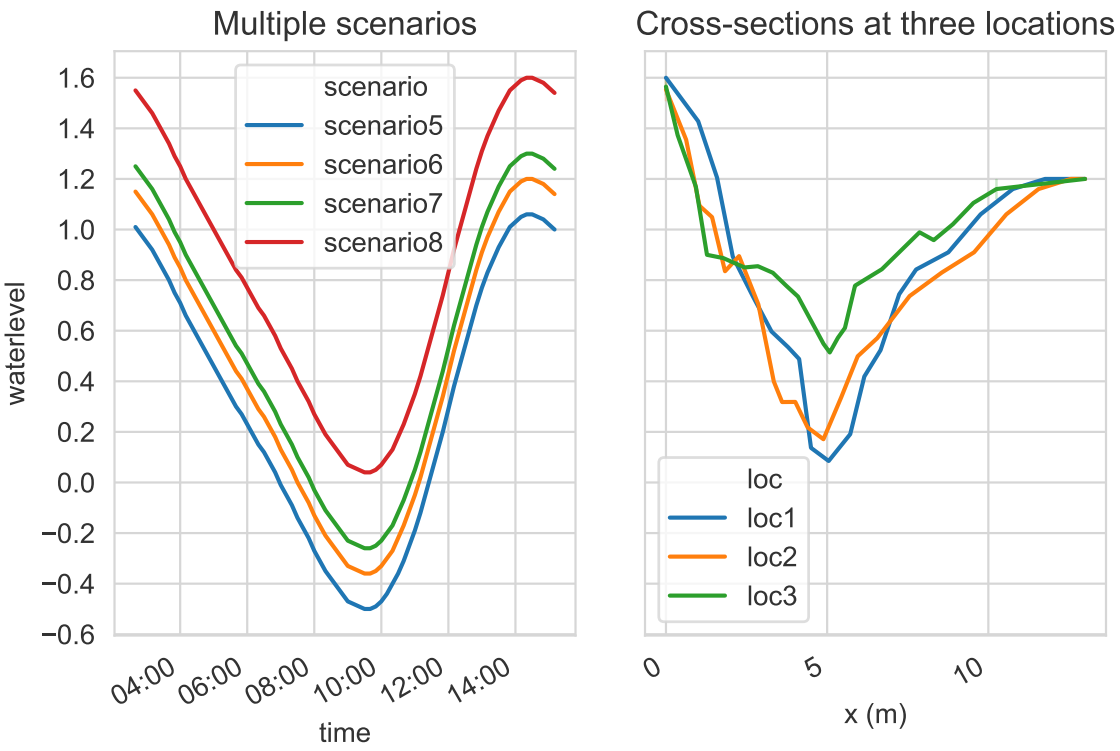
Multiple scenarios
Cross-sections at three locations
waterlevel
time
x (m)
scenario
scenario5
scenario6
scenario7
scenario8
loc
loc1
loc2
loc3
1.6
1.4
1.2
1.0
0.8
0.6
0.4
0.2
0.0
−0.2
−0.4
−0.6
04:00
06:00
08:00
10:00
12:00
14:00
0
5
10

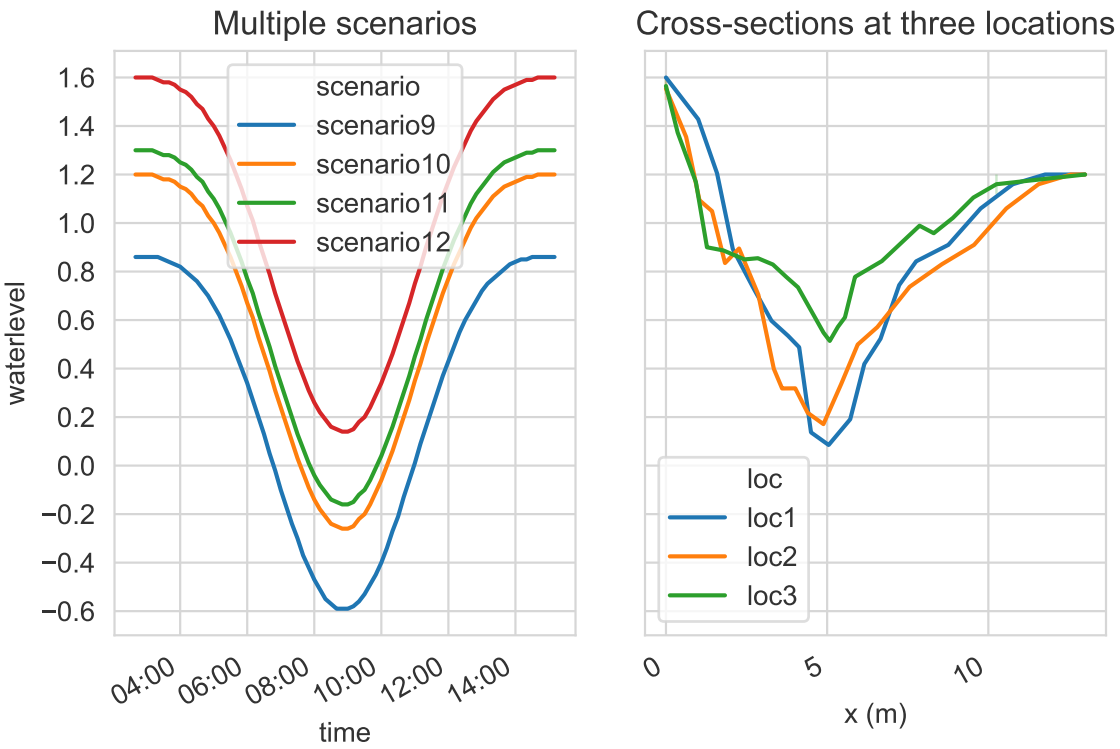
Multiple scenarios
Cross-sections at three locations
waterlevel
time
x (m)
scenario
scenario9
scenario10
scenario11
scenario12
loc
loc1
loc2
loc3
1.6
1.4
1.2
1.0
0.8
0.6
0.4
0.2
0.0
−0.2
−0.4
−0.6
04:00
06:00
08:00
10:00
12:00
14:00
0
5
10

E

Tidal Curves for Situations

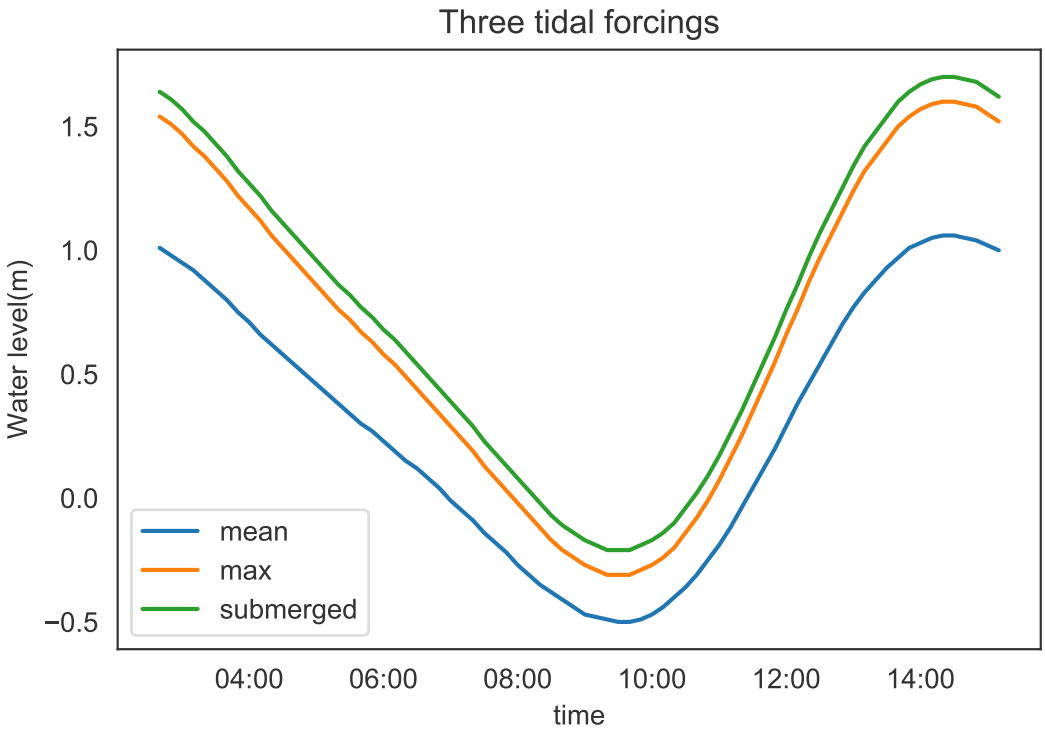

F Results of Numerical Model

F.1. Tidal Forcing

F.1.1. Flow Velocities

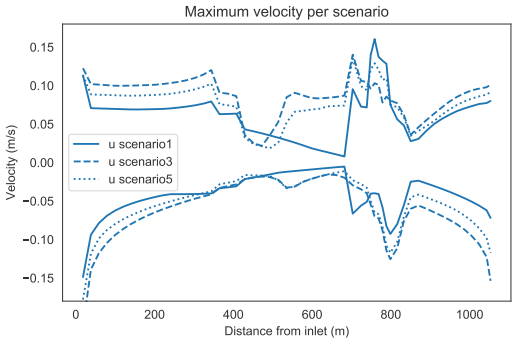

(a) Maximum flood and ebb velocities for multiple scenarios

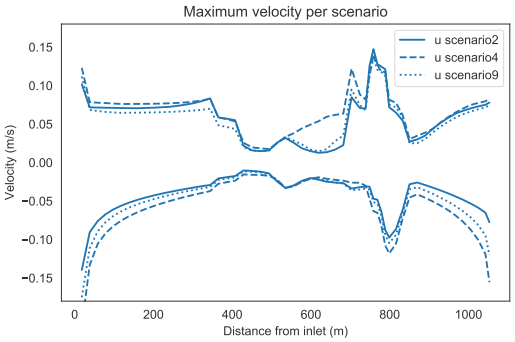

(b) Maximum flood and ebb velocities for multiple scenarios

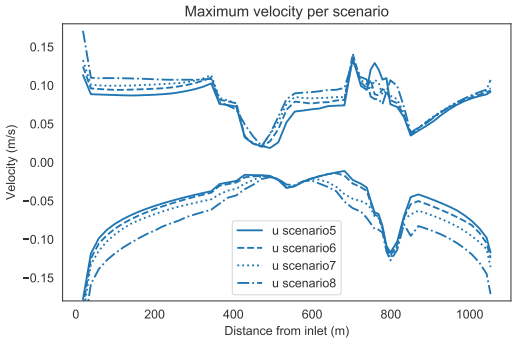

(c) Maximum flood and ebb velocities for multiple scenarios

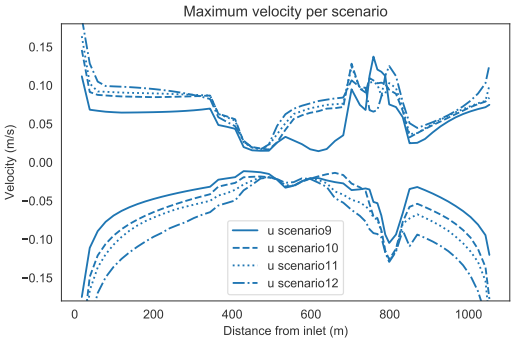

(d) Maximum flood and ebb velocities for multiple scenarios

Figure F.1: Maximum flow velocities along the channel. The tidal forcing is depicted in the two top plots of Figures 5.6.

F.1.2. Bed Shear Stress

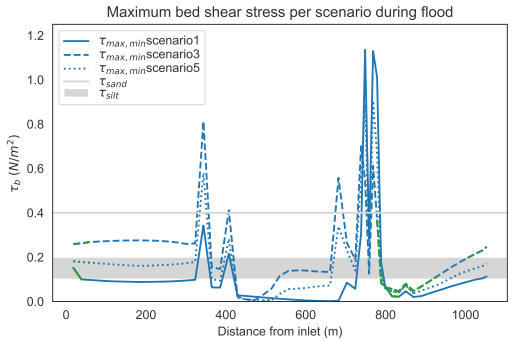

(a) Maximum bed shear stress for multiple scenarios

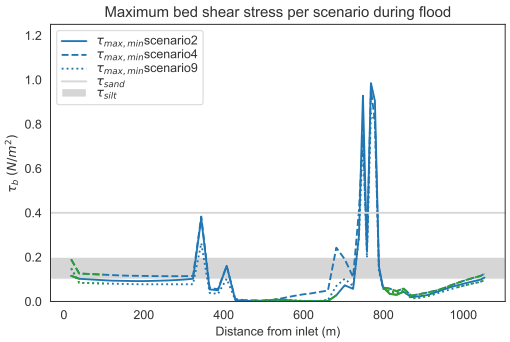

(b) Maximum bed shear stress for multiple scenarios

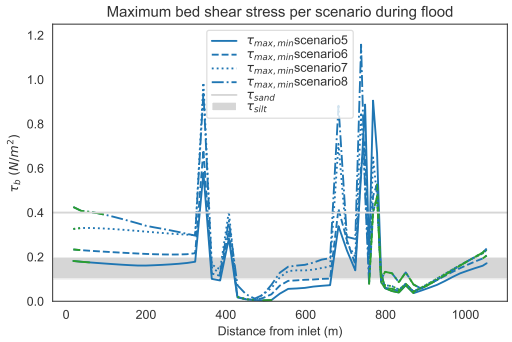

(c) Maximum bed shear stress for multiple scenarios

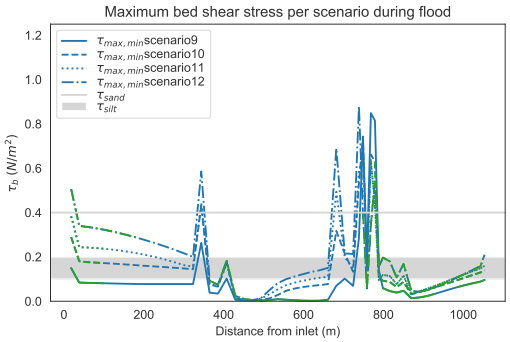

(d) Maximum bed shear stress for for multiple scenarios

Figure F.2: Maximum shear stress along the channel. τ_{sand} and τ_{silt} give the values for the critical bed shear stress. The tidal forcing is depicted in the two top plots of Figures 5.15 and 5.16. When the absolute maximum bed shear stresses during ebb are larger than the absolute maximum bed shear stresses during flood, the color of the line is green

F.1.3. Sedimentation

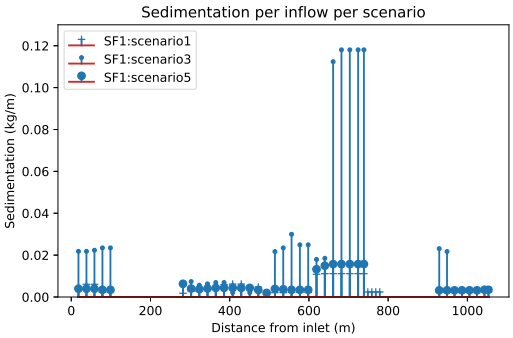

(a) Sedimentation for SF1 for multiple scenarios

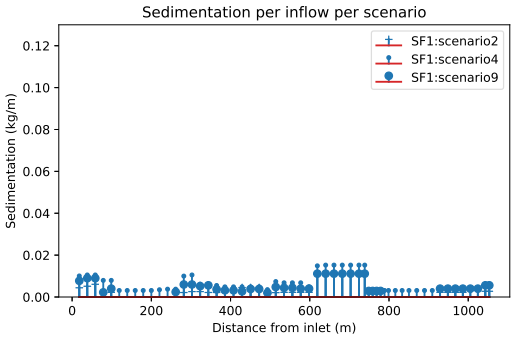

(b) Sedimentation for SF1 for multiple scenarios

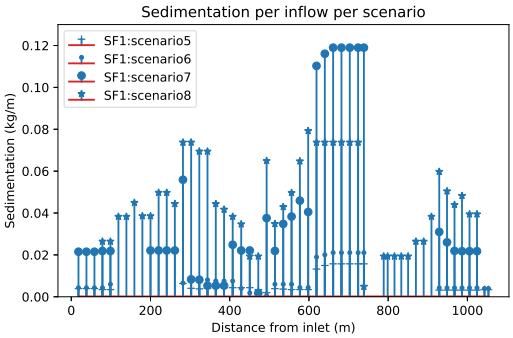

(c) Sedimentation for SF1 for multiple scenarios

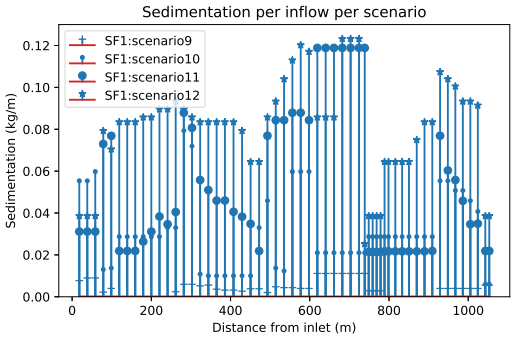

(d) Sedimentation for SF1 for multiple scenarios

Figure F.3: Maximum sedimentation along the channel for the finer sediment: SF1. The input parameters for this sediment fraction are listed in Table 5.2. The tidal forcing is depicted in Figures 5.6.

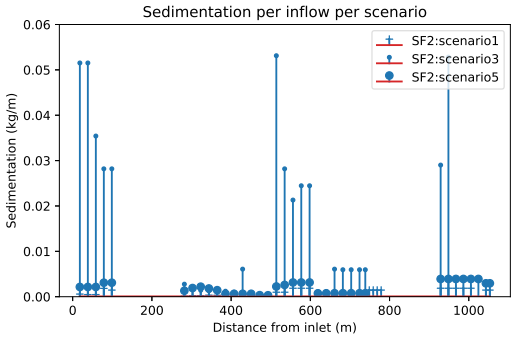

(a) Sedimentation for SF2 for multiple scenarios

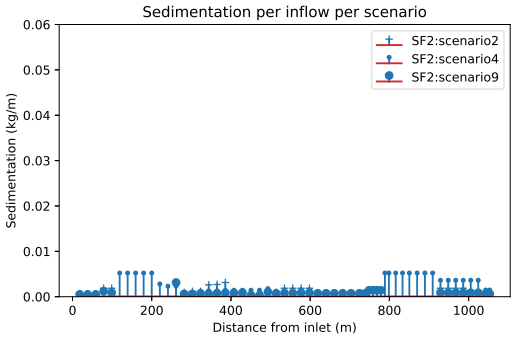

(b) Sedimentation for SF2 for multiple scenarios

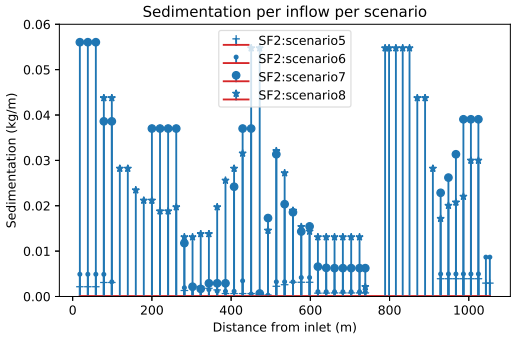

(c) Sedimentation for SF2 for multiple scenarios

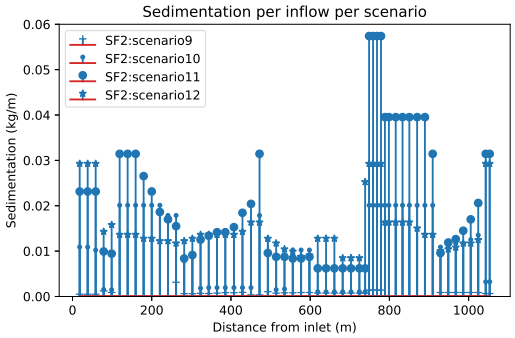

(d) Sedimentation for SF2 for multiple scenarios

Figure F.4: Maximum sedimentation along the channel for the coarser sediment SF2. The input parameters for this sediment fraction are listed in Table 5.2. The tidal forcing is depicted in Figure 5.6.

F.2. System Adjustments

F.2.1. Flow Velocities

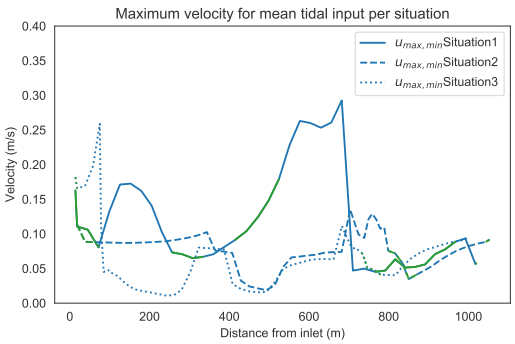

(a) Maximum velocity for multiple scenarios

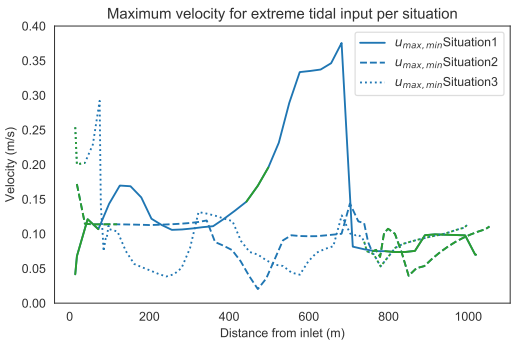

(b) Maximum velocity for multiple scenarios

Figure F.5: Maximum velocity along the x-axis of the creek system for three tidal curves (Appendix E) and three different scenarios. The green line segments indicate ebb-dominance.

F.2.2. Bed Shear Stress

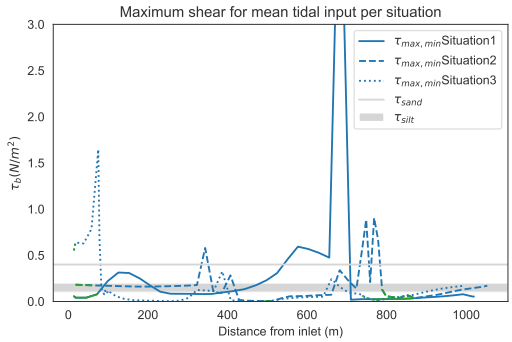

(a) Maximum bed shear stress for multiple scenarios

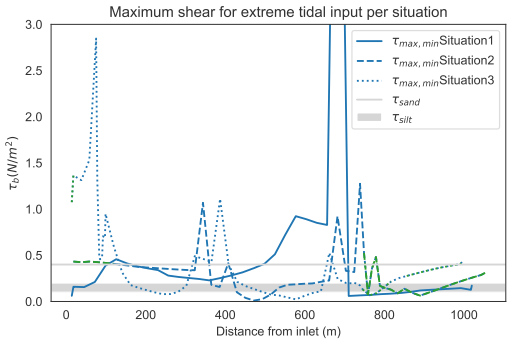

(b) Maximum bed shear stress for multiple scenarios

Figure F.6: Maximum shear along the x-axis of the creek system for three tidal curves and three different scenarios.

F.2.3. Sedimentation

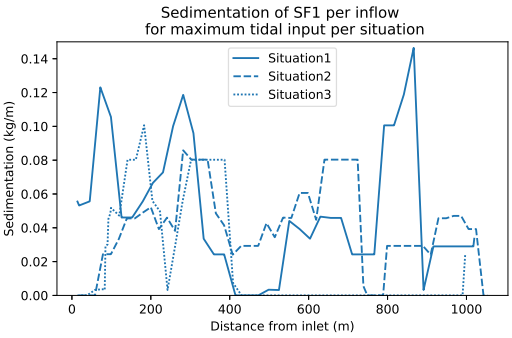

(a) Sedimentation for SF1 for multiple scenarios

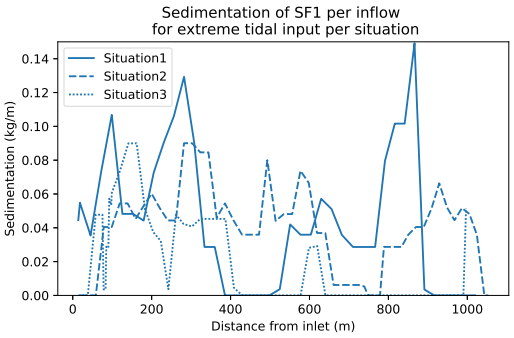

(b) Sedimentation for SF1 for multiple scenarios

Figure F.7: Maximum sedimentation of sediment fraction 1 along the x-axis of the creek system for three different scenarios.

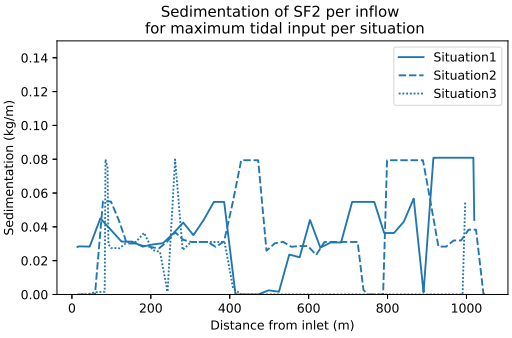

(a) Sedimentation for SF2 for multiple scenarios

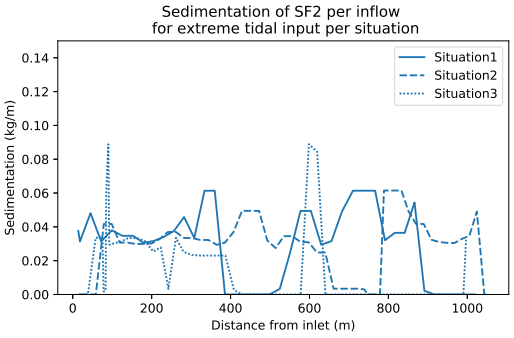

(b) Sedimentation for SF2 for multiple scenarios

Figure F.8: Maximum sedimentation of sediment fraction 2 along the x-axis of the creek system for three different scenarios.

Bibliography

[1] Miriam Coenders and Willem Luxemburg. *CIE4440 Hydrological Processes and Measurements*. Number September. 2017.

[2] Wiliam 1998 Coon. *Estimation of Roughness Coefficients*. 1998. ISBN 9781139541008. URL https://pubs.usgs.gov/wsp/2441/report.pdf.

[3] Tom Cox, Tom Maris, Pieter De Vleeschauwer, Tom De Mulder, Karline Soetaert, and Patrick Meire. Flood control areas as an opportunity to restore estuarine habitat. *Ecological Engineering*, 28(1):55–63, 2006. ISSN 09258574. doi: 10.1016/j.ecoleng.2006.04.001.

[4] Alma V. de Groot, Bregje K. van Wesenbeeck, and Jantsje M. van Loon-Steensma. Stuurbaarheid van kwelders. Technical Report november, 2013.

[5] D Dillingh. *Kenmerkende waarden kustwateren en grote rivieren*. Number 1207509-000. 2013. ISBN 1207509000.

[6] Patrick J. Doody. *Saltmarsh Conservation, Management and Restoration*. Springer Netherlands, 2007.

[7] A.C. Horrevoets, H.H.G. Savenije, J.N. Schuurman, and S. Graas. The influence of river discharge on tidal damping in alluvial estuaries. *Journal of Hydrology*, 294(4):213–228, jul 2004. ISSN 0022-1694. doi: 10.1016/J.JHYDROL.2004.02.012. URL https://www.sciencedirect.com/science/article/pii/S0022169404001052?via{%}3Dihub.

[8] Jonathan M. Huckle, Jacqueline A. Potter, and Rob H. Marrs. Influence of environmental factors on the growth and interactions between salt marsh plants: Effects of salinity, sediment and waterlogging. *Journal of Ecology*, 88(3):492–505, 2000. ISSN 00220477. doi: 10.1046/j.1365-2745.2000.00464.x.

[9] W E Odum. Comparative Ecology of Tidal Freshwater and Salt Marshes. *Annual Review of Ecology and Systematics*, 19(1):147–176, 1988. ISSN 0066-4162. doi: 10.1146/annurev.es.19.110188.001051.

[10] William E Odum, T J Smith, John K Hoover, and Carole C McIvor. The ecology of tidal freshwater marshes of the United States East Coast: a community profile. *US Fish and Wildlife Service*, OBS-83/17:Ch 2, 1984.

[11] Aline Pieterse, Jack A. Puleo, Thomas E. McKenna, and Jens Figlus. In situ measurements of shear stress, erosion and deposition in man-made tidal channels within a tidal saltmarsh. *Estuarine, Coastal and Shelf Science*, 192:29–41, 2017. ISSN 02727714. doi: 10.1016/j.ecss.2017.04.028. URL http://dx.doi.org/10.1016/j.ecss.2017.04.028.

[12] Zwevende Stof Rijn-maasmonding. Zwevende Stof Rijn-Maasmonding WL | delft hydraulics. 2006.

[13] H.H.G. Savenije. Salinity and tides in alluvial estuaries, 2nd completely revised edition: salinityandtides.com. *Open Access*, page 163, 2012.

[14] M.J.F. Stive and J. Bosboom. *Coastal Dynamics 1*. Delft Academic Press, 2015.

[15] Ven te Chow. *Open-Channel Hydraulics*. 1959.

[16] Steven Traynum and Richard Styles. Flow, stress and sediment resuspension in a shallow tidal channel. *Estuaries and Coasts*, 30(1):94–101, 2007. ISSN 15592731. doi: 10.1007/BF02782970.

[17] L.C. van Rijn. SIMPLE GENERAL FORMULAE FOR SAND TRANSPORT IN RIVERS, ESTUARIES AND COASTAL WATERS. Technical report, 1993.

[18] W. Vandenbruwaene, T. Maris, T. J S Cox, D. R. Cahoon, P. Meire, and S. Temmerman. Sedimentation and response to sea-level rise of a restored marsh with reduced tidal exchange: Comparison with a natural tidal marsh. *Geomorphology*, 130(3-4):115–126, 2011. ISSN 0169555X. doi: 10.1016/j.geomorph.2011.03.004. URL http://dx.doi.org/10.1016/j.geomorph.2011.03.004.

[19] Wouter Vandenbruwaene. Tidal channel development and the role of vegetation : fundamental insights and application for tidal marsh restoration Ontwikkeling van getijdengeulen en de rol van vegetatie : fundamentele kennis en toepassing voor schorherstel Wouter Vandenbruwaene. 2011.

[20] Wouter Vandenbruwaene, Tjeerd J. Bouma, Patrick Meire, and Stijn Temmerman. Bio-geomorphic effects on tidal channel evolution: Impact of vegetation establishment and tidal prism change. *Earth Surface Processes and Landforms*, 38(2):122–132, 2013. ISSN 01979337. doi: 10.1002/esp.3265.

[21] Z.B. Wang, C. Jeuken, and H.J. de Vriend. Tidal asymmetry and residual sediment transport in estuaries, 1999.

[22] B K Van Wesenbeeck, P Esselink, A P Oost, W E Van Duin, A V De Groot, R M Veeneklaas, T Balke, P Van Geer, A C Calderon, and A Smale. Kwelders En Schorren. 2014.

[23] J. C. Winterwerp, W. G. M. van Kesteren, B. van Prooijen, and W. Jacobs. A conceptual framework for shear flow-induced erosion of soft cohesive sediment beds. *Journal of Geophysical Research: Oceans*, 117(C10):n/a–n/a, 2012. doi: 10.1029/2012jc008072.